VNIVERSITAT DE VALÈNCIA

Escola Tècnica Superior d'Enginyeria ETSE-UV

DOCTORAL PROGRAMME IN ELECTRONIC ENGINEERING

DOCTORAL THESIS

Study of Electromagnetic Shielding Effectiveness Measurement Methods: Theoretical, Simulation and Experimental Approaches

Author:
Andrea Amaro Pérez

Supervisor:
Dr. Eng. José Torres País
Tutor:
Dr. Eng. Adrián Suárez Zapata

Universitat de València (UV)
Department of Electronic Engineering

Valencia, Spain – July 2025

Declaration

D. JOSÉ TORRES PAÍS, Doctor en Ingeniería Electrónica, Profesor Titular del Departamento de Ingeniería Electrónica de la Escola Tècnica Superior d'Enginyeria de la Universitat de València

D. ADRIÁN SUÁREZ ZAPATA Doctor en Ingeniería Electrónica, Profesor Ayudante Doctor del Departamento de Ingeniería Electrónica de la Escola Tècnica Superior d'Enginyeria de la Universitat de València

HACEN CONSTAR QUE:

ANDREA AMARO PÉREZ, Graduada en Ingeniería Electrónica de Telecomunicación y Máster en Ingeniería Electrónica, ha realizado bajo su dirección y tutorización el trabajo titulado *"Study of Electromagnetic Shielding Effectiveness Measurement Methods: Theoretical, Simulation and Experimental Approaches"*, que se presenta en esta memoria para optar al grado de Doctor por la Universitat de València.

Y para que así conste a los efectos oportunos, y dando su conformidad para la presentación de este trabajo delante del Tribunal de Tesis Doctoral que corresponda, firma el presente certificado, en Valencia, a 15 de Julio de 2025.

Fdo. D. José Torres País

JOSE GABRIEL\|TORRES\|PAIS Firmado digitalmente por JOSE GABRIEL\|TORRES\|PAIS Fecha: 2025.07.15 14:36:00 +02'00'

Fdo. D. Adrián Suárez Zapata

SUAREZ ZAPATA ADRIAN - 48588658P Firmado digitalmente por SUAREZ ZAPATA ADRIAN - 48588658P Fecha: 2025.07.15 14:23:49 +02'00'

UNIVERSITAT DE VALÈNCIA

ESCOLA TÈCNICA SUPERIOR D'ENGINYERIA
Departamento de Ingeniería Electrónica

Av. De la Universidad s/n, 46100 Burjassot (Valencia)

Acta de Calificación de Tesis Doctoral

Tesis Doctoral: Study of Electromagnetic Shielding Effectiveness Measurement Methods: Theoretical, Simulation and Experimental Approaches.

Autora: ANDREA AMARO PÉREZ

Director: Dr. JOSÉ TORRES PAÍS

Tutor: Dr. ADRIÁN SUÁREZ ZAPATA

El Tribunal nombrado para juzgar la Tesis Doctoral citada anteriormente, compuesto por los doctores:

Presidente: _____

Vocal: _____

Secretario: _____

Acuerda otorgarle la calificación de _____

Y para que así conste a los efectos oportunos, firmamos el presente certificado.

En Valencia, el _____ de _____ de 2025

Note to the Reader

According to the University of Valencia Doctorate Regulation[1] this Ph.D. dissertation is presented as a compendium of at least three publications in international journals containing the results of the conducted work.

Furthermore, in accordance with the aforementioned regulation and with the aim of fostering the language of the University of Valencia in research and educational activities, this Ph.D. dissertation starts with an extended abstract in one of the official languages of the Valencian Community (Spanish). Page XXI includes a short abstract in English followed by the research context, motivation, objectives, theoretical fundamentals, methodology, results, and conclusions.

[1]Reglament sobre el depòsit, avaluació i defensa de la Tesis Doctoral. (Aprovat per l'Acord 252/2024, de 23 de juliol, del Consell de Govern, i modificat mitjançant Acord 364/2024, de 17 de desembre)

Resumen

1. Contexto de investigación y motivación

La creciente complejidad de los sistemas electrónicos modernos, impulsada por el desarrollo de tecnologías de comunicación avanzadas como el 5G, ha generado nuevos retos en materia de compatibilidad electromagnética (EMC). Entre ellos, destaca la necesidad de asegurar niveles adecuados de apantallamiento frente a interferencias electromagnéticas (EMI), especialmente en entornos de alta frecuencia o dispositivos con alta densidad de integración. Esta situación plantea una presión creciente sobre las metodologías de caracterización disponibles, que deben adaptarse a las nuevas exigencias de frecuencia, geometría, precisión y representatividad.

Los métodos de medida estandarizados, como los definidos en la norma ASTM D4935-18 o IEEE 299-2006, constituyen una base sólida para la caracterización de la efectividad de apantallamiento electromagnético (SE). No obstante, en muchos casos, estos procedimientos no pueden ser utilizados debido a las restricciones en el tamaño de muestra, la sensibilidad a errores, o la limitada operabilidad en el rango de frecuencia. Esto hace necesario explorar nuevas metodologías que permitan obtener la SE en contextos donde los métodos estándar resultan inaplicables.

En este sentido, la presente tesis doctoral se sitúa en la intersección entre la investigación académica en EMC y las necesidades prácticas del entorno industrial. Su desarrollo ha sido llevado a cabo en el marco del grupo de investigación Diseño de Sistemas de Comunicaciones (DSDC) de la Universitat de València, y está vinculada a la Cátedra EMC WE-UV, orientada a la transferencia de conocimiento y desarrollo de soluciones aplicadas en el ámbito de la compatibilidad electromagnética. Asimismo, parte del trabajo experimental se ha realizado en el marco del proyecto estratégico SMART5G, financiado por el Ministerio de Ciencia e Innovación y centrado en tecnologías habilitadoras para sistemas de comunicación de nueva generación, en colaboración con el centro tecnológico AIMPLAS. El enfoque metodológico se complementa con colaboraciones internacionales, como la establecida con la Universidad de Roma “La Sapienza” para el desarrollo de configuraciones de medida especializadas.

La motivación principal de esta investigación reside en la necesidad de establecer métodos de medida alternativos que permitan evaluar de manera fiable la efectividad de apantallamiento en materiales reales, bajo condiciones que reflejen su aplicación final. Este objetivo responde tanto a una necesidad científica, relacionada con la validez física de las medidas, como a una necesidad tecnológica, vinculada a la versatilidad, la rapidez y la aplicabilidad industrial de los ensayos.

De este planteamiento se deriva la hipótesis central de la tesis:

> **En contextos en los que los métodos estandarizados no pueden aplicarse debido a restricciones de frecuencia, geometría o naturaleza del material:**
>
> **¿es posible estudiar un enfoque alternativo de medida que permita una evaluación rigurosa de la efectividad de apantallamiento, coherente con los principios físicos que rigen el comportamiento electromagnético del sistema?**

Para validar esta hipótesis, se han diseñado y evaluado distintas estrategias metodológicas, incluyendo adaptaciones de configuraciones coaxiales basadas en estándares existentes, así como el desarrollo completo de un sistema de medida no estandarizado de tipo Absorber Box. Este último método ha sido complementado con simulaciones electromagnéticas mediante el método de los elementos finitos (FEM), con el fin de crear modelos equivalentes que actúen como gemelos digitales de los sistemas experimentales y permitan analizar su comportamiento bajo distintas condiciones.

Además de su contribución al conocimiento académico, esta tesis tiene una clara vocación de transferencia tecnológica. Los resultados obtenidos, tanto en términos de configuraciones experimentales como de estrategias de validación, pueden integrarse en entornos de ensayo industriales, servir de base para nuevas guías técnicas, o contribuir en procesos de normalización y estandarización. En este sentido, parte de los desarrollos han sido ya compartidos en congresos nacionales e internacionales y están siendo aplicados en entornos de caracterización, lo que refuerza la aplicabilidad práctica del trabajo.

2. Objetivos

Teniendo en cuenta el contexto de la investigación, la motivación y la hipótesis anteriormente definidos, el objetivo general de la presente tesis doctoral se define de la siguiente manera:

Estudiar, desarrollar y validar metodologías alternativas para la caracterización de la efectividad de apantallamiento electromagnético en materiales planos, especialmente en aquellos casos en los que los procedimientos estandarizados existentes no resultan aplicables o presentan limitaciones significativas. Estas nuevas estrategias experimentales deben garantizar resultados fiables, reproducibles y físicamente interpretables, incluso en configuraciones no convencionales, rangos extendidos de frecuencia o materiales complejos.

En este sentido, se proponen los siguientes objetivos específicos (O.E.) para realizar la investigación de estos estudios doctorales que permitan dar solución a las dificultades previamente planteadas:

- O.E.1: Analizar las limitaciones técnicas y prácticas de los métodos estandarizados de medida de la efectividad de apantallamiento, particularmente en contextos de alta frecuencia, geometrías complejas o materiales difíciles de mecanizar.

- O.E.2: Aplicar y evaluar métodos de medida basados en sondas coaxiales derivadas de estándares existentes, adaptando el sistema a la caracterización de materiales planares utilizados en entornos de alta frecuencia.

- O.E.3: Estudiar y aplicar métodos de medida no estandarizados que permitan evaluar muestras con geometrías complejas o dimensiones incompatibles con los métodos convencionales, con el fin de ampliar el rango de aplicabilidad experimental.

- O.E.4: Caracterizar experimentalmente distintos tipos de materiales compuestos, tanto en configuraciones derivadas del estándar como en configuraciones alternativas, y analizar su comportamiento en términos de efectividad de apantallamiento en función de su composición, estructura y frecuencia.

- O.E.5: Realizar un estudio teórico de la efectividad de apantallamiento para configuraciones ideales, que proporcione una referencia teórica con la que interpretar los resultados obtenidos y para su comparación y validación.

- O.E.6: Desarrollar un modelo de simulación basado en el método de los elementos finitos que actúe como gemelo digital del sistema experimental, permitiendo simular el comportamiento y predecir la respuesta del material.

- O.E.7: Validar el modelo de simulación mediante comparación con resultados teóricos y datos experimentales, evaluando su precisión y utilidad como herramienta de apoyo en el diseño y análisis de materiales de apantallamiento.

- O.E.8: Contribuir a la definición de un marco metodológico que respalde el uso de técnicas alternativas de medida de la efectividad de apantallamiento, garantizando resultados fiables y representativos en escenarios de medida orientados a la aplicación.

3. Metodología

La presente tesis doctoral se desarrolla en formato de compendio de publicaciones científicas, cuya estructura ha sido diseñada para abordar de forma progresiva los objetivos planteados en este trabajo. A lo largo del proceso de investigación, se han publicado y presentado tres trabajos en revistas científicas indexadas en el *Journal Citation Reports* (JCR) y un artículo presentado en un congreso internacional de relevancia, todos ellos sometidos a procesos de revisión por pares. Cada uno de estos trabajos está incluido como parte estructural del cuerpo de la tesis y contribuye a dar respuesta a los objetivos específicos definidos en el Capítulo 1.

Tras una revisión del contexto de este ámbito de investigación realizado en el Capítulo 2, la tesis se articula a través de los Capítulos 3, 4, 5 y 6, cada uno de los cuales presenta un trabajo científico individual. La metodología se construye en torno al análisis, diseño, implementación y validación de métodos de medida de la efectividad de apantallamiento electromagnético de materiales planos. Finalmente, el Capítulo 7 recoge las conclusiones generales del trabajo y analiza las principales vías de transferencia tecnológica, resaltando el potencial de los métodos desarrollados para su aplicación en entornos industriales y su integración en futuras normativas o protocolos de medida. A continuación, se describe de manera detallada el contenido de los Capítulos 3, 4, 5 y 6, incluyendo el enfoque metodológico, el contexto tecnológico y experimental, y la colaboración con instituciones académicas y centros tecnológicos relevantes.

Capítulo 3 – Artículo de contribución a congreso I: Analysis of EMI Shielding Effectiveness for plastic fiber composites in the 5G sub-6 GHz band

El primer trabajo incluido en esta tesis, presentado en el 2021 IEEE International Joint EMC/SI/PI and EMC Europe Symposium, analiza la aplicabilidad de configuraciones coaxiales derivadas del estándar ASTM D4935-18 para la medida de la efectividad de apantallamiento electromagnético en materiales compuestos utilizados en aplicaciones en la banda sub-6 GHz, que forma parte del espectro FR1 empleado en tecnologías 5G. El contexto de este estudio se enmarca en las necesidades impuestas por los desarrollos tecnológicos actuales en el ámbito de las comunicaciones inalámbricas, concretamente en entornos 5G, donde se emplean frecuencias elevadas y materiales ligeros que deben integrarse en estructuras de dimensiones reducidas.

En este escenario, los métodos tradicionales de medida, como el basado en la norma ASTM D4935-18, encuentran limitaciones tanto en el rango de frecuencias como en las exigencias geométricas de las muestras. En concreto, el método estándar requiere un diámetro de muestra superior a 13 cm de una geometría muy específica, lo que impide su aplicación a compuestos complejos con estructuras rígidas difíciles de mecanizar. Además, cuando se trabaja a frecuencias del orden de gigahercios, aparecen efectos

parásitos y modos superiores que pueden comprometer la validez de la medida. Estas limitaciones motivan la necesidad de adaptar las configuraciones experimentales existentes para mantener la compatibilidad con las nuevas demandas del sector.

Para abordar esta problemática, se propone una adaptación del método ASTM D4935-18 que permita trabajar con muestras más pequeñas y que mantenga un comportamiento monomodo en el rango sub-6 GHz. La solución se basa en una sonda coaxial derivada de esta norma, con dimensiones reducidas y características optimizadas para operar en ese rango de frecuencia. Esta configuración fue seleccionada por su versatilidad y porque mantiene una continuidad con método estandarizado, lo que permite la comparación de los resultados obtenidos con otras instituciones.

El estudio se desarrolló en colaboración con el centro tecnológico AIMPLAS, encargado de la fabricación de los materiales compuestos. Se utilizaron distintas configuraciones de láminas compuestas de matriz polimérica reforzada con fibras plásticas, que incorporan elementos conductores tales como grafito niquelado, malla de cobre y nanotubos de carbono de paredes múltiples (MWCNT). Cada una de estas variantes fue caracterizada en términos de su respuesta electromagnética frente a una onda incidente utilizando un analizador de redes vectoriales (VNA) y una sonda coaxial adaptada.

Además de la caracterización de los materiales, se estudió la sensibilidad del método a variables como la alineación de la muestra, el tipo de contacto eléctrico, la repetibilidad de las medidas y la estabilidad del sistema en frecuencia. Este análisis permitió identificar los factores que influyen de forma crítica en la fiabilidad del método, así como sus limitaciones prácticas en cuanto al tipo de materiales que pueden caracterizarse con precisión.

Los resultados mostraron diferencias significativas en la efectividad de apantallamiento según el tipo de fibra utilizada como refuerzo y el material conductor incorporado. En particular, se observó que la presencia de nanotubos de carbono dispersos en el interior de la matriz mejora la atenuación, mientras que el uso de estructuras tipo malla generó variaciones dependientes de la frecuencia que podrían limitar la estabilidad del apantallamiento en ciertas bandas. Asimismo, el estudio permitió verificar que el método adaptado mantiene su validez en el rango sub-6 GHz, siempre que se asegure la continuidad eléctrica entre la muestra y la sonda coaxial.

Estos resultados permiten concluir que es viable extender el uso de configuraciones derivadas del estándar ASTM D4935-18 a contextos no contemplados inicialmente, siempre que se realicen adaptaciones geométricas adecuadas y se controle cuidadosamente el procedimiento experimental. Este trabajo representa, por tanto, un primer paso hacia el desarrollo de metodologías flexibles y fundamentadas físicamente para la medida de SE, en línea con los objetivos generales de esta tesis doctoral.

Capítulo 4 – Artículo científico I: EMI Shielding Effectiveness Study for Innovative Carbon Nanotube Materials in the 5G Frequency Region

El segundo trabajo incluido en esta tesis se centra en la extensión y validación de un método de medida basado en línea coaxial, adaptado específicamente para alcanzar la frecuencia de 18 GHz. Este trabajo representa una evolución metodológica respecto al capítulo anterior, con el objetivo de ampliar el rango de aplicabilidad de los sistemas coaxiales derivados del estándar ASTM D4935-18 hacia la región de microondas, cada vez más relevante en aplicaciones vinculadas a tecnologías inalámbricas avanzadas, como el 5G o el radar automotriz.

A frecuencias superiores a 1.5 GHz, los métodos de medida estándar dejan de ser adecuados debido a la aparición de modos de propagación superiores en la guía de onda, así como a restricciones derivadas del tamaño mínimo de la muestra, que en configuraciones convencionales supera los 13 cm. Estos factores comprometen la validez física de la medida y limitan la caracterización de materiales funcionales con geometrías reales. Ante esta situación, se propone y evalúa una sonda coaxial miniaturizada, diseñada para operar en condiciones monomodo hasta 18 GHz, cuya geometría permite reducir significativamente las dimensiones requeridas de la muestra sin comprometer la calidad de la medida.

La sonda fue diseñada y desarrollada por la Universidad de Roma “La Sapienza”, con quien se llevó a cabo una colaboración. Esta sonda mantiene los principios fundamentales del método estandarizado, pero permite aplicar este método de medida en un rango de frecuencia mucho más amplio, concretamente hasta alcanzar los 18 GHz.

A nivel experimental, se caracterizaron diferentes composiciones de materiales innovadores con nanotubos de carbono (CNTs) como material funcional. Se utilizaron tanto películas delgadas como compuestos multicapa, y se analizó la influencia de la concentración de CNT, la morfología superficial y la estructura de capas en la respuesta electromagnética de los materiales. Las medidas se realizaron mediante un sistema basado en analizador vectorial de redes en configuración de dos puertos, con calibración completa para minimizar errores sistemáticos.

Además del comportamiento de los materiales, se estudió la fiabilidad del sistema de medida: se analizó la sensibilidad a la alineación de la muestra, el nivel de repetibilidad entre medidas consecutivas y el efecto de errores de contacto. También se exploró la relación entre las propiedades electromagnéticas de los materiales (como la conductividad superficial) y su respuesta en términos de SE en función de la frecuencia.

Los resultados demostraron que la sonda miniaturizada permite realizar medidas estables y reproducibles en todo el rango considerado, con niveles de sensibilidad suficientes para distinguir pequeñas variaciones en la estructura del material. Se observó, además, que

el apantallamiento electromagnético mejora de forma significativa con el incremento de la concentración de nanotubos de carbono, debido al aumento de la conductividad efectiva y a la mejora en los mecanismos de reflexión y absorción.

Este trabajo valida el uso de métodos coaxiales miniaturizados como herramienta eficaz para la caracterización electromagnética de materiales funcionales en el rango de microondas. A nivel metodológico, supone una demostración práctica de que es posible extender el alcance de las metodologías derivadas del estándar ASTM D4935-18 más allá de los límites frecuenciales originalmente contemplados, mediante adaptaciones estructurales que preservan la física del sistema. Este enfoque encaja plenamente con el objetivo central de esta tesis: establecer métodos de medida alternativos aplicables en contextos reales, más allá de los métodos convencionales.

Capítulo 5 – Artículo científico II: Shielding Effectiveness Measurement Method for Planar Nanomaterial Samples Based on CNT Materials up to 18 GHz

El tercer trabajo incluido en esta tesis doctoral introduce un nuevo enfoque metodológico para la caracterización de la efectividad de apantallamiento electromagnético mediante el desarrollo de un método de medida no estandarizado, basado en una configuración de tipo Absorber Box. A diferencia de los capítulos anteriores, en los que se trabajó con adaptaciones de métodos coaxiales normativos, este estudio se centra en una metodología alternativa que permite superar limitaciones estructurales y geométricas impuestas por configuraciones convencionales.

La necesidad de este enfoque surge al enfrentarse a la caracterización de materiales compuestos que, por su rigidez o geometría final, no pueden ser mecanizados ni adaptados a las configuraciones coaxiales tradicionales. Este es el caso de ciertos laminados reforzados con fibras, ampliamente utilizados en sectores como el transporte o la electrónica estructural, donde las dimensiones, curvaturas o capas funcionales del material impiden su integración en sondas estandarizadas sin alterar su integridad o funcionalidad. Como alternativa, se propone un método basado en una configuración tipo Absorber Box, en la que la muestra se coloca sobre una abertura y el campo se transmite a través de ella desde una antena emisora situada en el exterior de una cavidad absorbente hacia una antena receptora alineada en el interior. Esta disposición elimina la necesidad de adaptar mecánicamente el material al sistema de medida, y permite una caracterización efectiva de muestras planas sin requerir preparación específica. A diferencia de otros métodos, no se necesita mecanizar ni cortar la muestra a una forma concreta, siendo suficiente con una lámina plana del material. Además, el sistema no requiere contacto directo entre la muestra y los elementos de medida, lo que facilita el ensayo de materiales frágiles, rígidos o de geometrías no normalizadas.

La metodología fue desarrollada en el marco del proyecto de líneas estratégicas SMART5G, cuyo objetivo general es la investigación de materiales alternativos para la construcción de carcasas de baterías para vehículos eléctricos ligeros compatibles con sistemas de comunicación de nueva generación. En este contexto, el método de Absorber Box se planteó como una herramienta flexible para evaluar materiales funcionales en condiciones representativas de aplicación real, sin depender de cámaras anecoicas completas. El desarrollo experimental se llevó a cabo en colaboración con el centro tecnológico AIMPLAS, que proporcionó los materiales compuestos.

Desde el punto de vista estructural, el sistema consiste en una caja metálica recubierta internamente con material absorbente de banda ancha, en cuyo interior se sitúa una antena receptora. La muestra se coloca sobre una abertura en la parte superior de la caja, y una antena emisora se sitúa justo por encima, permitiendo así medir el nivel de transmisión vertical a través del material. La configuración es altamente versátil, compatible con muestras planas de diferentes tamaños y aplicable a frecuencias de hasta 18 GHz, dependiendo del diseño de las antenas y del material radio-absorbente (RAM) que recubre el interior de la cavidad.

Los ensayos se realizaron sobre una serie de composites reforzados con CNTs, fabricados mediante técnicas de laminación y consolidación en matrices poliméricas. Se estudiaron distintas concentraciones de nanotubos, geometrías de refuerzo y orientaciones de fibra, analizando la respuesta electromagnética global de cada configuración. Las medidas experimentales pusieron de manifiesto la sensibilidad del sistema a cambios en la composición y estructura interna de las muestras, validando su utilidad para evaluar materiales con estructuras complejas y no homogéneas.

Desde el punto de vista metodológico, se realizó un análisis de la repetibilidad y estabilidad del sistema, incluyendo la sensibilidad a la colocación de la muestra, la calidad del material radio-absorbente del interior de la cavidad y el alineamiento de las antenas. Se verificó que, con un diseño adecuado y un procedimiento de medida bien definido, el método proporciona resultados coherentes y reproducibles a lo largo del rango de frecuencias evaluado.

Este trabajo representa una contribución clave a los objetivos de esta tesis, al demostrar que es posible implementar métodos de medida no estandarizados que mantengan una base física sólida y que sean capaces de caracterizar materiales avanzados en condiciones reales. El enfoque de caja absorbente propuesto proporciona una alternativa práctica a los métodos normativos, especialmente en contextos donde la mecanización de muestras o el uso de cámaras anecoicas completas no es viable. Este estudio refuerza la tesis central de este trabajo: la validez de métodos experimentales alternativos para la evaluación de SE, siempre que estén correctamente diseñados, controlados y justificados a nivel físico.

Capítulo 6 – Artículo científico III: Determination of Electromagnetic Shielding Effectiveness Using an Enhanced Absorber Box Method: Theoretical, Simulation, and Experimental Approaches

El cuarto y último trabajo incluido en esta tesis doctoral se centra en desarrollo y validación de una versión mejorada del método Absorber Box, mediante un enfoque combinado que integra teoría, simulación y verificación experimental. Este estudio constituye un paso metodológico esencial para confirmar que este tipo de configuraciones no estandarizadas pueden proporcionar resultados fiables y trazables, siempre que estén correctamente diseñadas y calibradas.

Mientras que en el capítulo anterior se presentaba el desarrollo experimental del sistema Absorber Box y su aplicación práctica en la caracterización de materiales compuestos reforzados, este trabajo complementa dicho desarrollo con una validación más profunda basada en modelos de simulación y fundamentos teóricos. El objetivo principal es establecer una correspondencia clara entre los resultados experimentales obtenidos y las predicciones teóricas basadas en modelos físicos, así como estudiar en detalle el comportamiento del campo electromagnético en el interior del sistema.

Para ello, se desarrolló un modelo tridimensional de la configuración experimental utilizando el software ANSYS HFSS, basado en el método de los elementos finitos. El modelo reproduce con alta fidelidad la geometría de la caja absorbente, las propiedades del material absorbente, las antenas de transmisión y recepción, así como la colocación de la muestra bajo prueba. Esta aproximación permite generar un gemelo digital del sistema, con el que se pueden explorar múltiples escenarios, ajustar parámetros críticos del diseño y obtener información detallada del comportamiento del campo eléctrico dentro de la cavidad.

Como parte del proceso de validación, se diseñaron modelos ideales de materiales con propiedades electromagnéticas conocidas (permeabilidad, permitividad y conductividad), para los cuales se calcularon teóricamente los niveles de atenuación por reflexión y absorción. A continuación, se simuló el comportamiento en términos de SE de estos materiales y los resultados obtenidos se compararon directamente con los cálculos analíticos. Este enfoque permitió evaluar el grado de acuerdo entre teoría y simulación, y detectar posibles desviaciones asociadas a efectos geométricos o numéricos.

Además de los resultados globales de transmisión (S_{21}), el modelo permitió observar la distribución del campo eléctrico en el interior del sistema, revelando fenómenos como la difracción en los bordes de la muestra, la concentración de energía en regiones específicas y el efecto del tamaño de la muestra sobre la atenuación medida. Este análisis resultó especialmente útil para explicar ciertas discrepancias observadas en medidas

reales, así como para optimizar la configuración del sistema desde el punto de vista del diseño físico.

En la fase experimental, se utilizaron materiales comerciales avanzados suministrados por Würth Elektronik, cuyas propiedades electromagnéticas fueron caracterizadas previamente por el fabricante. Estas muestras se utilizaron para evaluar el comportamiento del sistema Absorber Box en condiciones reales de medida. Los resultados experimentales obtenidos mostraron un buen nivel de consistencia en el rango de frecuencias evaluado (0.7–18 GHz), especialmente en las bandas media y alta. Las desviaciones observadas en las frecuencias más bajas se atribuyeron principalmente a fenómenos de difracción y a las limitaciones físicas impuestas por el volumen de la cavidad.

Este trabajo representa una culminación del enfoque metodológico propuesto en esta tesis. No solo confirma que los métodos no estandarizados como el basado en la Absorber Box pueden proporcionar resultados válidos y representativos, sino que además demuestra que el uso de herramientas de simulación numérica de alta fidelidad puede actuar como soporte técnico fundamental para su diseño, calibración y análisis. A través de esta validación, se consolida el valor del método Absorber Box como una herramienta fiable para la caracterización de materiales en entornos de alta frecuencia, reforzando así la hipótesis central de esta tesis doctoral: que los métodos alternativos, teóricamente y experimentalmente bien fundamentados, son viables para la caracterización electromagnética en aplicaciones modernas que exceden los límites de los procedimientos normativos convencionales.

4. Conclusiones

Esta tesis doctoral se ha centrado en el estudio, desarrollo y validación de metodologías alternativas para la caracterización de la efectividad de apantallamiento electromagnético en materiales planos, en respuesta a las limitaciones de los métodos estandarizados ante nuevas demandas tecnológicas, especialmente en contextos de altas frecuencias y geometrías no convencionales.

Partiendo de la hipótesis de que métodos no estandarizados pueden proporcionar resultados válidos y fiables si están justificados, experimentalmente demostrados y acompañados de una validación teórica/simulada, se han definido y cumplido una serie de objetivos que estructuran el conjunto del trabajo.

En primer lugar, se ha llevado a cabo un análisis crítico de los métodos estandarizados existentes, identificando sus restricciones principales en cuanto al rango de frecuencias operativo, el formato de las muestras y las condiciones de medida. Este análisis, junto con la revisión teórica y normativa recogida en el Capítulo 2, ha permitido establecer el

marco técnico en el que se justifican los métodos alternativos propuestos, cumpliendo así el objetivo específico O.E.1.

A continuación, se han implementado dos enfoques metodológicos diferenciados. Por un lado, se han desarrollado adaptaciones de métodos derivados del estándar ASTM D4935-18, orientadas a mantener la validez física del procedimiento original en rangos de frecuencia y condiciones no previstas inicialmente (O.E.2). En el Capítulo 3 se aplicó una sonda coaxial adaptada para operar en la banda sub-6 GHz con muestras de pequeño tamaño, mientras que en el Capítulo 4 se utilizó una sonda miniaturizada que permite extender el rango hasta 18 GHz. En ambos casos, los sistemas se calibraron y aplicaron a materiales compuestos reales, verificando su fiabilidad, sensibilidad y estabilidad.

Por otro lado, se ha propuesto y evaluado un método no estandarizado (O.E.3), basado en la configuración Absorber Box, cuyo desarrollo y validación se recogen en los Capítulos 5 y 6. Este método ha demostrado ser especialmente útil para caracterizar materiales rígidos o con geometrías difíciles de mecanizar, al no requerir contacto directo ni preparación específica de la muestra. El sistema permite medidas reproducibles en un rango amplio de frecuencias y con buena discriminación entre distintos niveles de apantallamiento. Su aplicación se ha llevado a cabo sobre muestras reales en colaboración con el centro AIMPLAS y en el contexto del proyecto estratégico SMART5G, lo que refuerza su validez en entornos reales.

En cuanto al objetivo O.E.4, se ha caracterizado experimentalmente un conjunto de materiales funcionales mediante ambos enfoques metodológicos, observando coherencia en los resultados y permitiendo analizar la respuesta electromagnética de distintas configuraciones de nanocompuestos y refuerzos.

Para proporcionar una base sólida al comportamiento observado, se ha realizado un estudio teórico de los mecanismos electromagnéticos involucrados en los métodos de medida utilizados, con especial atención a los procesos de reflexión, absorción y propagación en estructuras reales, cumpliendo así el objetivo O.E.5. Este estudio ha permitido interpretar de forma más rigurosa los resultados experimentales y orientar el diseño del modelo de simulación que se describe a continuación.

Con el objetivo de dotar de mayor trazabilidad al método Absorber Box y profundizar en su comprensión física, se ha desarrollado un modelo de simulación basado en el método de los elementos finitos, cumpliendo el objetivo O.E.6. El modelo reproduce fielmente la geometría del sistema de medida, las propiedades del absorbente, las condiciones de excitación y las características del material bajo prueba. Mediante este modelo se han simulado parámetros de transmisión (S_{21}), distribuciones del campo eléctrico y fenómenos como la difracción en bordes de muestra.

Posteriormente, se ha validado el modelo mediante su comparación con cálculos teóricos y datos experimentales (O.E.7), observándose un alto grado de coincidencia, especialmente en bandas de frecuencia medias y altas. Las desviaciones detectadas en frecuencias bajas han permitido identificar y analizar las limitaciones inherentes del sistema de medida, como el tamaño de la cavidad y los efectos geométricos en la zona de transición muestra-aire.

Finalmente, el conjunto del trabajo ha permitido establecer un marco metodológico flexible y fundamentado para la caracterización de la efectividad de apantallamiento en materiales planos, cumpliendo el objetivo O.E.8. Dicho marco combina la robustez de los métodos estandarizados con la versatilidad de métodos de medida alternativos, y se apoya en la simulación como herramienta de validación y optimización. Esta propuesta metodológica no solo amplía el rango de aplicación de las técnicas de medida de SE, sino que también facilita su transferencia al entorno industrial y su aplicación en un entorno real.

Abstract

The rapid expansion of telecommunications technologies, particularly the global deployment of 5G, has heightened concerns about electromagnetic interference (EMI) and its impact on electronic devices. Accurate characterization of shielding effectiveness (SE) at high frequencies is crucial. However, traditional measurement methods, such as ASTM D4935-18 and IEEE 299-2006, exhibit limitations that hinder the evaluation of shielding materials in the frequency range used by 5G and other emerging applications.

In particular, ASTM D4935-18 is limited to 1.5 GHz, while IEEE 299-2006 requires anechoic chambers and large samples, making it unsuitable for advanced materials with reduced dimensions. To address these limitations, alternative methods have been explored, including specialized coaxial probes, which allow for the evaluation of small samples containing carbon nanotube (CNT) fillers. However, when working with full composite materials reinforced with fibers, manufacturing constraints prevented the fabrication of samples compatible with this method. This led to the development of an alternative methodology based on the use of an Absorber Box for SE measurement at high frequencies.

This research aims to develop, validate, and optimize a measurement method based on an Absorber Box, overcoming the limitations of traditional methodologies. The proposed approach enhances accuracy and extends the frequency range, reducing diffraction effects and other errors associated with conventional techniques. The methodology includes an analysis of existing measurement techniques, an experimental evaluation of the coaxial probe method, and the design and optimization of the Absorber Box. Finite element method (FEM) simulations and laboratory experiments validate the precision and reproducibility of the new measurement system.

The findings of this research will make a significant contribution to the field of electromagnetic compatibility (EMC) by providing innovative tools for evaluating shielding effectiveness in high-frequency applications, particularly in the 5G spectrum.

Keywords: Electromagnetic Interference (EMI), Shielding Effectiveness (SE), high-frequency measurement, 5G technology, ASTM D4935-18, IEEE 299-2006, coaxial probe, Absorber Box, Finite Element Method (FEM), Electromagnetic Compatibility (EMC).

Acknowledgements

It is difficult to put words to the journey behind this thesis. It has not only been an academic project, but a stage full of people, learning and moments that have left their mark.

First of all, I would like to begin by thanking José Torres, my thesis director, for his guidance, his trust and for being, in the best of senses, the 'culprit' for this to have become a reality. Also, to Adrián Suárez, my tutor, thank you for always being available, for your patience and for your support.

To my colleagues at the Catedra EMC Würth Elektronik, Pedro, Roberto, Víctor and Marc, thanks for everything, for sharing good times and the occasional despair. I would like to express my sincere gratitude to Würth Elektronik, especially to its CTO, Alexander Gerfer, as well as to Steffen Muetsch, Jorge Victoria, and Antonio Alcarria, for their continued support of the Chair and this project since its inception. I also extend my thanks to all the colleagues at the Würth Elektronik office in Valencia, whose commitment and collaboration have been essential throughout the entire process.

To all the DSDC team, thank you also for those coffees and for making the day to day more bearable, for those little moments.

To my parents Rosmary and Paco, for always being there. For giving me the space to grow and the encouragement to continue, even when they didn't quite understand what this was all about. To my sister Paola, for being my reference, without you, I would not be me.

To Adrián, my partner, thank you for your patience, your company and your unconditional way of being.

To Maite and Eloy, for showing up with kind words and calm just when I needed them the most.

To my friends, for using only your LinkedIn profile to support my publications, for being my biggest fans. For making me laugh.

And finally, thanks to all the people who, in one way or another, have been part of this journey. This thesis is also a little bit yours.

The preparation of this doctoral thesis has been funded by the Grants for the recruitment of predoctoral research staff (ACIF 2021), from the Department of Innovation, Universities, Science and Digital Society. D.G. of Science and Research.

Agradecimientos

Es difícil poner palabras al recorrido que hay detrás de esta tesis. No ha sido solo un proyecto académico, sino una etapa llena de personas, aprendizajes y momentos que han dejado huella.

En primer lugar, quiero comenzar agradeciendo a José Torres, mi director de tesis, por su guía, su confianza y por ser, en el mejor de los sentidos, el 'culpable' de que esto se haya hecho realidad. También a Adrián Suárez, mi tutor, gracias por estar siempre disponible, por tu paciencia y por tu apoyo.

A mis compañeros de la Cátedra EMC WE-UV**,** Pedro, Roberto, Víctor y Marc, gracias por todo, por compartir buenos momentos y alguna que otra desesperación. Quiero expresar mi más sincero agradecimiento a Würth Elektronik, en especial a su CTO, Alexander Gerfer, así como a Steffen Muetsch, Jorge Victoria y Antonio Alcarria, por el continuo apoyo brindado a la Cátedra y a este proyecto desde sus inicios. También a todos los compañeros de la oficina de Würth Elektronik en Valencia, cuyo compromiso y colaboración han sido fundamentales a lo largo de todo el proceso.

A todo el equipo del DSDC, gracias también por esos cafés y por hacer el día a día más llevadero, por esos ratitos.

A mis padres Rosmary y Paco, por estar siempre ahí. Por darme el espacio para crecer y el ánimo para continuar, incluso cuando no entendían muy bien en qué consistía todo esto. A mi hermana Paola, por ser mi referente, sin ser tú, no sería yo.

A Adrián, mi pareja, gracias por tu paciencia, tu compañía y tu forma incondicional de estar.

A Maite y Eloy, por darme paz con unas palabras amables cuando más me hacía falta.

A mis amigos, por usar solo su perfil de LinkedIn para apoyar mis publicaciones, por ser mis mayores fans. Por hacerme reír.

Y, por último, gracias a todas las personas que, de una manera u otra, han formado parte de este camino. Esta tesis también es un poco vuestra.

La elaboración de esta tesis doctoral ha sido financiada por las Subvenciones para la contratación de personal investigador predoctoral (ACIF 2021), de la Conselleria de Innovación, Universidades, Ciencia y Sociedad Digital. D.G. de Ciencia e Investigación.

Table of contents

Declaration III
Acta de Calificación de Tesis Doctoral V
Note to the Reader VII
Resumen IX
1. Contexto de investigación y motivación IX
2. Objetivos X
3. Metodología XII
4. Conclusiones XVIII
Abstract XXI
Acknowledgements XXIII
Agradecimientos XXV
Table of contents XXVII
List of figures XXIX
Chapter 1. Introduction 31
1.1 Research context and motivation 31
1.2 Research objectives 32
1.3 Thesis structure 33
1.4 Thesis framework 34
Chapter 2. Background 39
2.1 Electromagnetic Compatibility and Shielding Fundamentals 39
2.2 Shielding Effectiveness 41
2.3 Shielding Materials: From Metals to Nanocomposites 46
2.4 Shielding Effectiveness Measurement Methods 49
2.4.1 Standardized Measurement Methods 50
2.4.2 Methods Derived from Standards 53
2.4.3 Non-Standardized Measurement Methods 56
2.5 Absorber Box Simulation Model Definition 61

2.6 Summary 63

Chapter 3. ASTM-derived Method for Sub-6 GHz Shielding Characterization 65
3.1 Conference paper I 65
3.2 Summary 73

Chapter 4. Miniaturized Coaxial Probe for Shielding Measurements up to 18 GHz..... 75
4.1 Scientific article I 75
4.2 Summary 88

Chapter 5. Non-Standardized Shielding Characterization of Complex Planar Materials 89
5.1 Scientific article II....89
5.2 Summary 108

Chapter 6. Improved Absorber Box Method with Simulation-Based Validation..... 109
6.1 Scientific article III....109
6.2 Summary 125

Chapter 7. Conclusions and technological transfer..... 127
7.1 Conclusions....127
7.2 Technological transfer....129
7.2.1 Measurement Setups....129
7.2.2 Contribution to IEEE 2715-2023 standard document 130
7.2.3 Technical dissemination through User Guides....131

REFERENCES 133

Appendix A. SCIENTIFIC CONTRIBUTIONS 137
A.1 Peer-reviewed scientific articles in journals....137
A.2 Peer-reviewed scientific articles in conferences 137

Appendix B. LIST OF ABBREVIATIONS..... 139

List of figures

Figure 1.1 DSDC (Diseño de Sistemas Digitales y de Comunicaciones). 35
Figure 1.2 Catedra EMC - Würth Elektronik....35
Figure 1.3 SMART5G project. 35
Figure 1.4 Consortium partners. 36
Figure 1.5 Generalitat Valenciana and European Union. 36
Figure 1.6 SWAT (Smart Wireless Applications and Technologies) group....37
Figure 1.7 INTA (Instituto Nacional de Técnicas Aeroespaciales). 37
Figure 2.1 EMC coupling model: source → coupling Path → victim. 40
Figure 2.2 EMI Shielding of Source to Prevent Coupling to External Equipment. 40
Figure 2.3 EMI Shielding of Receptor to Prevent Coupling to Internal Equipment....41
Figure 2.4 Electromagnetic wave interaction with shielding material. 42
Figure 2.5 Definition of Near-Field and Far-Field Regions in Antenna Theory. 45
Figure 2.6 Typical Components Used in the Formulation of Composite Structures. 46
Figure 2.7 Carbon nanotubes. (a) Single-walled CNTs. (b) Multi-walled CNTs. 47
Figure 2.8 Reinforcement fibers. (a) Biaxial carbon fiber. (b) Biaxial glass fiber. 48
Figure 2.9 Classification of SE Measurement Methods. 50
Figure 2.10 ASTM D4935-18 Measurement method and sample geometry. 51
Figure 2.11 IEEE 299-2006 Measurement Method. 52
Figure 2.12 Sections of two different ASTM-derived coaxial sample holders. 54
Figure 2.13 Nested reverberation chamber measurement method. 55
Figure 2.14 7 mm Coaxial airline measurement method and sample geometry. 57
Figure 2.15 Waveguide measurement method and sample geometry. 58
Figure 2.16 Dual TEM Cell Measurement method. 59
Figure 2.17 Schematic of the Absorber Box measurement setup. 60
Figure 2.18 3D simulation model of the Absorber Box setup....62

Figure 7.1 Technological transfer strategy 129
Figure 7.2 Absorber Box schematic measurement setup 130
Figure 7.3 Extract from the IEEE P2715 standard (DOI: 10.1109/IEEESTD.2023.10115252) 131
Figure 7.4 User Guide of the WE-EMIP 132

Chapter 1. Introduction

This introductory chapter outlines the context and unresolved challenges of the research topic addressed in this doctoral thesis. Therefore, the initial hypothesis and the expected achievements in relation to the thesis objectives are presented.

1.1 Research context and motivation

As the electromagnetic scenario of modern technology continues to expand, driven by the deployment of high-frequency communication systems, advanced driver-assistance platforms, and densely integrated electronics, the ability to characterize electromagnetic interference (EMI) and evaluate the shielding performance of devices and materials has become increasingly critical. Ensuring electromagnetic compatibility (EMC) in this context is not only a regulatory requirement but also a design necessity in sectors such as telecommunications, transport, and aerospace.

To quantify shielding effectiveness (SE), various measurement techniques have been developed, many of which are codified in international standards, such as ASTM D4935-18 or IEEE 299-2006 [1], [2]. These methods offer well-defined procedures for measuring the attenuation of electromagnetic fields by a material under specific geometrical and boundary conditions. However, as technologies evolve and applications push into new frequency bands and structural formats, the limitations of standardized measurement methods become apparent. Sample geometry constraints, fixture compatibility, and limited bandwidth are among the practical challenges that arise when attempting to characterize modern materials or integrated shielding solutions [3].

This challenge is not merely technical but methodological. Whereas new shielding materials continue to be developed, the measurement frameworks used to evaluate them have not always kept pace. In many cases, researchers adapt existing methods or develop new ones entirely, often without a clear reference to a standard or a validation procedure. This evolving scenario creates not only a technical challenge but also a methodological demand: in many practical situations, it is often impossible to meet the conditions specified by standard procedures. As new material formats and system constraints emerge, researchers are increasingly required to adapt existing methods or develop entirely new ones, tailored to the specific characteristics of the application at hand.

From this context emerges a central question that frames the **hypothesis** of this thesis:

> *In contexts where standardized methods cannot be applied due to frequency, geometry, or material constraints:*
>
> *Is it possible to study an alternative measurement approach that enables a rigorous evaluation consistent with the physical principles of electromagnetic shielding?*

In line with this hypothesis, the thesis emphasizes not the materials themselves but the methods used to characterize their shielding performance. It investigates how measurement techniques can be adapted or developed to meet the practical and technical demands of modern applications, particularly where standard procedures are insufficient. By combining experimental development with simulation-based validation, this work aims to contribute to a more comprehensive and flexible methodological framework for evaluating electromagnetic shielding effectiveness.

1.2 Research objectives

Taking into account the context of the research, motivation, and the previously defined hypothesis, the general objective of this doctoral thesis is as follows:

The research focuses on the study, implementation, and validation of alternative methods for measuring the shielding effectiveness of planar materials, with the aim of ensuring their suitability for modern electromagnetic compatibility applications that extend beyond the scope of standardized procedures.

In this regard, the following specific objectives (S.O.) are proposed to guide the research and address the methodological and technical challenges identified:

- S.O.1: Analyze the limitations of conventional standardized methods for shielding effectiveness measurements in the context of new material formats, frequency ranges, and test conditions.

- S.O.2: Apply alternative measurement methods derived from standardized coaxial transmission line procedures, adapted to extend their usability to a broader range of frequencies and sample types.

- S.O.3: Explore and apply non-standardized measurement approaches suitable for characterizing planar materials in scenarios where conventional methods cannot be applied due to their limitations.

- S.0.4: Characterize the shielding performance of various alternative materials using both the adapted and the non-standardized methods, in order to assess their measurement range and reliability.

- S.0.5: Perform a theoretical study of shielding effectiveness for ideal configurations, in order to provide a reference framework for interpreting, comparing, and validating the obtained results.

- S.0.6: Develop a Finite Element Method simulation model of the developed non-standardized method, serving as a digital twin of the experimental setup, to enable analysis of field distribution and transmission behavior.

- S.0.7: Validate the simulation model by comparing its results with theoretical predictions and experimental data, thus evaluating its accuracy and suitability for supporting measurement interpretation.

- S.0.8: Contribute to the definition of a methodological framework that supports the use of alternative shielding effectiveness measurement techniques under realistic, application-driven conditions.

1.3 Thesis structure

This doctoral thesis is organized into seven chapters covering the evolution of the implemented research work. The main body comprises a collection of three peer-reviewed scientific articles and one peer-reviewed scientific conference article that address the research objectives listed in Section 1.2.

Chapter 1 introduces the general context of the work, the motivation behind the study, and the hypothesis that drives the research. It also defines the main objectives and outlines the organization of the thesis.

Chapter 2 provides the theoretical foundation and literature review necessary to understand the scope and relevance of the research. It introduces the fundamentals of electromagnetic compatibility, shielding mechanisms, and the concept of shielding effectiveness. The chapter also reviews standardized, derived, and non-standardized measurement methods, and presents the simulation framework developed for absorber-based test systems.

Chapter 3 presents the first experimental study, which explores the limitations of the ASTM D4935-18 standard for shielding effectiveness measurements in the sub-6 GHz range. While the method is well-established, as frequency increases, the dimensions of the coaxial fixture must be reduced, which in turn requires smaller and more precisely

machined samples. This chapter, developed in the context of *Conference Paper I*, proposes an adapted coaxial configuration that facilitates more practical and versatile measurements.

Chapter 4 expands the frequency range of the coaxial methodology up to 18 GHz. In this chapter, a miniaturized coaxial probe is used to characterize novel alternative materials, with results published as *Scientific Article I*. This chapter explores the trade-offs in fixture design and calibration when pushing coaxial systems beyond their conventional limits.

Chapter 5 introduces an alternative measurement strategy based on an Absorber Box configuration. This method is particularly suited for evaluating fiber-reinforced composites that cannot be tested using coaxial fixtures. The chapter, corresponding to *Scientific Article II*, highlights the flexibility and performance of this non-standardized setup over a wide frequency range.

Chapter 6 complements the experimental work with the development of a Finite Element Method simulation model of the Absorber Box system. The model serves as a digital twin of the real setup, allowing validation against theoretical predictions and experimental results. This study, detailed in *Scientific Article III*, reinforces the physical consistency and reliability of the proposed method.

Finally, Chapter 7 summarizes the main conclusions drawn from the research, highlighting the contributions to the field and the potential for technological transfer. It also discusses the application of the developed methods in measurement system design, education, and product development.

This structure reflects the progression of the research from theoretical grounding and experimental implementation to simulation-based validation, offering a comprehensive and integrated perspective on the measurement of electromagnetic shielding effectiveness.

1.4 Thesis framework

The present doctoral thesis summarizes the author's research efforts from 2021 to 2025 as a Ph.D. candidate at the University of Valencia.

Specifically, this doctoral thesis has been developed within the framework of academic research carried out at the Universitat de València, in the context of the DSDC (Diseño de Sistemas Digitales y de Comunicaciones) research group. The group has broad expertise in high-frequency systems, electromagnetic compatibility, and instrumentation for characterization and measurement in advanced electronic environments, providing the technical and scientific foundation for the research activities undertaken in this work.

Figure 1.1 DSDC (Diseño de Sistemas Digitales y de Comunicaciones).

In parallel, the research has been supported by the **Catedra EMC-Würth Elektronik**, a long-term academic collaboration between the Universitat de València and **Würth Elektronik** that promotes education, research, and innovation in the field of EMC. The Catedra complements the activity of the university by fostering initiatives that connect academic knowledge with industrial practice. Within this framework, the research has benefited from technical discussions, access to resources, and opportunities for collaboration oriented towards real-world EMC applications.

Figure 1.2 Catedra EMC - Würth Elektronik.

Part of the research presented in this thesis was carried out within the **SMART5G project**, which was founded in 2021 under the Spanish Strategic Lines program for public-private collaboration. The project, titled “Research and Development of Smart Stations and New Materials for Optimizing Urban Mobility through Energy Management and 5G Applications,” focuses on enabling technologies for connected and sustainable mobility. Its overarching goal is the investigation of alternative materials for the construction of battery enclosures for light electric vehicles, ensuring compatibility with next-generation 5G communication systems.

Figure 1.3 SMART5G project.

The consortium includes the Universitat de València, AIMPLAS - Plastics Technology Center, ELIX Polymers, and ITERA Engineering, combining expertise in materials, electronics, and intelligent systems. Within this context, the Universitat de València, through the DSDC research group, contributes to the electromagnetic characterization and simulation of shielding materials designed for high-frequency 5G environments. This role is essential within the project, which provides a highly relevant technological framework for addressing critical EMC challenges, particularly those involving the design, evaluation, and validation of shielding strategies suited to the stringent demands of next-generation communication systems.

Figure 1.4 Consortium partners.

As part of the activities conducted under SMART5G, the research has also included a collaboration with **AIMPLAS – Plastics Technology Center**, which supported the design and fabrication of composite materials evaluated during the experimental campaigns. This collaboration enabled the integration of material development with electromagnetic performance testing, aligning with the project's multidisciplinary approach and application-driven goals.

The doctoral research has been supported by a **predoctoral research grant** (ACIF - Grants for the hiring of predoctoral research personnel) awarded by the **Generalitat Valenciana**, which provided the necessary financial and institutional backing for the execution of experimental and simulation tasks, as well as for dissemination activities and participation in scientific collaborations.

Figure 1.5 Generalitat Valenciana and European Union.

This framework has enabled the development of a doctoral study with a strong experimental foundation, supported by theoretical modeling, collaborative partnerships, and alignment with current research priorities in the field of electromagnetic compatibility and high-frequency characterization.

The first stay was carried out at the **University of Granada**, within the **SWAT** (Smart Wireless Applications and Technologies) research group. During this period, a joint experimental campaign was conducted in collaboration with Würth Elektronik, focused on the shielding characterization of different commercial and experimental materials. This initiative led to the proposal and coordination of an interlaboratory comparison project, aimed at evaluating the reproducibility and variability of shielding effectiveness measurements across different setups and institutional facilities. The comparison involved the SWAT group at the University of Granada, the Universitat de València, and the National Institute for Aerospace Technology (INTA).

Figure 1.6 *SWAT (Smart Wireless Applications and Technologies) group.*

As part of this collaborative effort, a second stay was carried out at **INTA**, where the same material samples were measured using their fully characterized measurement systems. This allowed for a direct and systematic comparison of results obtained under different methodologies and experimental conditions, contributing to the broader validation of the alternative measurement approaches explored throughout this thesis.

Figure 1.7 *INTA (Instituto Nacional de Técnicas Aeroespaciales).*

Chapter 2. Background

This chapter introduces the theoretical background and literature review to provide the basis on which this Ph.D. study has been developed. Firstly, an overview of Electromagnetic Compatibility and Shielding Fundamentals, including its challenges. Then, a review of the current electromagnetic shielding strategies and a discussion of the main standardized and alternative SE measurement methods are presented.

2.1 Electromagnetic Compatibility and Shielding Fundamentals

Electromagnetic compatibility is defined as the ability of an electrical or electronic system to operate in its electromagnetic environment without introducing unwanted electromagnetic disturbances to other systems. This definition implies two essential requirements: on the one hand, the system must tolerate the electromagnetic disturbances present in its environment; on the other, it must not emit levels of electromagnetic energy that interfere with the operation of nearby equipment [4].

The growing complexity of electronic devices, combined with increased signal speeds, system integration, and high-frequency technologies, has significantly increased the likelihood of electromagnetic interactions. In many applications, these interactions can compromise signal integrity, degrade performance, or even cause system failure. As a result, ensuring electromagnetic compatibility has become a critical design objective in sectors such as communications, transportation, healthcare, and industrial automation [5].

A widely used conceptual framework to understand electromagnetic interactions is the source → coupling path → victim model (Figure 2.1). In this model, a system or component acts as a source of unwanted electromagnetic energy. This energy is transferred through a coupling path, which can be conductive, capacitive, inductive, or radiated, until it reaches a susceptible system, known as the victim. The coupling may occur through shared power or ground lines, electric or magnetic fields between conductors, or as propagating waves through free space. The model emphasizes that interference can be controlled by reducing emissions at the source, interrupting or attenuating the coupling path, or increasing the immunity of the victim system [4], [5].

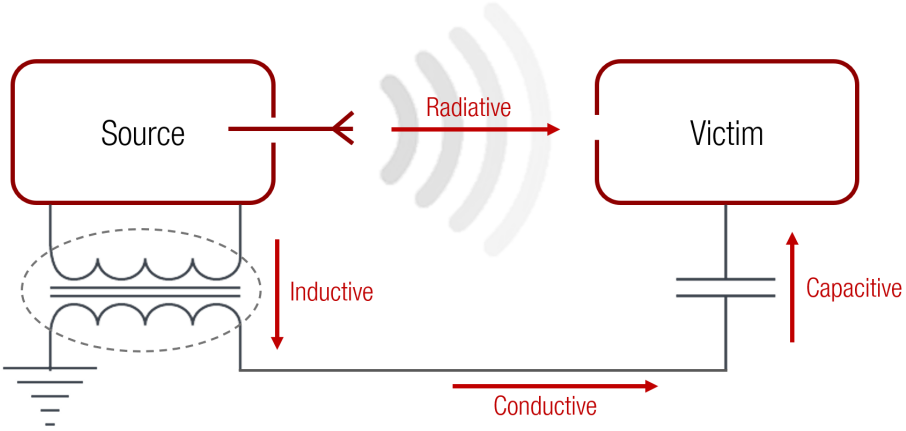

Figure 2.1 EMC coupling model: source → coupling Path → victim.

Electromagnetic interference refers to any electromagnetic phenomenon that results in the degradation of the performance of an electrical or electronic system. This degradation may manifest as signal distortion, data corruption, communication errors, or functional failure. Interference can originate from external sources, such as nearby transmitters or industrial equipment, or from internal components within the same system [6].

Modern electronic systems are particularly vulnerable to interference. In environments where reliability and safety are critical, such as in vehicles, aircraft, medical equipment, and industrial control systems, managing interference is not only a functional requirement but also a matter of regulatory compliance.

One of the most effective strategies to mitigate interference is electromagnetic shielding. It involves placing a barrier between the source and the susceptible system to reduce or block the transmission of electromagnetic energy (Figure 2.2 and Figure 2.3). This barrier is typically made of a material with suitable electrical conductivity or magnetic permeability, depending on the frequency and type of interference to be attenuated [4].

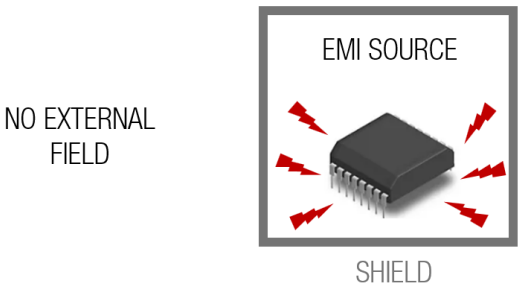

Figure 2.2 EMI Shielding of Source to Prevent Coupling to External Equipment.

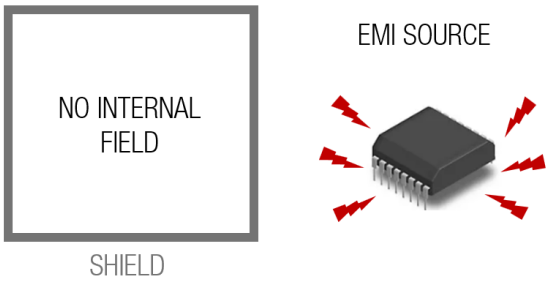

Figure 2.3 EMI Shielding of Receptor to Prevent Coupling to Internal Equipment.

When an electromagnetic wave encounters a shielding material, part of its energy is reflected at the surface, part is absorbed as it propagates through the material, and the remainder may be transmitted beyond it. The relative contribution of these mechanisms depends on several factors, including the electrical and magnetic properties of the material, its thickness, the frequency of the wave, and the angle of incidence.

These interactions are governed by the physical properties of the material and the characteristics of the incident field. Understanding how the shield modifies the field distribution is essential for evaluating its performance. The first mechanism that contributes to shielding is reflection. Absorption is the second major mechanism and becomes increasingly relevant when the wave penetrates the shield. The third mechanism, internal reflection, arises when part of the wave that has entered the material reflects back and forth within the shield due to its finite thickness. Together, these three contributions define the shielding effectiveness of a material [7].

2.2 Shielding Effectiveness

Electromagnetic shielding is used to reduce or prevent the transmission of electromagnetic energy from one region of space to another. The concept of shielding effectiveness provides a framework for evaluating this attenuation. It serves as the primary parameter used to describe the performance of a shielding material or structure, and it is widely applied in both material development and system-level electromagnetic compatibility assessment. Shielding effectiveness enables the comparison of different materials, geometries, and configurations on a common basis, and is used to establish technical specifications and regulatory thresholds across various industries [8].

Several factors influence the shielding behavior of a material, including its electrical conductivity, magnetic permeability, thickness, and the frequency of the incident field. These parameters affect how much of the electromagnetic energy is reflected, absorbed, or transmitted. A comprehensive analysis of shielding performance requires the ability to express this behavior in measurable terms. The following section presents the

mathematical formulation of shielding effectiveness and the primary physical mechanisms underlying electromagnetic attenuation.

For a plane electromagnetic wave incident normally on an infinite, homogeneous shielding material, the shielding effectiveness SE can be expressed as:

$$SE(dB) = 20\log_{10}\frac{E_{incident}}{E_{transmitted}} = 10\log_{10}\frac{P_{incident}}{P_{transmitted}} \quad (1)$$

where $E_{indicent}$ and $E_{transmitted}$ are the magnitudes of the electric field before and after the shield, respectively, and P represents power.

In practical scenarios, the total shielding effectiveness is the cumulative result of three main contributions:

$$SE = R + A + B \quad (2)$$

where R is the reflection loss (dB), A is the absorption loss (dB), and B is the multiple internal reflection correction (dB).

Each of these terms is associated with a distinct physical phenomenon that contributes to the attenuation of the incident wave (Figure 2.4).

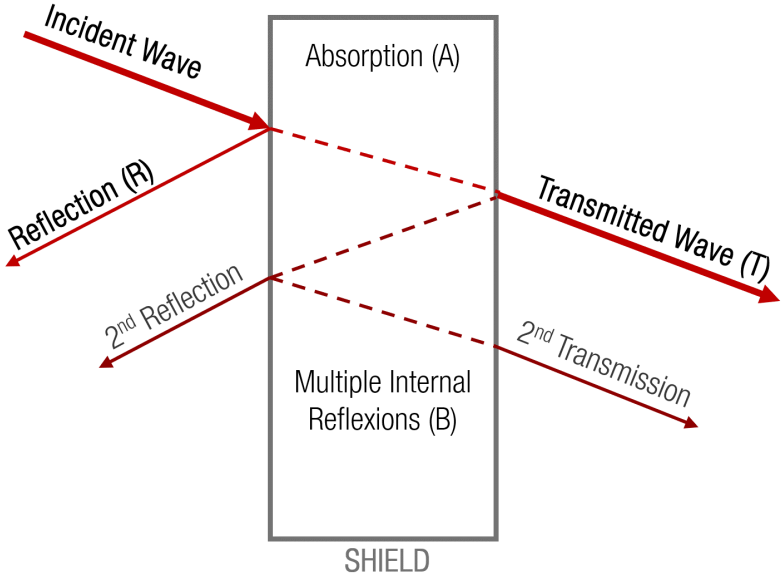

Figure 2.4 Electromagnetic wave interaction with shielding material.

Reflection Loss (R)

Reflection is the primary mechanism through which electromagnetic shielding is achieved at low frequencies, especially in materials with high conductivity. When a plane wave impinges on a conductive surface, a portion of the wave is reflected due to the impedance mismatch between the incident medium (usually air, with impedance $Z_0 \approx 377\Omega$ and the shielding material, which typically has much lower impedance.

The reflection loss for an electric field can be approximated by:

$$R = 20 \log_{10} \left(\frac{Z_0}{4Z_s} \right) \tag{3}$$

where Z_s is the surface impedance of the shield. For good conductors, the surface impedance is given by:

$$Z_s = \sqrt{\frac{j\omega\mu}{\sigma}} \tag{4}$$

where ω is the angular frequency, μ is the magnetic permeability of the material, and σ is its electrical conductivity. Reflection is particularly effective for electric fields and plane waves at high frequencies. However, for magnetic fields at low frequencies, especially below a few kilohertz, reflection is significantly less efficient unless the shield has high magnetic permeability (e.g., mu-metal).

Absorption Loss (A)

Absorption occurs as the wave propagates through the shielding material and is attenuated due to resistive losses. This attenuation is described by the skin effect, which causes electromagnetic waves to decay exponentially with depth inside conductive materials. The skin depth δ represents the distance at which the field strength is reduced to 1/e of its value at the surface and is given by:

$$\delta = \sqrt{\frac{2}{\omega\mu\sigma}} \tag{5}$$

The absorption loss is directly proportional to the thickness t of the shield relative to the skin depth:

$$A = 8.686 \cdot \frac{t}{\delta} \tag{6}$$

This shows that materials with high conductivity and permeability, as well as sufficient thickness, are more effective in absorbing electromagnetic energy. Unlike reflection, absorption becomes the dominant mechanism at higher frequencies and in thicker shields.

Multiple Internal Reflections (B)

When the shield is relatively thin compared to the skin depth or when it comprises porous or layered materials (as in many composites), multiple reflections can occur within the material. These internal reflections can partially re-radiate energy toward the source or forward into the shielded region, thereby reducing the overall effectiveness of the shield.

The multiple reflection term B is often negative, meaning it reduces the total SE. However, for sufficiently thick or highly absorptive materials where A > 10dB, the effect of multiple reflections becomes negligible and can often be ignored. The correction term is given by:

$$B = 20log_{10}(1 - e^{-2t/\delta}) \quad (7)$$

This term becomes significant for thin, low-conductivity materials, such as some polymeric composites or fabrics, and must be considered carefully when analyzing shielding at high frequencies or in lightweight applications.

In real-world applications, shields are rarely ideal. They contain seams, joints, apertures, and discontinuities, all of which can significantly degrade SE by introducing leakage paths. Moreover, the electromagnetic field may not always be normally incident, and materials are often heterogeneous and anisotropic. These complexities necessitate the use of empirical measurements and simulation tools, in addition to theoretical models. Furthermore, the type of electromagnetic field influences the shielding behavior. For instance, low-frequency magnetic fields are particularly difficult to shield and often require materials with very high magnetic permeability. Conversely, high-frequency plane waves are more readily attenuated by conductive materials due to reflection and the skin effect.

The electromagnetic field surrounding a source is divided into two primary regions: the near-field and the far-field. The near-field region exists close to the source, typically within a distance of $r < 2D^{\,2}/\lambda$. In this region, the electric and magnetic components of the field can exist independently and may not exhibit a fixed relationship. Depending on the nature of the source, either the electric or magnetic field may dominate. Conversely, the far-field region lies beyond the near-field, at distances greater than $2D^{\,2}/\lambda$ from the source. Here, the electromagnetic fields combine to form propagating waves with electric ($\vec{E}$) and magnetic ($\vec{H}$) components that are orthogonal and have a fixed relationship. In this region, the field impedance approaches that of free space ($\approx 377\Omega$), and the behavior of the fields becomes more predictable [9].

$$Z_0 = \frac{|\vec{E}|}{|\vec{H}|} = \sqrt{\frac{\mu_0}{\varepsilon_0}} \approx 377\Omega \tag{8}$$

The distinction between near-field and far-field regions is crucial when designing shielding solutions (Figure 2.5). In the near-field, the characteristics of the source dictate the shielding approach. For sources with strong electric fields, materials with high electrical conductivity, such as copper or aluminum, are effective because they reflect the electric fields. Conversely, for sources with strong magnetic fields, materials with high magnetic permeability, like mu-metal, are preferred, as they can absorb and redirect magnetic flux lines. In the far-field, where plane-wave conditions prevail, the shielding effectiveness is influenced by the material's ability to reflect and absorb electromagnetic waves. Conductive materials are generally effective due to their reflective properties and the skin effect, which confines currents to the surface layer, enhancing absorption losses.

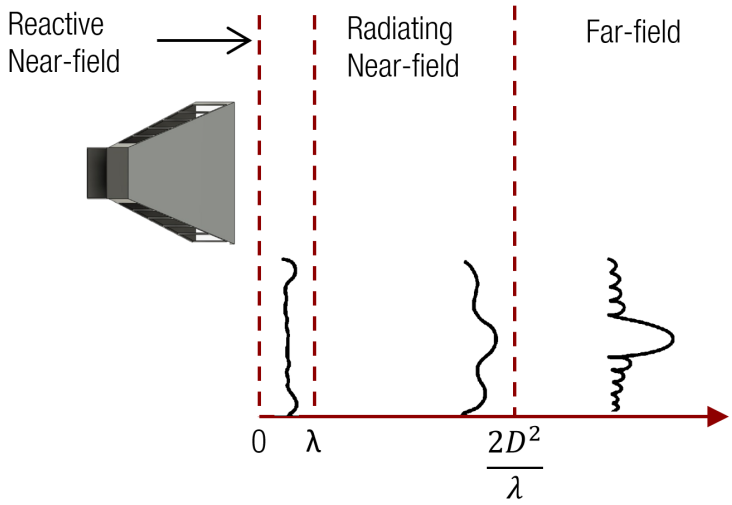

Figure 2.5 Definition of Near-Field and Far-Field Regions in Antenna Theory.

Understanding these regions helps in selecting suitable materials and designing shield geometries to effectively reduce electromagnetic interference.

2.3 Shielding Materials: From Metals to Nanocomposites

The performance of an electromagnetic shield depends not only on its geometry or mounting configuration, but also on the electromagnetic properties of the material used. In any shielding scenario, the material determines the attenuation mechanisms involved, particularly reflection and absorption, and ultimately governs the overall effectiveness of the solution. For this reason, even when the primary focus is on evaluating or improving measurement methods, it is essential to understand the types of materials typically involved in electromagnetic shielding applications and their implications for testing.

Traditionally, electromagnetic shielding has been implemented using metals such as copper, aluminum, steel, and their alloys. These materials are characterized by their high electrical conductivity and are especially effective in reflecting incident electromagnetic waves at the interface due to the resulting impedance mismatch. Metallic shields also exhibit low surface resistance, making them suitable for broadband protection, particularly in enclosures and connectors where continuous electrical paths can be maintained [10]. However, as technological applications have evolved, particularly in fields such as aerospace, automotive systems, wearable electronics, and high-frequency communications, the limitations of traditional metallic solutions have become increasingly apparent. Their relatively high density, mechanical rigidity, and susceptibility to corrosion can conflict with the design and functional requirements of modern systems. Moreover, their lack of flexibility and incompatibility with complex or layered structures restricts their use in some emerging technologies.

These challenges have led to the development of alternative shielding materials, often based on composite structures that aim to strike a balance between electromagnetic performance and other design constraints. Among these, polymer-based nanocomposites have become one of the most explored solutions. These materials typically consist of a dielectric matrix, such as polyethylene, polypropylene, epoxy, or other engineering polymers, combined with conductive or magnetic fillers (Figure 2.6). Depending on the formulation, such composites can attenuate electromagnetic waves through a combination of reflection, absorption, and in some cases, multiple scattering effects [11], [12], [13].

Figure 2.6 Typical Components Used in the Formulation of Composite Structures.

Conductive fillers, such as carbon nanotubes (CNTs), graphene, carbon black, metal nanoparticles, or silver-coated fibers, are used to enhance the composite's electrical conductivity and improve shielding through reflection [14], [15]. On the other hand, magnetic fillers, such as ferrites, iron oxides, or microwave absorbing ceramics, contribute to attenuation through magnetic losses and are particularly relevant at lower frequencies [16], [17], [18]. Among these materials, CNTs are of particular interest due to their high aspect ratio, intrinsic conductivity, and ability to form conductive networks at relatively low concentrations. CNTs can be classified as single-walled (SWCNTs) or multi-walled (MWCNTs), each with distinct electrical, mechanical, and morphological properties that influence their effectiveness as shielding fillers (Figure 2.7). Their versatility and performance make them especially attractive for developing lightweight, high-performance shielding composites, and they are featured in several of the experimental studies presented in this thesis.

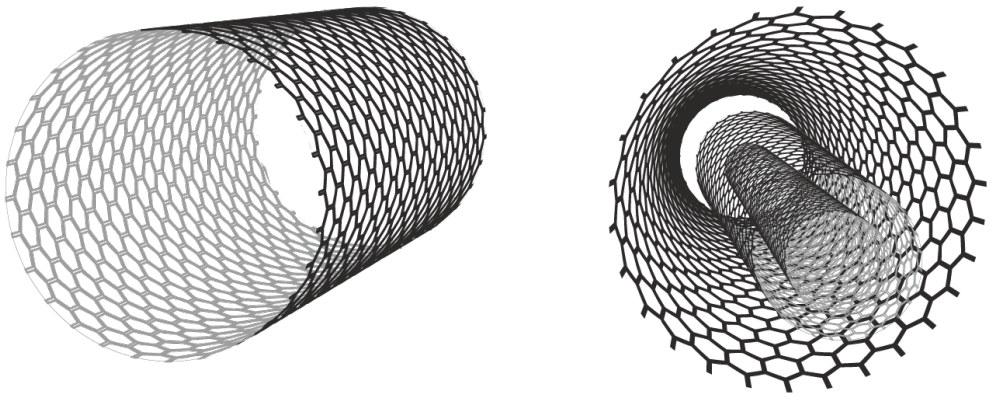

Figure 2.7 Carbon nanotubes. (a) Single-walled CNTs. (b) Multi-walled CNTs.

The flexibility of nanocomposite design enables a tunable response, where the shielding effectiveness can be optimized for a specific application by adjusting the filler concentration, dispersion, orientation, or by incorporating hybrid filler systems. Moreover, these materials are often lightweight, flexible, and compatible with industrial manufacturing processes, which makes them attractive for integration into structural or functional components.

In addition to nanocomposites, fiber-reinforced composites are increasingly used when mechanical integrity and dimensional stability must be preserved (Figure 2.8). Carbon fiber composites (CFC), in particular, offer moderate electrical conductivity along the fiber axis and can provide directional shielding performance. Glass fiber composites (GFC) are also used, especially when combined with conductive coatings or interleaved shielding layers. These materials are particularly relevant in transportation and aerospace

industries, where structural and EMI requirements must be met simultaneously [19], [20], [21].

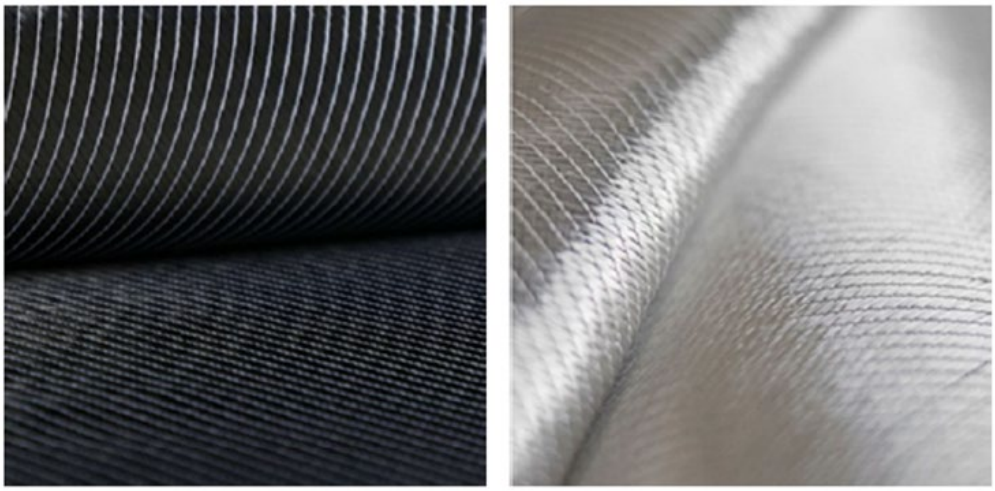

Figure 2.8 Reinforcement fibers. (a) Biaxial carbon fiber. (b) Biaxial glass fiber.

Table 2.1 Comparison of Shielding Materials

Material Type	Conductivity	Dominant Mechanism	Weight	Mechanical Properties
Metals	High	Reflection	High	Rigid, strong
Polymer-based Nanocomposites	Moderate to low (depends on filler)	Reflection - Absorption	Low	Flexible, tunable
Fiber-Reinforced Composites	Low to moderate (depends on fiber type)	Reflection (directional) + Absorption (if hybridized)	Moderate	High strength, structural integrity

Despite their advantages, characterizing the shielding properties of these advanced materials presents specific challenges. Their electromagnetic response is often anisotropic, heterogeneous, and sensitive to frequency and sample preparation. These characteristics make them ideal test cases for evaluating the robustness and adaptability of measurement methods, especially when standard fixtures are not easily applicable.

Although this thesis does not focus on the design or optimization of shielding materials as a primary objective, several of the experimental campaigns involve nanocomposites and reinforced laminates. Their use reflects the current trends in EMI research and serves to validate the flexibility and reliability of the measurement setups under realistic material conditions. The choice of such materials reinforces the need for alternative or adapted measurement techniques, particularly when traditional standards cannot accommodate non-metallic samples or when broader frequency coverage is required.

2.4 Shielding Effectiveness Measurement Methods

The characterization of shielding effectiveness is essential for assessing how materials interact with electromagnetic fields and how efficiently they attenuate unwanted energy. As electromagnetic interference becomes more critical in modern systems, reliable measurement techniques are necessary to guide material selection, validate performance, and ensure compliance with technical specifications.

Standardized methods have long provided a solid foundation for this purpose. Protocols developed by organizations such as ASTM and IEEE define procedures that are widely accepted in industry and regulatory environments. These methods offer clear criteria for sample preparation, fixture geometry, calibration, and data interpretation, ensuring repeatability and comparability across laboratories and applications.

However, the technological landscape has undergone considerable evolution in recent years. The emergence of high-frequency communication systems, such as 5G and automotive radar, has extended the operational spectrum into the millimeter-wave domain [22]. At the same time, the development of new shielding materials has introduced practical limitations that conventional standardized methods cannot always address. Many of these materials cannot be shaped into the sample geometries required by standard fixtures, and their performance must often be evaluated at frequencies well beyond the range originally specified in those protocols.

In this context, there is a growing need to adapt the measurement strategies. On the one hand, researchers have proposed modifications to existing standardized methods, such as extending their frequency range or adapting their geometry. On the other hand, entirely non-standardized measurement methods have been developed to provide flexible, application-specific solutions. These methods preserve the underlying principles of electromagnetic field measurement but introduce alternative setups that allow characterization of advanced materials under conditions closer to real-world use [3].

The following sections outline the primary techniques employed to measure shielding effectiveness. First, the standardized methods are described, focusing on their configuration, applicability, and limitations. Then, non-standardized approaches are

introduced, with an overview of their operating principles and relevance to current technological challenges.

Figure 2.9 illustrates the classification of shielding effectiveness measurement methods discussed in this chapter, including both standardized procedures, variants derived from them, and non-standardized alternatives developed to address the needs of advanced technologies.

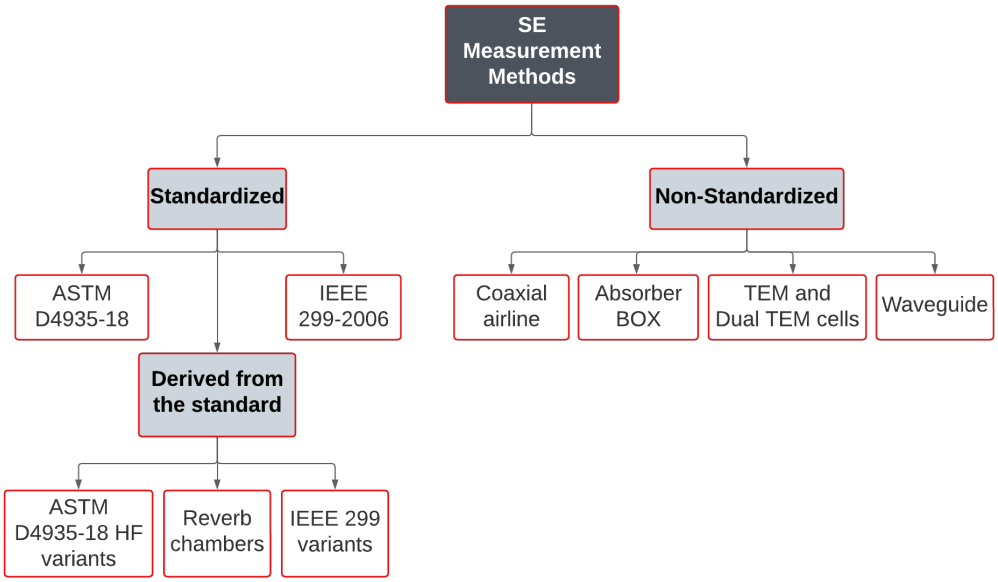

Figure 2.9 Classification of SE Measurement Methods.

2.4.1 Standardized Measurement Methods

Standardized methods provide a well-defined framework for measuring the shielding effectiveness of materials and enclosures. These methods are developed by international standardization bodies such as ASTM and IEEE, and they define not only the measurement principle but also the test fixture geometry, calibration procedures, and data interpretation protocols. Their widespread acceptance makes them essential for certification and benchmarking of commercial materials and systems. Among the most established are the ASTM D4935-18 coaxial transmission line method and the IEEE 299-2006 free-space method, each suited to specific frequency ranges, sample types, and application scenarios [1].

The ASTM D4935-18 standard defines a test procedure based on a coaxial transmission line fixture operating in transverse electromagnetic (TEM) mode. The shielding material is cut into a circular sample and mounted between two precisely machined coaxial flanges. A vector network analyzer (VNA) is used to measure the transmitted signal with and

without the sample in place, allowing the shielding effectiveness to be determined over a frequency range from 30 MHz to 1.5 GHz. The SE of the material under test can be written as:

$$SE(dB) = S_{21,ref} - S_{21,load} \quad (9)$$

where $S_{21,ref}$ is the transmission scattering parameters between the port 1 and port 2 measured when the coaxial fixture is loaded with the reference, and the $S_{21,load}$ is the transmission scattering parameters between the port 1 and port 2 measured when the coaxial sample holder (CSH) is loaded with the load specimen.

This method is widely used for planar, homogeneous materials due to its compact configuration, simplicity of implementation, and good measurement repeatability. However, it is constrained by the physical geometry of the fixture, which requires the sample to be a rigid, flat disk of standardized dimensions, and by its upper-frequency limit, which may be insufficient for modern high-frequency applications. The general measurement setup of the ASTM D4935-18 standard is shown in Figure 2.10.

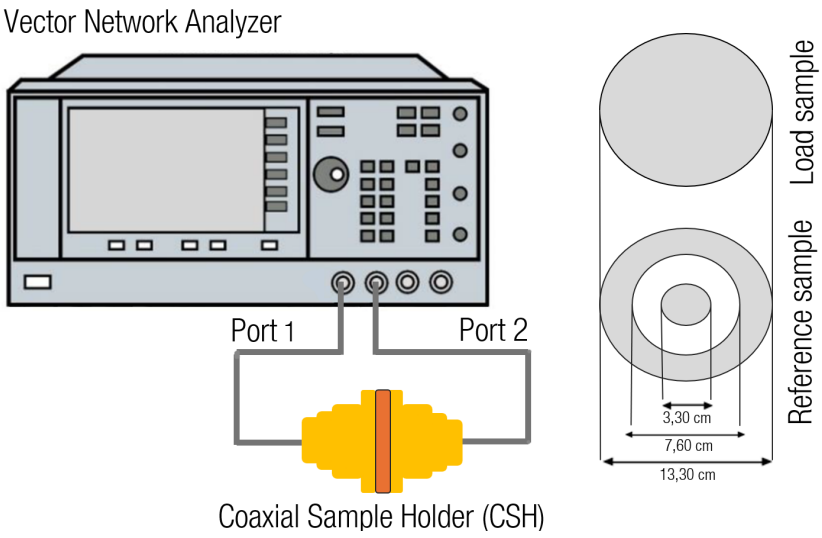

Figure 2.10 ASTM D4935-18 Measurement method and sample geometry.

In contrast, IEEE 299-2006 describes a free-space measurement method based on the use of a transmitting and a receiving antenna positioned on opposite sides of the test sample. The sample is typically mounted vertically and placed in an anechoic or shielded chamber to ensure controlled propagation conditions. The shielding effectiveness is calculated by comparing the received field strength or power level in the absence of the sample with that in its presence. This approach supports a wide frequency range,

extending from 9 kHz to 18 GHz depending on the antenna system used, with provisions to extend this range down to 50 Hz and up to 100 GHz, accommodating various testing requirements.

This standard is particularly suited for evaluating large panels, enclosures, or complex shielding structures with apertures and seams. It provides valuable insights into system-level shielding performance, but requires a large test environment and is more susceptible to measurement uncertainties arising from diffraction at sample edges, alignment issues, and the effectiveness of the absorber [2]. The general measurement setup of the IEEE 299-2006 standard is shown in Figure 2.11.

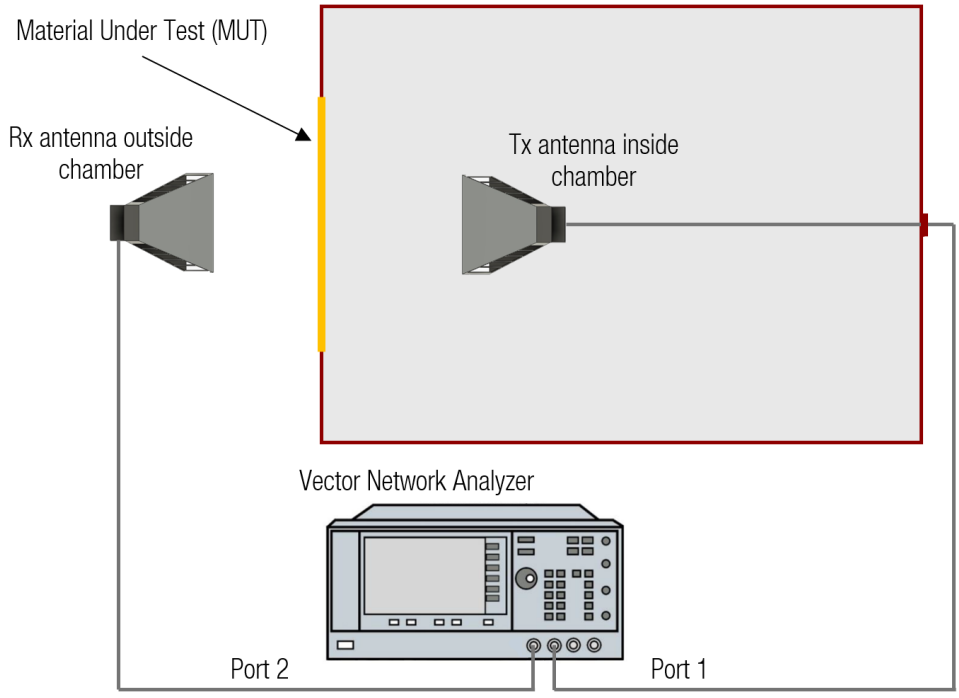

Figure 2.11 IEEE 299-2006 Measurement Method.

Both ASTM D4935-18 and IEEE 299-2006 are foundational in the field of electromagnetic shielding characterization. They provide robust methodologies for assessing material performance under well-defined conditions, serving as reference points for comparing experimental results. However, the evolving demands of electronic technologies, particularly in terms of frequency range, material flexibility, and sample geometry, have highlighted the need to go beyond the scope of these standardized protocols. This need has led to the development of measurement methods derived from these standards,

which aim to extend their applicability while preserving their core physical and methodological principles.

Table 2.2 Standardized Measurement Methods

Method	Frequency	Measurement Setup	Advantages	Limitations
ASTM D4935-18	30 MHz - 1.5 GHz	Coaxial transmission line (TEM)	Compact, repeatable, easy to implement	Requires rigid, flat samples, limited to 1.5 GHz
IEEE 299-2006	9 KHz - 18 GHz (extendable to 50 Hz - 100 GHz)	Free-space measurement with antennas	Suitable for large and complex structures	Susceptible to diffraction issues, requires large samples

2.4.2 Methods Derived from Standards

As electromagnetic technologies advance and new material systems emerge, the limitations of standardized measurement methods have become increasingly apparent. Procedures such as ASTM D4935 and IEEE 299-2006 provide a robust foundation for the evaluation of shielding effectiveness, but their implementation is often constrained by factors such as frequency bandwidth, fixture geometry, or sample preparation. To address these challenges, several derived methods have been developed that retain the measurement philosophy of the standards while introducing structural or procedural modifications. These adaptations allow for greater experimental flexibility and have been successfully implemented in both academic research and industrial validation campaigns, including the experimental studies presented in this thesis.

One of the most widely adopted derived approaches involves the miniaturization of coaxial transmission line fixtures originally based on the ASTM D4935-18 standard. In the standard configuration, the fixture is designed to operate reliably up to approximately 1.5 GHz under single-mode conditions. By reducing the transverse dimensions of the inner and outer conductors, the cutoff frequency of higher-order modes is increased, extending the usable bandwidth well into the gigahertz range, up to 8 GHz, 12 GHz, or even 18 GHz, depending on the fixture design and calibration (Figure 2.12).

These adaptations enable the characterization of small, planar samples, typically circular with diameters ranging from 7 to 18 mm. In Conference Paper I (Chapter 3), a reduced-size coaxial sample holder is used to measure the shielding effectiveness of fiber-reinforced polymer composites containing conductive fillers. Later, in Scientific Article I (Chapter 4), a further miniaturized fixture developed by La Sapienza University is employed

to characterize CNT-based thermoplastics up to 18 GHz, covering part of the 5G spectrum [23], [24], [25].

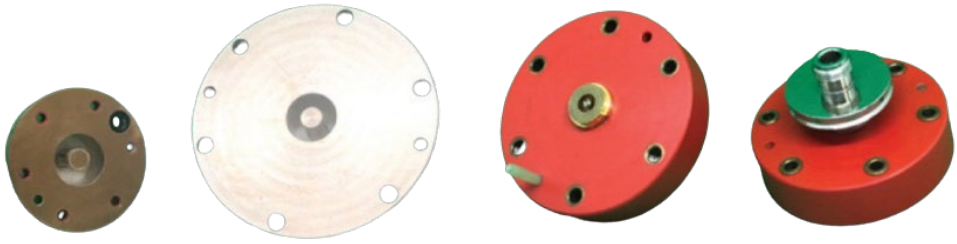

Figure 2.12 Sections of two different ASTM-derived coaxial sample holders.

While these adaptations preserve the measurement principle based on insertion loss in a coaxial line, they require precise mechanical tolerances, meticulous calibration, and careful flange alignment to ensure signal integrity. The method is highly reproducible when properly implemented, as demonstrated in interlaboratory studies involving institutions such as the Wroclaw University of Science and Technology, and provides excellent resolution for thin or conductive materials in broadband applications.

Another important family of derived techniques stems from modifications to the free-space setup described in IEEE 299-2006. In these configurations, the material under test is mounted over an aperture between two shielded or absorber-lined enclosures, and horn antennas are used to measure the transmitted field. These compact adaptations are particularly useful when testing large-area, flexible, or irregular samples that are incompatible with standardized holders [26]. Frequency coverage typically ranges from 1 GHz to 18 GHz, depending on antenna geometry and chamber design. One of the key advantages is the ability to carry out non-contact measurements, which reduces the influence of imperfect sample mounting or mechanical deformation. However, care must be taken to control unwanted reflections, diffraction, and leakage at the aperture edges. These methods retain the conceptual basis of the free-space approach while allowing measurements in more accessible and compact laboratory environments.

Reverberation-based adaptations represent another derived approach, particularly suitable for the broadband evaluation of complex or anisotropic materials. In the dual-chamber configuration showed in Figure 2.13, the sample is placed over an aperture between two coupled metallic enclosures, and the shielding effectiveness is determined by comparing the average field levels or transmitted power across the barrier [27], [28]. These systems support operation from around 500 MHz up to several gigahertz and enable measurements that incorporate angular and polarization diversity. The method approximates realistic electromagnetic environments and offers statistical stability across

a wide frequency band. Nonetheless, it requires large physical enclosures and robust electromagnetic isolation to prevent coupling artefacts. This approach has been adopted by institutions such as the Università Politecnica delle Marche and Cisco Systems for evaluating textile and multilayer composites, particularly in the context of system-level applications [29].

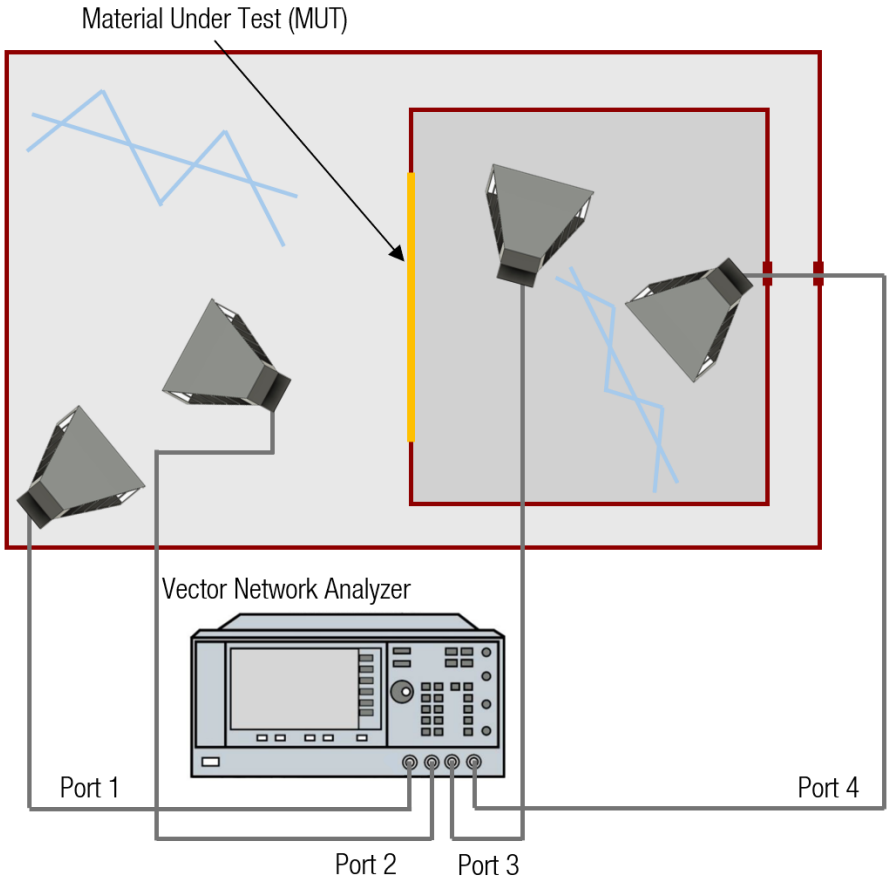

Figure 2.13 Nested reverberation chamber measurement method.

These derived methods show how the core structure of standardized techniques can be preserved while adapting the physical configuration to suit new demands. By adjusting geometry, extending frequency coverage, or modifying the test environment, it becomes possible to evaluate advanced shielding materials that cannot be measured using conventional fixtures. Their implementation by research institutions and their use in this thesis demonstrate their importance in the current landscape of electromagnetic characterization.

Table 2.3 Methods Derived from Standards

Method	Frequency	Measurement Setup	Advantages	Limitations
Extended coaxial method	Up to 18 GHz	Reduced coaxial fixture size	Allows measurement of smaller samples and broadband characterization	Sensitive to misalignment, reduced coupling at low frequencies
Compact free-space method	1 GHz - 18 GHz	Uses aperture and horn antennas	Does not require full anechoic chamber, flexible for large or flat samples	Requires precise alignment and absorber control
Reverberation-based environments	500 MHz - several GHz	Uses nested or vibrating metallic enclosures	Averages multiple angles and polarizations, suitable for large-area materials	Bulky setups, difficult to shield and isolate

2.4.3 Non-Standardized Measurement Methods

In many research and development contexts, shielding effectiveness must be evaluated in situations where neither standardized nor derived methods are applicable. These cases often involve unconventional sample geometries, material formats incompatible with fixture-based testing, or frequency ranges that exceed those covered by traditional techniques. To address these scenarios, several non-standardized measurement methods have been developed. Although not formally regulated, these techniques are widely used due to their versatility and their ability to adapt to specific experimental requirements. Their reliability depends on careful calibration, mechanical stability, and validation, but they provide valuable alternatives in cases where established methods fall short.

One widely used approach is the miniaturized coaxial airline method, which consists of a short, air-filled transmission line formed between two coaxial connectors. The sample is inserted as a discontinuity in the line, and the transmission and reflection parameters are measured using a vector network analyzer (Figure 2.14). This setup enables broadband characterization, ranging from several hundred megahertz to tens of gigahertz, depending on the connector design and the electromagnetic properties of the sample. The method is simple to implement and well suited for small, flat, and highly conductive materials. However, it is sensitive to edge effects, fixture leakage, and poor contact, particularly when working with non-metallic samples or materials that have low shielding levels.

Because the sample is not enclosed in a shielded structure, the method may also be susceptible to external coupling and environmental interference, which can limit its reproducibility [16].

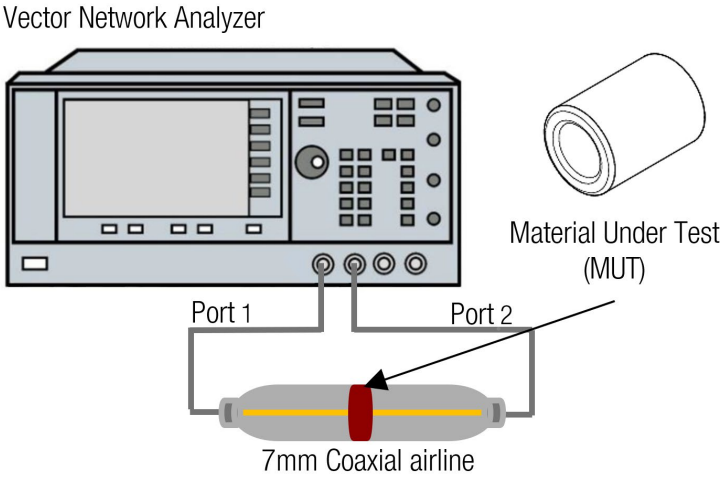

Figure 2.14 7 mm Coaxial airline measurement method and sample geometry.

Waveguide-based methods represent another widely accepted class of non-standard techniques for high-frequency characterization. In this configuration, the sample is mounted in the cross-section of a rectangular waveguide, and the shielding effectiveness is determined by measuring the insertion loss across the structure (Figure 2.15). The method operates in well-defined frequency bands, typically in the X-band (8.2–12.4 GHz), Ku-band (12.4–18 GHz), or K-band (18-26.5 GHz), depending on the dimensions of the waveguide. It is especially useful for coatings, thin films, and planar composites with uniform surface characteristics. The University of Twente, for example, has employed waveguide setups in interlaboratory comparisons organized under the IEEE P2715 initiative. The primary limitations of this method are its narrowband nature and the stringent machining requirements of the sample, which must match the waveguide aperture precisely to prevent leakage or excitation of higher modes [30].

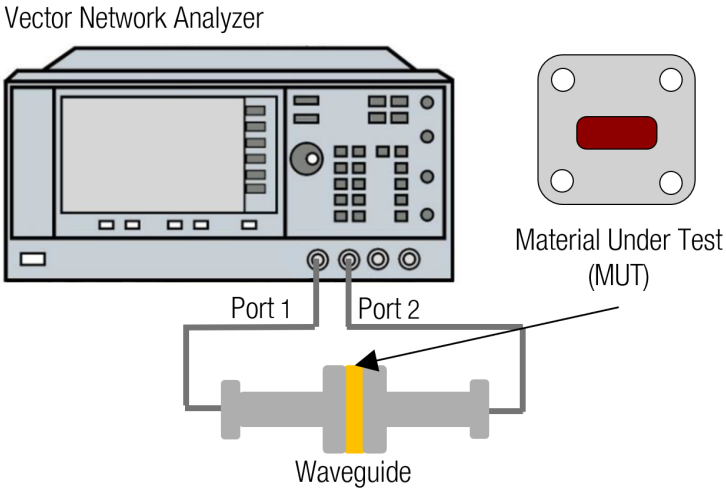

Figure 2.15 Waveguide measurement method and sample geometry.

A further non-standard method is the use of dual TEM cells, where the test material is placed over an aperture shared between two matched TEM enclosures (Figure 2.16). The shielding effectiveness is calculated from the transmitted power or voltage across the interface, often using a transfer impedance or insertion loss formulation. This configuration enables relatively broadband measurements, typically spanning a frequency range of a few megahertz to over 1 GHz, and provides a controlled electromagnetic environment with a uniform field distribution in the test region [31], [32]. The University of Twente has applied this method to characterize polymer-based laminates and other planar materials. Its compact structure and well-defined geometry make it an attractive alternative to coaxial or reverberation-based methods, although its frequency range is limited by the cell size and termination quality, and it may be sensitive to mismatches and edge coupling at the aperture.

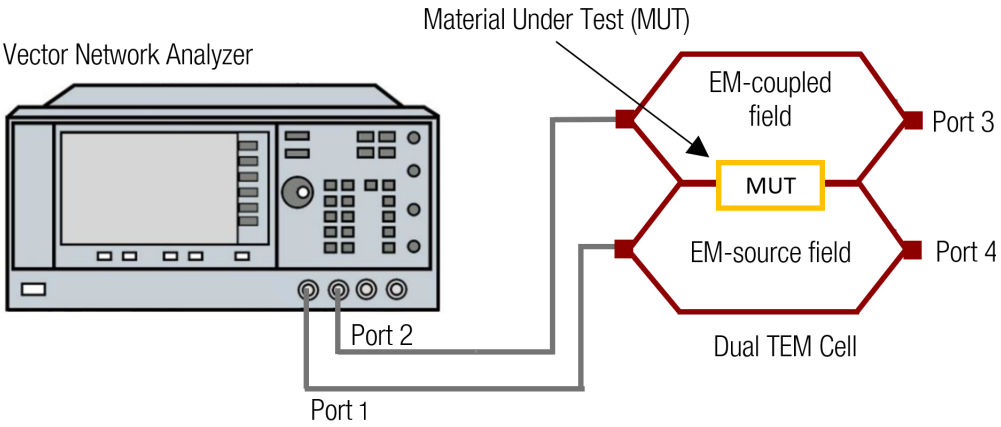

Figure 2.16 Dual TEM Cell Measurement method.

Among the most flexible and increasingly adopted non-standard methods is the Absorber Box configuration. In this setup, a transmitting antenna is placed inside a metallic or absorber-lined chamber, and the sample is positioned over an aperture through which the signal propagates vertically to a receiving antenna placed above. The enclosure is designed to suppress reflections and external coupling, approximating a quasi-free-space environment without the need for a full anechoic chamber. The system enables large-area sample testing, accommodates moderate mechanical tolerances, and operates effectively across a frequency range of 700 MHz to 18 GHz, depending on the antenna type and absorber performance. It is particularly useful for materials that are difficult to machine or clamp into conventional fixtures [33].

Figure 2.17 shows the schematic diagram of the Absorber Box measurement system. The setup consists of a transmitting and a receiving horn antenna placed on opposite sides of the material under test (MUT), which is mounted horizontally over a central aperture. The antennas are connected to the ports of a vector network analyzer, enabling the measurement of the transmitted signal (S_{21}) across the MUT. The entire enclosure is lined with absorbing material to suppress internal reflections and emulate quasi-free-space conditions. This simple yet effective configuration enables vertical wave propagation through planar samples without requiring precision clamping or adapting to a standard fixture.

The measurement procedure consists of two steps: first, a reference transmission measurement is performed with the aperture left open (air), and the corresponding $S_{21,air}$ parameter is stored. Then, the MUT is placed over the aperture and a second transmission measurement is taken, resulting in $S_{21,sample}$. The shielding effectiveness of the material is computed from the difference in transmission levels between both

measurements, quantifying the attenuation introduced by the sample as shown in equation 10. This simple yet effective configuration enables vertical wave propagation through planar samples without requiring precision clamping or adaptation to a standard fixture.

$$SE(dB) = S21_{sample} - S21_{air} \tag{10}$$

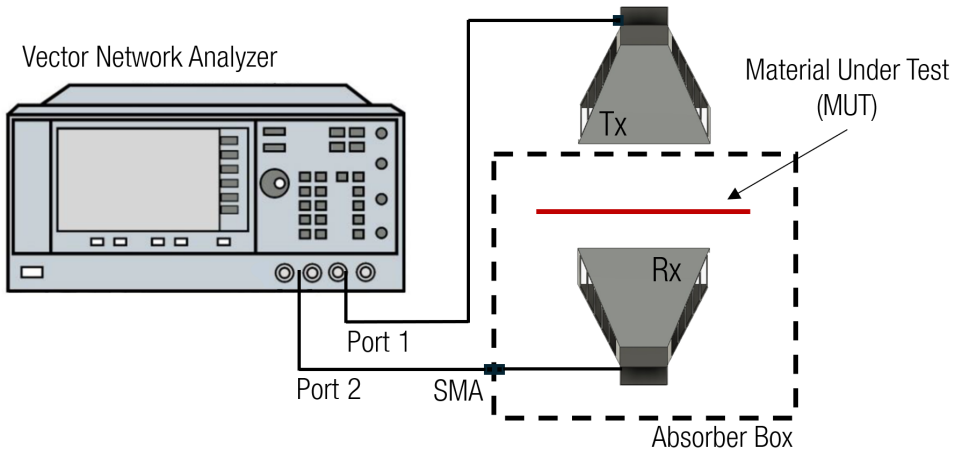

Figure 2.17 Schematic of the Absorber Box measurement setup.

This method is applied in Scientific Article II (Chapter 5) to characterize fiber-reinforced CNT composites whose rigidity and size make them incompatible with coaxial holders. In Scientific Article III (Chapter 6), the setup is further validated through full-wave electromagnetic simulations, which enable a detailed analysis of the field distribution, diffraction effects, and sample positioning. The configuration developed in this thesis builds upon Absorber Box designs used by the University of York, which implemented a dual-polarized version in the IEEE P2715 round robin campaign. The method offers a high dynamic range, good repeatability, and structural simplicity, making it an effective tool for characterizing planar shielding in applied research.

These non-standardized methods, when carefully implemented and calibrated, provide essential capabilities for evaluating the shielding behavior of materials that fall outside the scope of traditional techniques. Their adaptability, frequency reach, and ability to accommodate complex sample formats make them indispensable in the development of advanced electromagnetic shielding technologies.

Table 2.4 Non-Standardized Measurement Methods

Method	Frequency	Measurement Setup	Advantages	Limitations
Miniaturized coaxial airline	Few hundred MHz - tens of GHz	Short air-filled coaxial line	Broadband, fast to implement, suitable for thin and conductive samples	Sensitive to leakage and fringing, open structure
Waveguide method	Band-specific (X, Ku, K, Ka)	Sample placed in rectangular waveguide section	High precision within narrow bands, well-defined modes	Requires tight machining tolerance, narrowband
Dual TEM cell	Few MHz - 1 GHz	Two matched TEM enclosures within shared aperture	Controlled field, compact geometry, suitable for planar samples	Limited frequency range, sensitive to mismatches
Absorber Box	700 MHZ - 18 GHz	Vertical transmission through sample in absorber-lined box	Flexible setup, no sample machining needed, quasi free-space environment	Requires high absorber quality, susceptible to diffraction effects

2.5 Absorber Box Simulation Model Definition

As discussed throughout this chapter, the accurate measurement of shielding effectiveness depends not only on the choice of experimental method but also on a clear understanding of the physical phenomena involved in wave-material interactions. In non-standardized methods, such as the Absorber Box configuration described in Section 2.4.3, numerical simulation becomes a powerful tool to complement and extend experimental data. It enables the analysis of complex electromagnetic effects that are challenging to isolate through measurements alone, including edge diffraction, wave coupling, and non-uniform field distributions within the test system.

To investigate and validate the electromagnetic behavior of this setup, a Finite Element Method (FEM) simulation model was developed using the finite element method. Figure 2.18 illustrates the 3D geometry used in the simulation, where the enclosure, aperture, absorber layout, and horn antennas are modelled in detail. The sample under test is positioned between the antennas, and its interior surfaces are covered with radio-

absorbing material (RAM), which is accurately defined using complex permittivity and permeability data provided by the manufacturer. The simulated model serves as a digital twin of the physical system, enabling parametric studies and theoretical validation under controlled conditions.

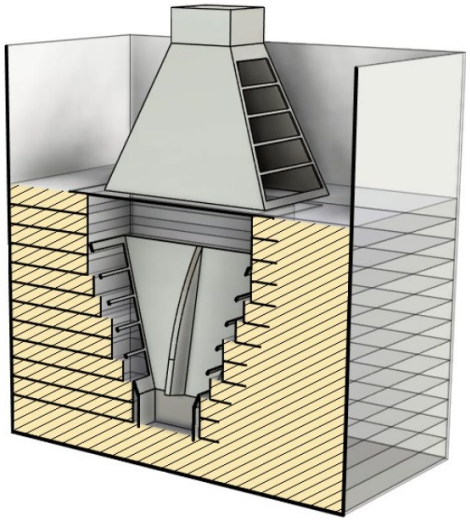

Figure 2.18 3D simulation model of the Absorber Box setup.

One of the key contributions of the simulation model is its ability to visualize and analyze the electric field distribution within the enclosure. This spatial information reveals how the electromagnetic wave interacts with the sample, how the field is shaped by the geometry of the cavity and aperture, and how potential sources of uncertainty, such as standing waves, edge effects, or absorber quality, may influence the final measurement. These insights are essential for improving field uniformity, minimizing unwanted reflections, and ensuring that the region where the sample is located approximates a plane-wave excitation as closely as possible.

The complete development and application of this simulation model are presented in detail in Scientific Article III (Chapter 6). There, the model is used to evaluate not only the transmission characteristics of the system but also its capacity to represent real-world measurement scenarios. The comparison with analytical predictions and the field-level simulation data collectively reinforces the method's validity and highlights the role of numerical modelling as a cornerstone of accurate and reproducible shielding effectiveness assessment.

2.6 Summary

This chapter introduces the fundamental concepts related to electromagnetic compatibility and interference, emphasizing the importance of shielding in electronic systems. The mechanisms that govern shielding behavior have been described, along with the definition and formulation of shielding effectiveness. Then, an overview of conventional and advanced shielding materials is presented. The chapter concludes with an exhaustive bibliographic review of the different measurement methods reported in previous studies conducted by various research institutions, including standardized procedures, derived variants, and non-standardized approaches.

Chapter 3. ASTM-derived Method for Sub-6 GHz Shielding Characterization

In this chapter, the experimental application of a coaxial measurement method, derived from ASTM D4935-18*, for characterizing shielding effectiveness in the sub-6 GHz band, are presented. The work was carried out in collaboration with AIMPLAS, who provided the composite material samples and the coaxial test fixture used for this study.*

3.1 Conference paper I

Title: Analysis of EMI Shielding Effectiveness for plastic fiber composites in the 5G sub-6 GHz band

Authors: Pedro A. Martinez, Jose Torres, Adran Suarez, Antonio Alcarria, Andrea Amaro, Begoña Galindo-Galiana, Carolina Losada-Fernandez, Victor Ramirez-Monsell and Blai Lopez-Rius

Published in: IEEE International Joint Symposium on Electromagnetic Compatibility (EMC), Signal and Power Integrity (SIPI) and EMC Europe, Raleigh, NC, USA, 2021, pp. 278-283. 19 October 2021

DOI: 10.1109/EMC/SI/PI/EMCEurope52599.2021.9559349

Citations: 10 (WoS, accessed on 14 July 2025).

Description: The conference is an international conference with a high scientific level supported by the IEEE Electromagnetic Compatibility Society and the EMC Europe Committee. The conference that promotes EMC research, innovation and international cooperation. The submitted contributions are subjected to the peer review process to assess the quality of the manuscript before it is published in the IEEE Xplore database, one of the most comprehensive interdisciplinary engineering databases in the world. The paper was accepted for oral presentation and indexed with a DOI. The author of this thesis presented the work during the conference.

Synopsis:

The transition toward connected, lightweight, and electrically autonomous platforms has created a growing demand for polymer-based shielding materials that can operate effectively in high-frequency environments. In particular, the sub-6 GHz band (FR1) used in 5G communications presents new challenges in terms of shielding performance, as existing solutions based on metallic materials are often incompatible with the mechanical, thermal, and integration requirements of next-generation electronic systems. Within this context, this chapter examines the development and characterization of fiber-reinforced composite laminates incorporating various conductive fillers, with a focus on applications in the automotive and aerospace sectors where both electromagnetic compatibility and weight reduction are crucial.

The study investigates eight composite structures based on an epoxy matrix reinforced with biaxial carbon or glass fiber fabrics, combined with different conductive additives: multi-walled carbon nanotubes, nickel-coated graphite, and copper mesh. These combinations were selected to evaluate the relative contribution of both the reinforcement and the conductive phase to the overall shielding effectiveness in the sub-6 GHz range. All samples were manufactured using a hand lay-up and vacuum bagging process, and precisely machined for measurement.

A coaxial transmission line holder inspired by the ASTM D4935-18 standard was used to characterize the shielding performance. Although this method was originally intended for operation up to 1.5 GHz, the fixture was adapted and combined with a high-dynamic-range vector network analyzer to extend the frequency range. The coaxial configuration enabled a controlled and repeatable environment for assessing the transmission parameters of each material. Additionally, simulations were used to support the analysis and to understand the behavior of the materials beyond the standard frequency range, providing qualitative insight into the interaction between the test specimens and the electromagnetic field in the GHz region.

The results demonstrate significant differences between the various combinations, particularly between glass fiber and carbon fiber-based laminates. The addition of conductive materials improved the performance of glass-fiber composites, with copper mesh achieving the highest attenuation. In contrast, carbon fiber composites already exhibited strong intrinsic shielding performance, and the effect of the conductive additives was less pronounced. The data confirm the potential of plastic composites to replace traditional metallic shields in applications where mechanical constraints and weight are limiting factors.

Analysis of EMI Shielding Effectiveness for plastic fiber composites in the 5G sub-6 GHz band

P. A. Martinez[1], J. Victoria[2], J. Torres[1], A. Suarez[1], A. Alcarria[2], A. Amaro[1], B. Galindo-Galiana[3], C. Losada-Fernandez[3], V. Ramirez-Monsell[3] and B. Lopez-Rius[3]
[1]*Department of Electronic Engineering, University of Valencia,* Valencia, Spain
adrian.suarez@uv.es
[2]*Product Management, Würth Elektronik eiSos GmbH & Co. KG,* Waldenburg, Germany
jorge.victoria@we-online.de
[3]*Sustainable and Future Mobility Group, Plastics Technology Centre AIMPLAS,* Valencia, Spain
bgalindo@aimplas.es

2021 IEEE International Joint EMC/SI/PI and EMC Europe Symposium | 978-1-6654-4888-8/21/$31.00 ©2021 IEEE | DOI: 10.1109/EMC/SI/PI/EMCEurope52599.2021.9559349

***Abstract*— The study and modeling of EMC are becoming more critical than ever due to the ubiquitous presence of electronic circuits in all aspects of our lives. Specifically, it is crucial to extend these studies to the new frequencies that, in a few years, will be a reality in modern telecommunications systems, such as 5G and its derived technologies. A specific critical field where the proper EMI shielding has been ensured to avoid EMC problems is the electric autonomous vehicles (EAVs). The huge number of electronics systems in new vehicles will dramatically extend the demands on the EMI shielding solutions used to attenuate the radiated emissions that could affect circuits in the vehicle. Metals or metal alloys are the most common EMI shielding materials since they demonstrate adequate shielding capacity against EMI. However, polymers have become up-and-coming materials for EMI shielding with the characteristics of lightweight, flexibility, cost-effective, easy processing, and resistance to corrosion. Consequently, it is necessary to develop EMI shielding materials based on polymers, plastic materials, and fiber composites that ensure compliance with the different standards that regulate 5G and the proper operation of possible systems susceptible to the intentional and unintended signals generated by this new technology. This contribution focuses on characterizing different composite structures' performance based on fibers combined with conductive materials in terms of shielding effectiveness, covering the 5G sub-6 GHz frequency range.**

Keywords—Shielding effectiveness, shielding materials, fiber composites, housing, sub-6 GHz, 5G technology, electric autonomous vehicles

I. INTRODUCTION

Electronic devices continually integrate more complex and more advanced functionalities. This involves increasing operating frequencies, the miniaturization of the electronic design, high component integration, reduction of the device housing, and using very low voltage signals [1], [2]. These design principles are often used to achieve a device with better performance and features; however, they increase the likelihood of generating complex electromagnetic interference (EMI) problems. The electronics can be sensitive to the surrounding electromagnetic environment, and it can also act as a noise source. Thus, it is essential important to manage electromagnetic noise for avoiding unwanted electromagnetic interactions with nearby systems [3], [4]. Therefore, the ability to control complex EMI problems by eliminating or reducing them is in high demand [5].

The ideal EMI shield is an infinitely conductive enclosure with no apertures or penetrations of any kind. From this perspective, solutions based on metallic shielding are widely used by designers, because they allow mitigating the effects of EMI that have not been foreseen in the design and/or manufacturing phases, and that could not be mitigated otherwise without having to redo the design and/or manufacturing processes [6]. However, the fact is that metals have many shortcomings, such as high density, poor corrosion resistance, and high processing costs, that has restricted their development.

With the emergence of 5G communications, it is necessary to design new EMI shielding materials and techniques in the direction of higher shielding effectiveness, wider shielding frequency, and better performance. In this context, plastic materials and conductive polymer composites have emerged from a continuous search for better performance in shielding applications, and they are more attractive in the field of electromagnetic shielding [7], [8]. Conductive polymer composites present an excellent alternative because of their low density, good chemical stability, flexibility, and easy processing, compared with metal-based materials. These materials provide an outstanding combination of electrical, thermal, and mechanical performance. Plastic materials make it possible a free design and weight reduction by about 40%, critical factors in the automotive sector that can allow a reduction of energy consumption, a key important role in electrically and autonomous driven vehicles [9]–[11].

Until recently, the main frequencies of interest were the AM and FM bands used by radio and frequencies below 3 GHz used by Bluetooth radio, Wi-Fi, and mobile phone networks. One of the 5G challenges is designing of new EMI shielding techniques that allow 5G to coexist with other technologies. In this way, it is necessary to develop EMI shielding materials that ensure compliance with the different standards that regulate 5G and the proper operation of possible systems susceptible to the intentional and unintended signals generated by this new technology.

A specific critical field where the proper EMI shielding has been ensured in order to avoid EMC problems is the electric autonomous vehicles (EAVs). EAVs are a growing registering a compound annual growth rate (CAGR) of 39.47% from 2019 to 2026, according to Allied Market Research [12]–[14]. The increase of electronics systems in the vehicles will extend the demands on the EMI shielding devices used to attenuate the radiated emissions that could affect circuits in the vehicle and their interconnectivity. The huge number of electronics systems in new vehicles will dramatically extend the demands on the EMI shielding

solutions used to attenuate the radiated emissions that could affect circuits in the vehicle. EMI shielding materials will need to perform over a wide range of frequencies in more applications as electronic systems take over more and more aspects of the vehicle's driving operations while adding as little as possible to the weight of the vehicle.

Moreover, these innovative materials will meet the requirements in terms of shielding effectiveness (SE) and frequency range to adapt to 5G technologies [15]. Composite materials combine lightweight with high mechanical performance. Nevertheless, their interaction with electromagnetic radiation has to be studied in order to adapt to new 5G frequencies without compromising density and mechanical performance. Different composite structures will be analyzed in the present study, comparing the reinforcing fiber and the addition of carbon nanotubes (MWCNT) and nickel-coated graphite as additives to improve EMI shielding effectiveness of epoxy matrix. The results could be applied in autonomous vehicles and drones for reducing platforms' electromagnetic signature.

Consequently, this contribution is focused on characterizing new plastic shielding materials in the Frequency Range 1 (FR1) of 5G technology that includes sub-6 GHz frequency bands. Some of these are bands traditionally used by previous standards, but they have been extended to cover potential new spectrum offerings from 410 MHz to 7125 MHz [15].

II. Shielding Composite Structures

For the development of composites with electromagnetic shielding properties, materials have been selected, including matrix, reinforcement, and conductive materials. Table I summarizes the materials used to manufacture the eight composite samples evaluated in this contribution. Each of these samples consists of a polymer (epoxy resin) matrix reinforced with fiber fabric layers. Two different fibers fabric are used as reinforcement in order to evaluate its contribution in terms of SE. This structure is combined with a conductive material with the aim of improving the SE. The conductive materials analyzed corresponds to a copper (Cu) mesh from Goodfellow, multi-walled carbon nanotubes (MW-CNT) nanoparticles from Nanocyl, and nickel-coated graphite particles from Hart Materials.

TABLE I. Materials used to form the composite structures

Material type	Description
Matrix	Cycloaliphatic epoxy system - Resoltech
Reinforcement	Biaxial carbon fiber fabric - SGL
Reinforcement	Biaxial glass fiber fabric - Metyx
Conductive	Copper mesh - Goodfellow
Conductive	MW-CNT - Nanocyl
Conductive	Graphite-Nickel - Hart Materials

The selected reinforcements and conductive materials employed for the manufacturing of composites with EMI shielding properties are shown in Fig. 1. The biaxial carbon fiber fabric and biaxial glass fiber fabric selected as reinforcements are shown in Fig. 1(a) and Fig. 1(b), respectively. The selected conductive materials are shown in Fig.1(c)–(e)).

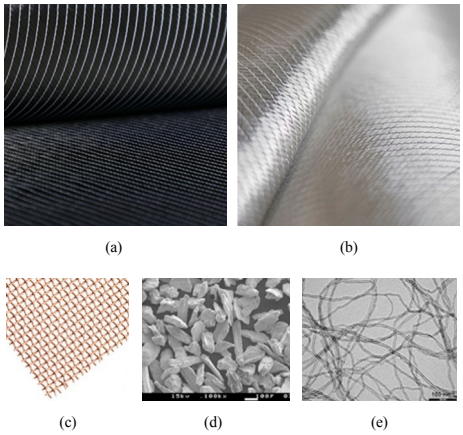

Fig. 1. Selected materials for the manufacturing of composites with EMI shielding properties. (a) Biaxial carbon fiber fabric. (b) Biaxial glass fiber fabric. (c) Copper mesh. (d) Graphite-Nickel. (e) MW-CNT.

Composite laminates have been manufactured by hand lay-up and vacuum bagging process. Hand lay-up is the simplest composite manufacturing method, as shown in Fig. 3. The methodology consists of placing the reinforcement layers on the mould and impregnating them manually with the thermosetting resin. Consolidation rollers are used to thoroughly wetting the reinforcement and removing entrapped air. Subsequent layers of reinforcement are added and impregnated to build laminate thickness.

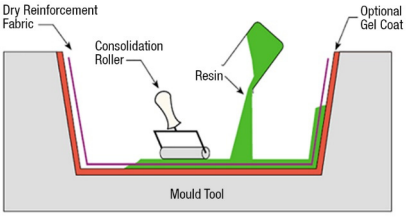

Fig. 2. Hand lay-up composite manufacturing process.

Vacuum bagging is applied to consolidate the composite laminate, as shown in Fig. 3. After hand lay-up, the uncured laminate is covered with a peel ply (a synthetic fabric with a fine weave that assists with demoulding and surface finish), a release film (a perforated film that helps to evacuate entrapped air uniformly. At the same time it evacuates any resin excess that bleeds out of the composite) and a breather fabric (a relatively thick non-woven fabric that absorbs the resin that passes through the release film). After this, the entire lay-up is then covered with a vacuum bag and sealed around the edges, apart from the connection to the vacuum pump. Activating the pump sucks all the air out of the space between the vacuum bag and the mould, causing the composite to be consolidated under 1 bar of pressure and at room temperature. Once the part is fully cured, the vacuum pump can be disconnected, the vacuum bag, breather fabric, release film, and peel ply removed and discarded, and the part removed from the mould.

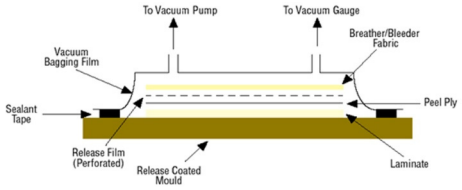

Fig. 3. Hand lay-up composite manufacturing process.

Within this processing methodology, the selected conductive materials have been included in their respective composite laminates following different methods:

1) MW-CNT: Dispersion of nanoparticles in the matrix using high-speed dispersing equipment. The mix has been used in the impregnation of all reinforcement layers of the composite laminates.

2) Graphite-Nickel: Manual mixing in the matrix. The mix has been applied between layers 3 and 4 of the composite laminates.

3) Cooper mesh: Placement of the mesh between layer 3 and 4 of the composite laminates, obtaining a sandwich structure.

Following the different described methodologies, eight composite laminates have been obtained. Their composition and thicknesses are summarized in Table II:

TABLE II. OBTAINED COMPOSITES AND THEIR REAL THICKNESSES

Reference	Reinforcement	Conductive material	Thickness (mm)
CF	6 x Carbon Fiber	-	2.30
CF + Cu	6 x Carbon Fiber	Copper	2.45
CF + MW-CNT	6 x Carbon Fiber	MW-CNT	2.30
CF + Gr-Ni	6 x Carbon Fiber	Graphite-Nickel	2.45
GF	6 x Glass Fiber	-	2.31
GF + Cu	6 x Glass Fiber	Copper	2.45
GF + MW-CNT	6 x Glass Fiber	MW-CNT	2.26
GF + Gr-Ni	6 x Glass Fiber	Graphite-Nickel	2.62

Finally, these composite laminates have been machined using a CNC machining equipment to obtain specimens with the appropriate dimensions for subsequent analysis. Fig. 4 shows an example of the specimens obtained after the machining tasks.

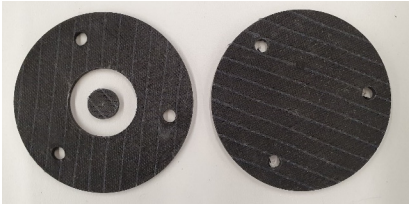

Fig. 4. Example of machined composite specimens for the EMI shielding test.

III. MEASUREMENT SETUP

There are multiple methods to measure electromagnetic shielding, but one of the most widely accepted is the ASTM 4935-18 standard. As for frequency range limitations, this method allows measuring planar samples in a narrow frequency range from 30 MHz to 1.5 GHz. These limits are based on the decrease in current displacement due to capacitive coupling at very low frequencies and overmodulation at higher frequencies where the wavelength is comparable to the size of the sample used in this method [16].

The method consists of the measurement of the insertion loss (IL) that results when introducing test samples in a coaxial two-conductor transmission line holder, supporting transverse electromagnetic (TEM) propagation mode. The Keysight E7051B Vector Network Analyzer (VNA) has been used to obtain the measurements. It allows measurements from 300 kHz to 8.5 GHz. It also has a dynamic range of 100 dB, which is sufficient to measure the SE of the selected materials and four Type-N female connectors with a characteristic impedance of 50 Ω [17]. The specimen holder is a coaxial transmission line with special taper sections and notched matching grooves to maintain a characteristic impedance of 50 Ω throughout the entire length of the holder as shown in Fig. 5. Note that the transmission line holder is based on the ASTM 4935-18 standard and it has been used to characterize samples beyond the frequency range defined by this. Thereby, the results obtained in the high frequency region should be considered as a qualitative approach.

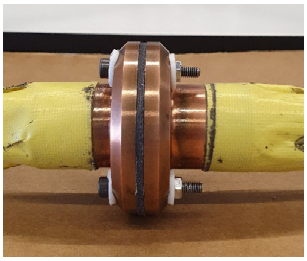

Fig. 5. Coaxial transmission line holder with a test sample introduced.

The procedure requires two types of specimens that must have the same thickness in order to make SE measurements, the reference, and the load specimens. The difference between the measurements of the load and the reference specimen provides the measurement of the SE, caused by the reflection and absorption of the material between the two flanks of the coaxial probe. The use of two different specimens is justified by the fact that the use of the reference specimen can compensate the effects of capacitive coupling by establishing a frequency-dependent reference level [18], [19].

The load specimen has a disk-like shape with a diameter equal to that of the outer flange. On the other hand, the reference specimen consists of two parts: a washer and a disk-shaped sample, matching the dimensions of the outer and inner conductors, respectively. Fig. 6 shows the measurement setup described previously and the dimensions of the specimens, both the reference and the load:

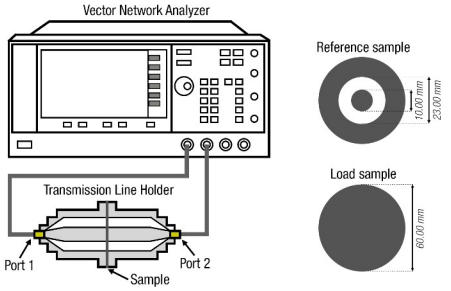

Fig. 6. Measurement test setup following the ASTM D4935-18 procedure.

Fig. 7 shows the experimental setup implemented to characterize the samples under test.

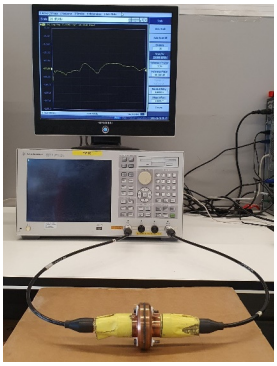

Fig. 7. Measurement test setup following the ASTM D4935-18 procedure.

The SE measurement (dB) can be expressed as the difference between the IL expressed in dB of the load specimen ($IL_{dB,l}$ and the IL of the reference one $IL_{dB,r}$):

$$SE_{dB} = IL_{dB,l} - IL_{dB,r}. \quad (1)$$

The $IL_{dB,l}$ e $IL_{dB,r}$ measurements can be done directly from the VNA due to the measurement method used, by placing the probe terminals between ports 1 and 2 of the network analyzer and selecting the measurement of S21, both for the reference and the load. Therefore, SE_{dB} can be expressed as

$$SE_{dB} = 20\log_{10}\left|\frac{S_{21,l}}{S_{21,r}}\right|. \quad (2)$$

Whereas the frequency range established by the ASTM 4935-18 standard is limited to frequencies below 1.5 GHz, measures have been carried out from 0 Hz to 8.5 GHz, to observe the tendency of the behavior of the different materials in the FR1 frequency range (410 MHz – 7125 MHZ) [20].

Fig. 8 shows the measurement of reference specimens of the different materials. These measurements provide an approximate representation of the behavior of these materials in a higher frequency range. It can be seen that the method provides flat responses, although it can be noted that there is an uncertainty range between 4 GHz and 5 GHz, which has not been considered large enough to discard measurements made at these frequencies.

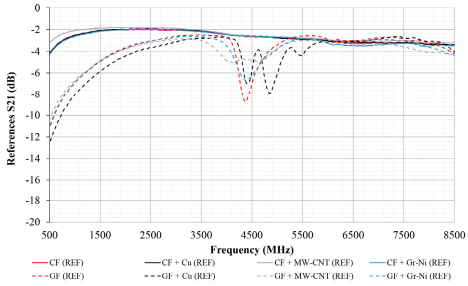

Fig. 8. S_{21} parameters obtained from the different reference specimens under test.

Copper mesh conductive material has been evaluated in terms of SE by obtaining the reference and load transmission parameters. This material can provide a significant SE performance and can be considered as a reference in order to determine composite laminates' performance evaluated in this contribution. Fig. 9 shows the SE for this conductive material.

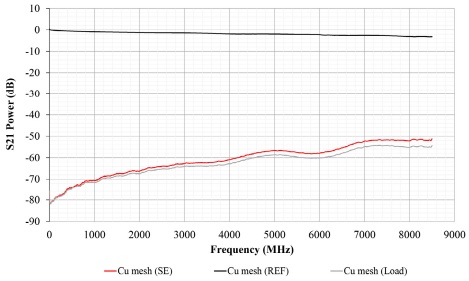

Fig. 9. Reference, Load and Shielding Effectiveness obtained for the copper mesh conductive material.

IV. Results and Discussion

This section is focused on showing the results corresponding to the measurement of eight sample composites under test. A comparison between the carbon fiber and glass fiber's SE performance is carried out by combining them with the three conductive materials.

Firstly, the different materials' shielding effectiveness is evaluated by considering the frequency range defined in the ASTM 4935-18 standard (30 MHz to 1.5 GHz). Fig. 10 shows the shielding effectiveness provided by the composite laminates samples based on CF reinforcement (dashed traces) and GL reinforcement (solid traces). It can be observed that the GF samples without any conductive material do not provide attenuation, whereas the CF sample can provide significant SE. The CF sample provides an attenuation between around -55 dB to -75 dB, considering the frequency range from 100 MHz to 1.5 GHz. When a conductive material is added to the CF reinforcement, a similar SE is obtained. The addition of the MW-CNT conductive material results in improving the SE response by about 3 dB. Specifically, if the 1 GHz frequency point is considered, the CF+MW-CNT sample shows an attenuation of -73.6 dB, whereas the CF sample of -70.3 dB. Regarding the CF+Gr-Ni and CF+Cu samples, the original CF material is able to provide a better response. If these two combinations are compared, the

CF+Gr-Ni is able to show higher SE values than CF+Gr-Ni from 550 MHz.

Nevertheless, the influence of the conductive materials analyzed for the CF sample is not correlated in the case of being combined with GF. Thereby, the GF+Cu is the GF-based combination that represents the best performance. However, the opposite of what happens with CF, GF's combination with the conductive material based on MW-CNT provides higher shielding effectiveness. The GF+Gr-Ni sample provides a similar response to GF+Cu up to 450 MHz, but its effectiveness is reduced from that frequency point.

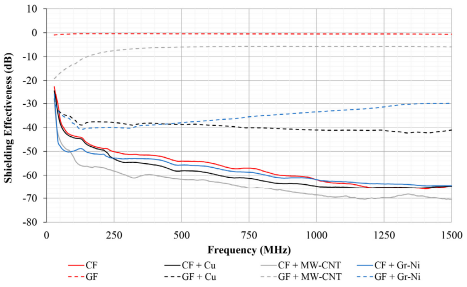

Fig. 10. Shielding effectiveness results for different composites materials under test in the frequency range defined in the ASTM 4935-18 standard.

As mentioned in section III, although the range defined in the standard is between 30 MHz and 1.5 GHz, measurements have been carried out in the frequency range from 300 kHz to 8.5 GHz. This is because the aim of the study is to observe the behavior at higher frequencies and get an approach of the SE value in frequencies above 1.5 GHz. Fig. 11 shows the SE of these materials covering the frequency range of FR1 sub-6 GHz (410 MHz – 7125 MHz).

In contrast with the results presented in Fig. 10, Fig. 11 shows the shielding effectiveness provided by the same composite laminates samples, but considering the sub-6 GHz bandwidth. It is observed that the trend of the SE response is maintained, so it is possible to obtain an approximation of the performance of the materials at higher frequencies.

By extending the frequency range beyond that described in the ASTM 4935-18 standard, it can be observed how certain parasite resonances become evident, particularly in the traces of the GF+Cu combination specimen, reaching values of approximately -10 dB at frequencies around 4.2 GHz. Note also an uncertainty bandwidth between 3.1 GHz and 4.0 GHz in the responses of the CF samples, where the resonance of the GF+Cu composite, reaches a value of -42 dB. This means that the most significant variations in the responses are found in those materials whose conductive material is copper.

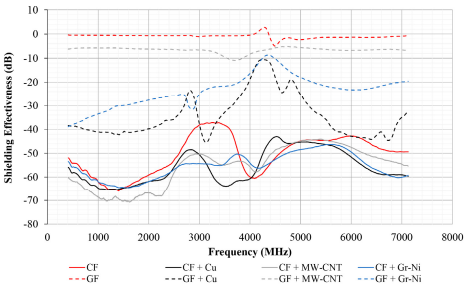

Fig. 11. Shielding effectiveness results for different composites materials under test in the sub-6 GHz (FR1) frequency range.

V. Conclusions

EMI shielding effectiveness in the FR1 frequency range of 5G has been studied. Two types of materials based on carbon fiber and glass fiber have been compared, adding to both three types of conductive materials to give them metallic properties. It has been observed how the different materials perform in the specified frequency range, giving a preliminary idea of how they might work at higher frequencies for applications requiring EMI shielding against the ever-increasing 5G technologies.

Firstly, it has been concluded that the CF presents a higher attenuation than the GF without introducing any conductive material. Furthermore, it has been observed that combining conductive materials with the CF composite gives very similar results to the original response, regardless of the material introduced. Concerning this, it would be concluded that the combination that provides the best results to CF composites is CF+MW-CNT, while for GF, the best combination is GF+Cu.

It has to be remarked that these types of characterizations are very relevant from a technological and industrial point of view. Specifically, for automotive and related sectors, the use of EMI shielding based on plastic materials has many advantages such as the manufacturing cost reduction.

Considering this, in the automotive sector, particularly the vehicle of the future, the weight of those elements in which specific structural characteristics of rigidity, protection against impact as well as vibration absorption are not required, is a frequent area of work, aimed above all at reducing the consumption of vehicles. This is why developing these types of plastic materials with metallic properties is very important nowadays.

Consequently, the selection of these plastic materials and their conductive composite polymers is not arbitrary, as it has been demonstrated. Some of the samples analyzed and, specifically, those based on CF composites, present a considerable attenuation to be able to replace metallic materials, thus eliminating the disadvantages that these materials entail.

References

[1] F. M. Idris, M. Hashim, Z. Abbas, I. Ismail, R. Nazlan, and I. R. Ibrahim, "Recent developments of smart electromagnetic absorbers based polymer-composites at gigahertz frequencies," *J. Magn. Magn. Mater.*, vol. 405, pp. 197–208, 2016, doi.org/10.1016/j.jmmm.2015.12.070.

[2] J. Victoria, A. Suarez, P. A. Martinez, A. Alcarria, A. Gerfer, and J. Torres, "Improving the Efficiency of NFC Systems Through Optimizing the Sintered Ferrite Sheet Thickness Selection," *IEEE Transactions on Electromagnetic Compatibility*, vol. 62, no. 4, pp. 1504–1514, 2020, doi: 10.1109/TEMC.2020.3003800.

[3] J. Victoria, et al., "Transmission Attenuation Power Ratio Analysis of Flexible Electromagnetic Absorber Sheets Combined with a Metal Layer," *Materials*, vol. 11, no. 9, p. 1612–1626, 2018, doi.org/10.3390/ma1091612.

[4] C. Paul, *Introduction to Electromagnetic Compatibility*. Hoboken, NJ, USA: Wiley, 2006.

[5] N. Matsushita, T. Nakamura, and M. Abe, ""Spin-sprayed Ni-Zn-Co ferrite films with high μr">100 in extremely wide frequency range 100 MHz-1 GHz," *J. Appl. Phys.*, vol. 93, no. 10, pp. 7133–7135, 2003, doi.org/10.1063/1.1558198.

[6] H. W. Ott, *Electromagnetic Compatibility Engineering*. New York, NY, USA: Wiley, 2011.

[7] X. Li, G. Wang, C. Yang, J. Zhao, and A. Zhang, "Mechanical and EMI shielding properties of solid and microcellular TPU/nanographite composite membranes," *Polym. Test.*, vol. 93, p. 106891, 2021, doi.org/10.1016/j.polymertesting.2020.106891.

[8] H.-C. Cheng, C.-R. Chen, S. Hsu, and K.-B. Cheng, "Electromagnetic Shielding Effectiveness and Conductivity of PTFE/Ag/MWCNT Conductive Fabrics Using the Screen Printing Method," *Sustainability*, vol. 12, no. 15, p. 5899, 2020, doi.org/10.3390/su12155899.

[9] W. Seiler, "EMI shielding for thermoplastic housings," *Freudenberg Sealing Technologies*, 2019. [Online]. Available: https://www.fst.com. [Accessed: Jan. 12, 2021]

[10] A. Naseer, et al., "Reinforcement of Electromagnetic Wave Absorption Characteristics in PVDF-PMMA Nanocomposite by Intercalation of Carbon Nanofibers," *Electron. Mater. Lett.*, vol. 15, pp. 201–207, 2019, doi.org/10.1007/s13391-018-00104-9.

[11] DSM Engineering Plastics, "DSM provides a full spectrum of engineering plastics for electronic applications in the connected car," *DSM Engineering Plastics*, 2017. [Online]. Available: https://www.dsm.com. [Accessed: Jan. 12, 2021]

[12] Allied Market Research, "Autonomous Vehicle Market by Level of Automation (Level 3, Level 4, and Level 5) and Component (Hardware, Software, and Service) and Application (Civil, Robo Taxi, Self-driving Bus, Ride Share, Self-driving Truck, and Ride Hail) - Global Opportunity Analysis and Industry Forecast, 2019-2026," *Allied Market Research*, 2019. [Online]. Available: https://www.alliedmarketresearch.com. [Accessed: Jan. 12, 2021]

[13] M. K. Khan and A. Quadri, "Augmenting cybersecurity in autonomous vehicles: Innovative recommendations for aspiring entrepreneurs," *IEEE Consumer Electronics Magazine*, doi: 10.1109/MCE.2020.3024513.

[14] L. Zongwei, J. Hao, T. Hong, and Z. Fuquan, "An Overview of the Latest Progress and Core Challenge of Autonomous Vehicle Technologies," *MATEC Web Conf.*, vol. 308, no. 06002, 2020, doi.org/10.1051/matecconf/202030806002.

[15] S. Aerts et al., "In-situ Measurement Methodology for the Assessment of 5G NR Massive MIMO Base Station Exposure at Sub-6 GHz Frequencies," *IEEE Access*, vol. 7, pp. 184658–184667, 2019, doi: 10.1109/ACCESS.2019.2961225.

[16] Standard Test Method for Measuring the Electromagnetic Shielding Effectiveness of Planar Materials, ASTM International Std. D4935-18, 2018.

[17] Keysight Technologies, "Agilent ENA 2, 3 and 4 Port rf Network Analyzers," E5071B 300 kHz to 8.5 GHz datasheet, 2008.

[18] K. Tserpes, V. Tzatzadakis, and J. Bachmann, "Electrical Conductivity and Electromagnetic Shielding Effectiveness of Bio-Composites." *J. Compos. Sci.*, vol. 4, no. 28, 2020, doi.org/10.3390/jcs4010028.

[19] T. W. Więckowski, , J. M. Janukiewicz, "Methods for Evaluating the Shielding Effectiveness of Textiles," *Fibres & Textiles*, vol. 14, no. 5, 2006.

[20] H. Vasquez, L. Espinoza, K. Lozano, H. Foltz, and S. Yang, "Simple device for electromagnetic interference shielding effectiveness measurement," *IEEE EMC Soc. Newslett.*, vol. 220, pp. 62–68, 2009.

3.2 Summary

This chapter highlights the practical limitations of applying ASTM D4935 directly to modern shielding materials and operating frequencies. While the standard remains robust in its principle, its physical constraints, in terms of required sample geometry and restricted frequency range, make it incompatible with the testing of many composite structures intended for 5G or automotive use. By adapting the measurement fixture and using more compact samples, the methodology was successfully extended beyond 1.5 GHz, offering qualitative insights in the sub-6GHz (FR1) frequency range. These findings justify the continued refinement of coaxial-based methods and serve as the foundation for the next chapter, where a miniaturized probe is introduced to further increase the usable frequency range and reduce sample size requirements.

This study directly addresses S.O.1 and S.O.2, by identifying the limitations of standardized methods and applying a derived configuration adapted to new test conditions. Furthermore, it sets the foundation for S.O.4, by beginning to explore the applicability of adapted methods to advanced composite materials, a topic that is developed in subsequent chapters.

Chapter 4. Miniaturized Coaxial Probe for Shielding Measurements up to 18 GHz

This chapter presents the extension of the coaxial transmission line method for shielding effectiveness measurements up to 18 GHz using a miniaturized probe configuration. This adaptation allows shielding effectiveness measurements of planar samples in the upper microwave range, where standard fixtures are no longer suitable due to mode propagation and geometric limitations. The measurement fixture used in this study was provided by the University of Rome "La Sapienza", as part of a collaborative effort developed within the framework of this work.

4.1 Scientific article I

Title: EMI Shielding Effectiveness Study for Innovative Carbon Nanotube Materials in the 5G Frequency Region

Authors: Andrea Amaro, Adrian Suarez, Alessio Tamburrano, Jose Torres, Fabrizio Marra, Pedro A. Martinez, Begoña Galindo, Neus Soriano, Jorge Victoria and Antonio Alcarria

Published in IEEE Transactions on Electromagnetic Compatibility, Volume 65, Issue 1, February 2023. Pages: 177 – 185. 18 October 2022

DOI: 10.1109/TEMC.2022.3209708

Impact factor (2023): JCR: 2.0

Quartile (2023): SJR: Q1 (Electrical and Electronic Engineering)

Citations: 8 (WoS, accessed on 14 July 2025).

Description: IEEE Transactions on Electromagnetic Compatibility (ISSN 0018-9375; CODEN: IEMCAE) is a peer-reviewed journal published by the Institute of Electrical and Electronics Engineers (IEEE). The journal focuses on all aspects of electromagnetic compatibility (EMC), including electromagnetic environments, interference control, EMC and EMI modeling, high-power electromagnetics, EMC standards, measurement

methods, computational electromagnetics, signal and power integrity, transmission lines, electrostatic discharge, lightning effects, and EMC in wireless and optical technologies, as well as in printed circuit board and system design. The impact factor, quartile, and rank information have been obtained from the Journal Citation Reports (JCR) and SCImago Journal Rank (SJR) databases, based on the publication year (2020). The citations have been consulted in the Web of Science database.

Synopsis:

The integration of 5G technologies into high-density electronic systems, particularly in sectors such as autonomous electric vehicles, has introduced new challenges in mitigating electromagnetic interference. As operating frequencies increase and traditional shielding solutions based on metallic enclosures become less viable due to weight and rigidity, there is growing interest in alternative materials that are lightweight, processable, and effective over a broad frequency spectrum. Among these, polymer nanocomposites with conductive fillers such as carbon nanotubes offer a promising solution, combining electrical functionality with mechanical versatility.

This chapter presents the electromagnetic characterization of polypropylene-based composites containing multi-walled CNTs at three different concentrations. The materials were fabricated via melt mixing, and their electrical conductivity was evaluated to establish the relationship between shielding performance and electrical conductivity in the gigahertz range. One of the most relevant aspects of this study lies in the measurement approach. A coaxial transmission line holder was specifically designed and manufactured by modifying the dimensions of the fixture defined in the ASTM D4935-18 standard. This adaptation enables the extension of the measurement range up to 18 GHz while preserving the transverse electromagnetic propagation mode. This frequency range includes part of the 5G spectrum, including sub-6 GHz band, which is gaining increasing importance in practical applications.

The use of this adapted coaxial holder allows for the precise evaluation of the shielding effectiveness of small, planar samples with high reproducibility and spectral resolution. The results show that shielding performance improves with increasing CNT concentration, with the highest-loading sample reaching mean attenuation values around 24 dB and peaking at 25.6 dB at 10 GHz. While the increase in effectiveness with filler content is evident, the relationship is not strictly linear, indicating the influence of factors such as filler dispersion, network formation, and material saturation.

The outcomes reported in this work validate the potential of CNT-based nanocomposites as effective electromagnetic shielding materials for high-frequency applications. Moreover, the use of a derived high-frequency coaxial method highlights the importance

of adapting measurement techniques to meet the demands imposed by emerging technologies and new material systems.

EMI Shielding Effectiveness Study for Innovative Carbon Nanotube Materials in the 5G Frequency Region

Andrea Amaro, *Student Member, IEEE*, Adrian Suarez, *Member, IEEE*, Alessio Tamburrano, *Senior Member, IEEE*, Jose Torres, *Senior Member, IEEE*, Fabrizio Marra, Pedro A. Martinez, *Member, IEEE*, Begoña Galindo, Neus Soriano, Jorge Victoria, *Member, IEEE*, and Antonio Alcarria, *Member, IEEE*

***Abstract*—It is crucial to extend the electromagnetic compatibility (EMC) studies to the new frequency regions where modern telecommunication systems operate, specifically those related to the fifth-generation (5G) technology standard for broadband cellular networks. Electric autonomous vehicles (EAVs) are systems that feature 5G technology on board and for which it is essential to ensure the proper management of EMC to prevent malfunctions. Given the considerable development of the EAV-related sector, new materials and solutions for EMI shielding with properties that reduce interference in the frequency regions of 5G technology are being investigated. Today, meatal-based solutions are the most common EMI shielding materials used to mitigate EMC problems. Nevertheless, with the appearance of EAVs, it is needed the design of novel materials that provide a significant balance in terms of shielding effectiveness (SE) and mechanical properties. Thereby, carbon nanotubes (CNTs) are an attractive alternative to conventional EMI shielding materials due to their characteristics. The lightweight condition, flexibility, cost-effectiveness, easy processing, and resistance to corrosion made this new type of material perfect to be used in the field of EAVs. This contribution focuses on describing and characterizing three nanocomposite materials manufactured by loading a polymer matrix with 5%, 7%, and 10% CNT concentrations, respectively. The SE measurement is carried out with a coaxial sample holder based on the standard ASTM D4935-18. This measurement setup makes it possible to determine the performance of the three materials under test up to 18 GHz, covering part of the operation frequencies of 5G systems.**

***Index Terms*—ASTM D4935-18, carbon nanotubes (CNTs), coaxial sample holder (CSH), electromagnetic compatibility (EMC), electromagnetic interferences (EMI), fifth-generation (5G) technology, shielding effectiveness (SE), shielding materials.**

Manuscript received 2 May 2022; revised 14 August 2022; accepted 19 September 2022. Date of publication 18 October 2022; date of current version 16 February 2023. *(Corresponding author: Andrea Amaro.)*

Andrea Amaro, Adrian Suarez, Jose Torres, and Pedro A. Martinez are with the Department of Electronic Engineering, University of Valencia, 46010 Valencia, Spain (e-mail: andrea.amaro@uv.es; adrian.suarez@uv.es; jose.torres@uv.es; pedro.a.martinez@uv.es).

Alessio Tamburrano and Fabrizio Marra are with the Department of Astronautical, Electrical and Energy Engineering, Sapienza Università di Roma, 00184 Rome, Italy (e-mail: alessio.tamburrano@uniroma1.it; fabrizio.marra@uniroma1.it).

Begoña Galindo and Neus Soriano are with the AIMPLAS Technological Institute of Polymers, 46980 Valencia, Spain (e-mail: bgalindo@aimplas.es; nsoriano@aimplas.es).

Jorge Victoria and Antonio Alcarria are with the Würth Elektronik eiSos, 74638 Waldenburg, Germany (e-mail: jorge.victoria@we-online.de; antonio.alcarria@we-online.de).

Color versions of one or more figures in this article are available at https://doi.org/10.1109/TEMC.2022.3209708.

Digital Object Identifier 10.1109/TEMC.2022.3209708

I. Introduction

THE importance of electromagnetic interferences (EMI) shielding relates to the high demand of today's society for the reliability of electronics and the rapid growth of the development of new telecommunications systems [1], [2], [3]. Nowadays, due to the ubiquitous presence of electronic circuits in all aspects of life, the study and modeling of electromagnetic compatibility (EMC) are more important than ever, especially in relation to extending these studies to the new frequencies.

The new fifth-generation (5G) standard has a significant impact on the communication industry since a great variety of innovate technologies are derived from it. The main difference between 5G and previous generations is the operating frequency. The 5G spectrum is divided into two regions: FR1, also known as the sub-6 GHz frequency range, and FR2, also called the millimeter-wave frequency range. Thereby, 5G technology faces the challenge of the environmental problems arising from the EM field generated by its antennas and how to prevent this from affecting other sensitive systems [4]. Therefore, one current challenge concerns the design of new EMI shields to promote the coexistence of 5G with other technologies.

One of the possible victim systems is the electric autonomous vehicle (EAV). The trend to develop a safe EAV is growing up, especially as the 5G network becomes more widespread worldwide. 5G, at least ten times faster than 4G, will improve communications between vehicles with innovative driving technologies [5]. Nevertheless, the massive number of electronic systems in new 5G operating vehicles will dramatically increase the demand for electromagnetic (EM) shielding materials with properties suitable to ensure low EMI in 5G radiation frequencies [6], as the use of devices for the attenuation of radiated emissions could affect car circuits, provoke interferences and resulting in traffic accidents [7].

EM shielding materials present the ability to obstruct and minimize the signal emitted through backward reflection of the field waves or by means of the absorption and dissipation of the radiation inside the material [8], [9]. Traditional metal shields

can effectively attenuate EMI generated by 5G applications, but they have generally some drawbacks, such as lack of flexibility [8], bulkiness, weight, volume [10], or low corrosion resistance. Conductive polymer composites are a good alternative due to their properties, such as low density, good chemical stability, flexibility, and easy-processing compared with metal-based materials [11]. This is why polymer-based materials are taking on a special relevance, showing a good performance when loaded with fillers that enhance their properties, such as carbon nanotubes (CNTs), thus eliminating the disadvantages of metal-based materials [11], [12].

In order to avoid the limitations of using metal shields in EAV systems and other applications with similar requirements on weight, significant scientific efforts have been devoted to study polymer-based EMI composite performance [13], [14], [15], [16], [17]. These alternative shields are generally based on polymeric materials loaded with additives in such a way as to enable them to absorb EM energy. The additives can be electrically conductive and/or can have dielectric/magnetic properties significantly different from those of the polymeric matrix.

Thereby, the incorporation of either conducting or ferromagnetic particles can modify the electrical conductivity/permeability of the composite to obtain an effective reflection/absorption shield. Depending on the nature of the filler, the material response to incident EM waves can be linked to a specific mechanism or to a combination of many [16]. Different types of additives such as metal flakes, silicon carbide, titanium dioxide, zinc oxide, or talc particles have been reported in the literature, showing the effect of their size, shape, concentration, electrical resistivity, and dispersion degree in the host matrix on the EM properties. The investigation of lightweight EMI shielding materials will allow the possibility of increasing the safety of 5G communications in autonomous driving as well as improving the vehicle's consumption and autonomy [17].

Currently, there are many studies on the measurement and behavior of CNTs in which it is possible to see how the SE can vary depending on the frequency range and the selected material.

Several studies show measurements of about 13 dB at 10 wt% CNF loading [18]. Yang et al. [19] obtained a value of approximately 20 dB of MWCNT/PS (multiwalled CNTs/polystyrene) composites with an MWCNT loading of 7 wt%.

Other studies show the EMI SE of MWCNT/PP (multiwalled CNTs/polypropylene) composite as a function of MWCNT content and shielding plate thickness, where for a sample thickness of 1 mm and an MWCNT content of 5% and 7.5%, achieves an average SE value of 7.7 dB and 22.3 dB, respectively. The latter shows an increase with frequency, reaching the value of 19.7 dB at a frequency of 10 GHz [20]. In another work from 2013, there is a comparison of MWCNT/portland cement composites as a function of the concentration of MWCNTs in the X-band. In it, an SE between 7 and 10 dB is achieved for a sample of 3 wt%, and an SE greater than 27 dB is reported for a concentration of 15 wt% [21].

This contribution studies the shielding effectiveness (SE) provided by nanocomposites based on CNTs, one of the most commonly investigated additives in literature in the last few years. Thereby, this article describes the manufacturing procedure used in order to obtain the best dispersion in the material under test (MUT) [22], [23], [24]. Moreover, how the CNTs concentration modifies the electrical conductivity of the MUT and how this is related to SE is also analyzed. In particular, the performance of three CNT samples with different particles concentration is investigated, considering a portion of the 5G frequency region (up to 18 GHz), including the FR1 and part of the FR2 spectrum. The measurement procedure consists on measuring the SE of the different planar material specimens with a coaxial sample holder (CSH) based on the standard ASTM D4935-18 [25], [26].

This manuscript is organized as follows. First, Section II illustrates the selected shielding materials that are studied in this research. This section also describes the manufacturing process of the three samples. Section III defines the measurement setup used to determine the SE. Subsequently, the results obtained from the measurements are presented in Section IV. This section also analyses and discusses the performance of the three samples up to 18 GHz. Finally, the main conclusions of the research are summarized in Section V.

II. Shielding Materials Characterization

The selected materials and their manufacturing procedure are described in this section. CNT dispersion within the polymer matrix has a significant influence on the nanocomposite's final properties, including the electrical properties and the microwave susceptor capacity [27], [28]. Different processing parameters have been considered and which combination of them provides the best degree of dispersion in each sample. Finally, the electrical conductivity of the extruded samples is analyzed since higher electrical conductivity indicates a better ability to reduce interferences in the microwave frequency region [29], [30].

A. Definition of CNT Selected Materials

Graphene, graphite, and CNTs are the main allotropic structures of carbon used for the absorption of EM radiation [31].

CNT is a unique form of carbon filament/fiber, conceivable as a two-dimensional hexagonal lattice of carbon atoms rolled up to form a tubular structure with diameter in the scale of nanometers. The introduction of CNTs into a polymeric matrix increases the electrical conductivity as well as the permittivity of the material [32], [33]. This, in turn, results in an increase in the number of conductive links and, thus, to an improvement of the SE.

Since their discovery [34], the exceptional mechanical, electrical, and thermal properties of CNTs [35], [36] have made them potential candidates for high-tech applications. These structures are divided into two groups: single-walled CNTs (SWCNT) with a diameter even less than 1 nm and MWCNT, consisting of nested SWCNT weakly bound together by van der Waals forces, having an external diameter increasing with the number of shells and even on the order of several tens of nanometers [30], [37], [38]. The latter type has been selected for the current study.

Notice that carbonaceous particles-based materials are excellent for absorbing EM radiation, and then converting that energy into thermal one. These materials can show high values of the imaginary part of complex permittivity (ε'') and, therefore, also

TABLE I
LIST OF SAMPLES PRODUCED

Sample code	Description
CNT5	Sheet of polymer matrix + 5% CNT
CNT7	Sheet of polymer matrix + 7% CNT
CNT10	Sheet of polymer matrix + 10% CNT

high values of the loss tangent (tan δ). Carbonaceous particles absorb EM radiation due to the presence of delocalized π electrons, which can move freely [39], [40].

The samples manufactured for this research are based on polypropylene copolymer (coPP Moplen RP210G), properly selected due to its nonpolar nature and microwave transparency. The CNT nanocomposites were prepared by melt mixing procedure using a co-rotating twin-screw extruders. The effectiveness of the heating process was tested by paying particular attention to the filler dispersion [29], [41], [42].

Table I lists the three different samples evaluated in this contribution.

The intrinsic properties of the polymer nanocomposites depend directly on the number of microcapacitors and the polarization centers of the material.

An increase in CNT loading results in an increase in the relative permittivity and thus, in the number of these microcapacitors. In turn, the increase in CNTs increases the amount and mobility of charge carriers improving the electrical conductivity of the material, which is related to the improvement of the SE. Therefore, three samples with increasing CNT concentration have been chosen to observe how the amount of filler affects the SE [33], [43].

B. Sample Manufacturing and Processing Parameters

The manufacturing procedure is based on microwave technology, a high-energy-efficient fabrication method for producing plastic materials. The use of CNT as processing additive has a double functionality as they act as mechanical reinforcement and electrically conductive fillers.

The nanocomposites were obtained in a co-rotative twin screw extruder COPERION W&P ZSK25 as shown in Fig. 1. This extruder has a diameter of 25 mm and an L/D ratio of 40. Samples with different dispersion grades were produced by varying several processing parameters.

CNT dispersion within the polymer matrix has a significant effect on the final properties of the nanocomposite. For this reason, it is essential to reduce the presence of agglomerates, which could decrease the performance of the final nanocomposite in terms of mechanical, electrical, and thermal properties. The dispersion of CNTs highly depends on the nature of the polymer matrix. In some polar polymers such as polycarbonate [44], polyvinyl alcohol [45], and polyamide [46] CNTs are easily dispersed. However, polyolefins are considered the less suitable matrices to disperse CNTs. Despite that, good properties can be achieved by optimizing the processing conditions.

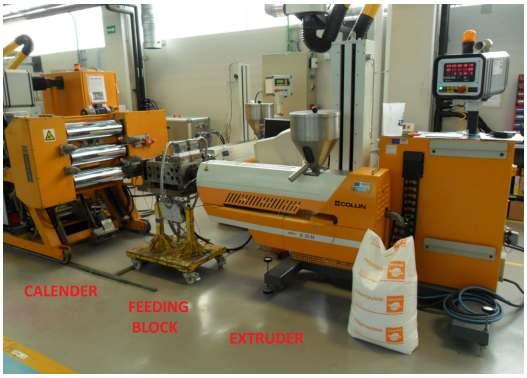

Fig. 1. Pilot plant cast-sheet coextrusion line.

TABLE II
PROCESSING PARAMETERS FOR CNT-BASED FORMULATIONS

Sample code	CNT5	CNT7	CNT10
Melt T (°C)	212	211	212
Pressure (bar)	72	82	100
rpm	85	90	90
Torque (N/m2)	4.9–25%	5.0–26%	5.3–26%
Drawing (%)	1.25	1.25	1.3
Die Gap (μm)	900	900	900
Rolls T (°C)	80	80	80
Sheet thickness (μm)	900	950	950

All the samples are processed through the same technology, sheet extrusion, and under the same conditions. Output parameters are differed due to the higher content of CNT, which increases the compound viscosity.

Table II summarizes the processing parameters of the extruder, optimized to maximize the degree of dispersion in the different CNT samples. The good quality of the resulting material based on CNT is observed in Fig. 2, where the sheet shows high homogeneity and a gleaming black piano surface.

C. Electrical Conductivity of Extruded Sheets at Pilot Plant

Nanocomposites characterized by a better filler dispersion generally exhibit more significant electrical properties than compounds in which MWCNT form bundles. The measurement of the dc electrical resistance is not only fundamental for evaluating the effect of the concentration of filler on the electrical properties of the material and therefore obtaining the percolation curve, but it is also useful for providing indications regarding the state of particle aggregation.

The manufactured sheets were cut to lower dimensions of 15 $\times$ 15 cm. The resistance between electrodes of all the sheets is studied in order to evaluate the relation between the electrical properties of the samples and their attenuation factor.

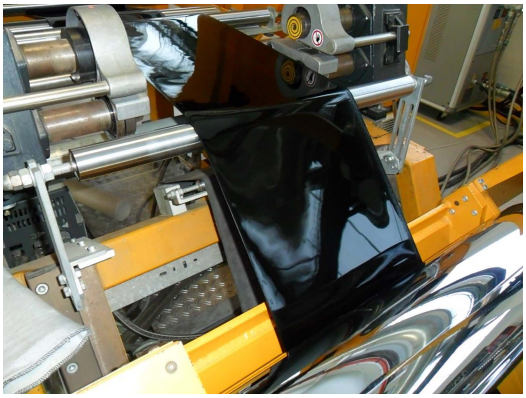

Fig. 2. Sheet production of coPP Moplen 210G + 7% CNT.

Tests on samples CNT5, CNT7, and CNT10 provided an electrical resistance of 540 Ω, 110 Ω, and 20 Ω, respectively. Then, based on the standard ISO 3915, the resistivity (ρ) of the samples is calculated according to the following equation:

$$\rho = R\frac{b}{l} \tag{1}$$

where b is the width of the electrodes in centimeters and l is the distance between them. It follows that CNT5, CNT7, and CNT10 have a conductivity of 0.0018 S/sq, 0.009 S/sq, and 0.05 S/sq, respectively.

III. SE Measurement Setup

There are several methods to measure the SE of planar materials, among which are the shielded-room variations derived from the standard MIL-STD 285 [47] and de IEEE 299 [48], the coaxial transmission line based-on methods [49], [50], time-domain measurements [51], transverse EM (TEM), and dual TEM approaches [52], [53], [54]. Currently, all these methods have different limitations when it comes to the measurement of planar materials, especially in terms of frequency limitation, but one of the most widely used is that described by ASTM D4935-18 [25].

The measurement method employed in this study is based on the test method described in ASTM D4935-18 standard that defines a procedure for measuring the EM SE of a planar material for a plane, far-field EM wave. The frequency range limits are based on decreasing displacement current as a result of decreased capacitive coupling at lower frequencies and on excitation of modes other than the TEM at higher frequencies for the size of the CSH. This procedure applies to the measurement of SE of planar materials under normal incidence, far-field, plane-wave conditions, considering E and H tangential to the surface of the material. Therefore, according to the ASTM D4935-18 standard, the measurement setup described in this contribution makes it possible to determine the net SE caused by reflection and absorption.

The method consists of measuring the insertion loss that results when introducing test samples in a coaxial two-conductor transmission line holder, supporting TEM propagation mode. Test methods based on the use of coaxial TEM cells for evaluating the SE of a material are based on the mathematical equivalence between the ideal case of an infinite planar shield placed in free space and illuminated orthogonally by a plane wave, and the case of a material sample inserted in a transmission line [55].

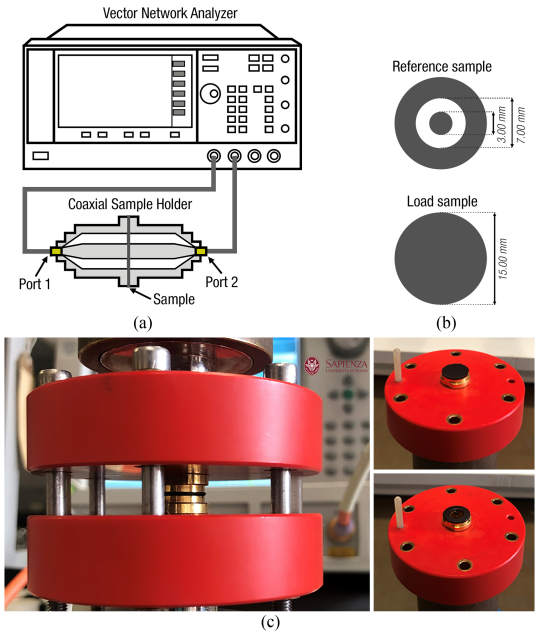

Fig. 3. Measurement procedure with the high-frequency CSH. (a) Sketch of the measurement test setup based on the ASTM D4935-18 procedure. (b) Shape and size of samples required for the SE measurement with the high-frequency CSH. (c) CSH with the MUT (load and reference specimens) for the SE measurements up to 18 GHz [26].

The test fixture of the ASTM D4935-18 consists of a two-port flanged CSH with a characteristic impedance of 50 Ω. Notice that the major limit of the standard's CSH concerns its operating frequency range, as the method allows the characterization of planar samples in a narrow band from 30 MHz to 1.5 GHz. The frequency limits are based on the decrease in current displacement due to capacitive coupling at very low frequencies and overmodulation at higher frequencies where the wavelength becomes comparable to the sample size [25].

A smaller and modified versions of the CSH based on the measurement procedure described in ASTM D4935-18 have been manufactured and described in [56], [26] to extend the measurements up to 18 GHz. Therefore, the coaxial sample holder of [26] has been used to evaluate the performance of the materials sample of Table I in part of the frequency region employed by 5G technologies.

The two halves of the CSH have been connected through coaxial cables to the two-ports of a vector network analyzer (VNA) for the measurement of the scattering parameters [Fig. 3(a)].

The used VNA (Anritsu VectorStar MS4647A, [57]) allows tests from 10 MHz up to 70 GHz with a dynamic range between 85 and 100 dB (depending on the frequency), but sufficient to measure the SE of the MUTs.

The sample holder is a coaxial probe with a characteristic impedance of 50 Ω. The diameter of the central conductor is 3 mm. The outer conductor has an inner diameter of 7 mm and an outer diameter of 15 mm, where it goes into contact with the MUT. The total contact area between the sample and the external conductor is only 138.23 mm^2.

The two cell sections are inserted into PVC supporting rings. To tighten the two halves together, either dielectric or metal screws can be used because being not electrically in contact with the cell's outer conductor [26].

The test requires two specimens of the same material and thickness, the reference, and the load. In particular, the load specimen has a disk-like shape with a diameter equal to that of the outer CSH flange; the reference specimen has two parts: a washer and a disk-shaped sample, matching the dimensions of the outer and inner conductors, respectively. Their dimensions are reported in Fig. 3(b). The use of two different specimens is justified because the reference one can partially compensate the effects of capacitive coupling by establishing a frequency-dependent reference level [15], [58].

The difference between the measurements of the load and the reference specimen provides the SE, caused by the reflection and absorption of the material sandwiched between the two flanges of the coaxial cell [Fig. 3(c)]. Hence, the SE in decibels can be expressed as follows:

$$SE = 20log_{10}\left|\frac{S_{21,R}}{S_{21,L}}\right| \quad (2)$$

where $S_{21,R}$ and $S_{21,L}$ are the measured transmission scattering parameter of the reference and load specimen, respectively.

IV. Results and Discussion

This section is focused on showing the results and comparison of the SE measurements carried out for the three CNT-based samples having different filler percentage compositions.

The sample manufacturing process can result in samples with different dispersion grades and homogeneities. Several samples have been taken from the same sheet to check how the dispersion grade affects the SE. In this way, is possible to verify that the dispersion of the material is good if the traces are similar to each other. Note that it has not been possible to take the same number of samples from all of the sheets, given the complexity of the mechanization to prepare the samples with the required dimensions when the CNT loading is increased.

First, Fig. 4 shows the SE provided by the CNT5 samples. It is observed that the traces are very close, indicating the good homogeneity of the composite and the reliability of the measurement system. The mean value obtained from the measurement of the CNT5 samples is 8.32 dB. In particular, at the frequency of 10 GHz, assumed from now on as a reference frequency, we have a SE value of 8.75 dB.

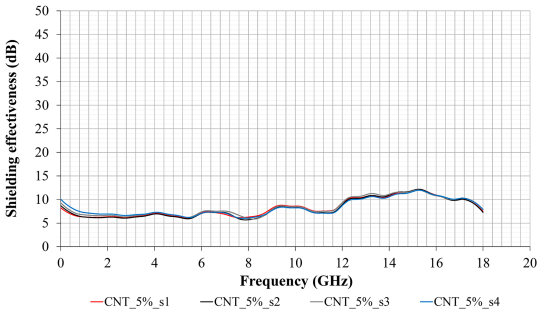

Fig. 4. SE results for different samples of the 5% CNT MUT.

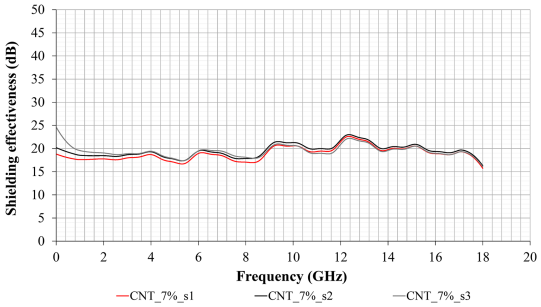

Fig. 5. SE results for different samples of the 7% CNT MUT.

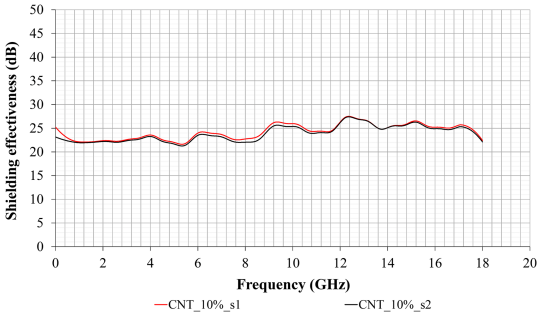

Fig. 6. SE results for different samples of the 10% CNT MUT.

Fig. 5 shows the results obtained by measuring three samples of the CNT7. As it can be observed, the responses of the different samples of this material are in good agreement with respect to each other. The most appreciable difference of about 6 dB can be observed in the low-frequency region. Above 8.50 GHz, the difference is negligible. In this case, the mean value is 19.29 dB; at the reference frequency of 10 GHz the SE value is 20.82. dB.

Fig. 6 shows the CNT10 SE results. In particular, two samples are measured: the two traces are significantly coincident and do not present considerable variations throughout the entire frequency range. The most notorious difference is appreciated

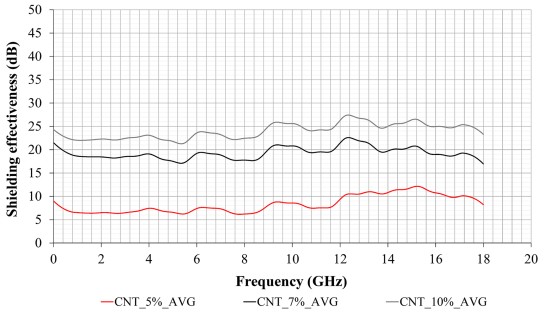

Fig. 7. SE results for CNT samples with the three different concentrations.

at the minimum frequency of 30 MHz, where the two traces differ by approximately 2 dB. The mean value obtained from the measurement of the CNT10 samples is 23.98 dB. A SE value of 25.60 dB is obtained at 10 GHz.

Fig. 7 shows the average curves, calculated using the different samples. response, for each CNT concentration. It can be clearly observed that as the CNT loading increases also the SE provided by the material increases. Moreover, excluding the low frequency data (i.e. up to a few hundreds of MHz) where generally, as known in the literature, the reference sample is not able to perfectly correct the measurement, and those close to the cut-off frequency of the guide, the general trend of the curves shows that the SE increases with increasing frequency due to absorption phenomena. The mean value obtained for the CNT5 trace corresponds to 7.95 dB and the difference between the global extrema (the maximum and minimum values of the curve in the considered frequency range) is 5.99 dB. For CNT7 sample the mean value is 19.21 dB and 5.63 dB is the maximum SE variation, lower than the one obtained for CNT5 sample. The mean for the CNT10 sample is 23.88 dB, with a variation of 6.16 dB between the global extrema.

The difference in CNT concentration between the CNT5 and CNT7 nanocomposite samples, which is 2%, results in an average SE increase of 11.26 dB. Instead, although the difference in concentration between the CNT7 and CNT10 samples is more significant (3% of CNT), the difference in SE is only 4.67 dB. This means, as expected that the SE does not increase linearly with the increase in concentration of CNTs. Nevertheless, it is confirmed that with a higher filler loading (CNT10), the electrical conductivity is improved and, therefore, the shielding effectiveness of the material increases.

Martínez et al. [4] compared in the frequency range of 300 kHz . 8 GHz several samples of a carbon fiber (CF) reinforced composite, changing the type of the inner layer of the material. In particular, the comparison between a sample with a multi-walled carbon nanotube (MWCNT) based-layer and a sample with a copper mesh layer is performed and the effects on the SE is analyzed. The samples were measured according to the ASTM D4935-18 standard. The results show that in the lower frequency range (up to 3 GHz), the MWCNT-based sample shows a better performance, resulting in a higher attenuation than that provided by the material with the copper mesh. At the frequency of 8 GHz, the latter sample provides an attenuation of 46.53 dB, whereas, the one with MWCNT fillers shows a value of 55.55 dB. In the intermediate frequency range, the responses are very similar, and the values are comparable. Those results suggest that MWCNTs are a good alternative to copper in EM shielding applications. In this contribution, for the CNT10 sample it is obtained an SE of 22.44 dB at 8 GHz. Notice that, since in this paper only the CNT-based load has been characterized, and not the final CF reinforced material, which alone, without the contribution of nanocomposite layer provides a significant attenuation, the result here obtained can be considered important and significant for many applications in the field of shielding.

The values obtained in other previous studies on the EM behavior of CNT-based materials are very different because the manufacturing process, and then, the obtained properties of the samples, have a significant influence on the final SE measurement. For example, it has been demonstrated that for a final MWCNT/PS composite sample loaded with 7wt% of MWCNT, a SE of 20 dB @ 10 GHz is obtained [21], whereas for a MWCNT/PP material with a concentration of 7.5wt% of MWCNTs the SE is 22.3 dB at the same frequency [22]. Comparing those values with the mean SE of 23.98 dB @ 10 GHz measured in this study for the CNT10 sample, it confirms that the obtained results present a considerable EM attenuation for the coPP + 10% CNT material. This improvement demonstrates that the manufacturing process employed allows to increase the amount of CNT in the final material while providing a good dispersion.

V. Conclusion

The performance of three nanocomposites based on the dispersion of nanotubes within a polymer matrix has been analyzed in terms of EMI shielding effectiveness. The characterization has been carried out covering the frequency range up to 18 GHz with the aim of investigating the behavior of this kind of materials to reduce EMI in systems sensitive to 5G technologies. The materials studied have been manufactured by introducing three different concentrations of CNTs in order to evaluate their performance by using a measurement setup based on the ASTM D4935-18.

It has been concluded that the amount of carbon nanotubes dispersed significantly influences the effective electrical conductivity of the composite, and consequently the SE of the material. If the electrical conductivity results are compared with the results obtained in terms of SE, it is possible to observe that higher electrical conductivity results in higher attenuation. In particular, the CNT7 and CNT10 nanocomposites have demonstrated to provide a significant SE in a wide frequency range. Nevertheless, there is no proportional relationship between the increase of the concentration of CNTs and the electrical conductivity, and then the mean value of SE.

It was also shown that, given the values obtained from previous studies on the measurement of SE of CNT-based composites, significant SE results were obtained in this study, which makes

these materials a suitable alternative to conventional solutions for the 5G frequency region in the EMC field.

Consequently, it should be noted that these types of characterizations are very relevant from a technological and industrial point of view. In particular, EMI shielding based on innovative nanocomposite materials has many advantages for automotive and related sectors, such as the manufacturing cost and weight reduction compared to traditional shielding.

REFERENCES

[1] K. A. Mcrae, "Electromagnetic shielding in today's environment," in *Proc. Nat. Conf. Publication, Inst. Eng.*, 1994, pp. 495–498.

[2] P. A. Martinez et al., "Design and study of a wide-band printed circuit board near-field probe," *Electronics*, vol. 10, no. 18, Sep. 2021, Art. no. 2201, doi: 10.3390/electronics10182201.

[3] J. Victoria, A. Suarez, P. A. Martinez, A. Alcarria, A. Gerfer, and J. Torres, "Improving the efficiency of NFC systems through optimizing the sintered ferrite sheet thickness selection," *IEEE Trans. Electromagn. Compat.*, vol. 62, no. 4, pp. 1504–1514, Aug. 2020, doi: 10.1109/TEMC.2020.3003800.

[4] P. A. Martinez et al., "Analysis of EMI shielding effectiveness for plastic fiber composites in the 5G sub-6 GHz band," in *Proc. IEEE Int. Joint EMC/SI/PI EMC Eur. Symp.*, 2021, pp. 278–283, doi: 10.1109/EMC/SI/PI/EMCEurope52599.2021.9559349.

[5] "DSM provides a full spectrum of engineering plastics for electronic applications in the connected car," *DSM Eng. Plastics*, Sep. 2017. [Online]. Available: https://www.dsm.com

[6] L. Zongwei, J. Hao, T. Hong, and Z. Fuquan, "An overview of the latest progress and core challenge of autonomous vehicle technologies," in *Proc. MATEC Web Conf.*, 2020, vol. 308, Art. no. 06002, doi: 10.1051/matecconf/202030806002.

[7] American Chemistry Council Plastics Division, "Vehicle lightweighting maintains safety," 2019. [Online]. Available: https://www.automotiveplastics.com/wp-content/uploads/Vehicle-Lightweighting-Maintains-Safety.pdf

[8] J. M. Thomassin, C. Jerome, T. Pardoen, C. Bailly, I. Huynen, and C. Detrembleur, "Polymer/carbon based composites as electromagnetic interference (EMI) shielding materials," *Mater. Sci. Eng.: R, Rep.*, vol. 74, no. 7, pp. 211–232, 2013, doi: 10.1016/j.mser.2013.06.001.

[9] J. Victoria et al., "Transmission attenuation power ratio analysis of flexible electromagnetic absorber sheets combined with a metal layer," *Materials*, vol. 11, no. 9, Sep. 2018, Art. no. 1612, doi: 10.3390/ma11091612.

[10] E. F. Vance and W. Graf, "The role of shielding in interference control," *IEEE Trans. Electromagn. Compat.*, vol. 30, no. 3, pp. 294–297, Aug. 1988, doi: 10.1109/15.3308.

[11] J. D. Sudha, S. Sivakala, R. Prasanth, V. L. Reena, and P. Radhakrishnan Nair, "Development of electromagnetic shielding materials from the conductive blends of polyaniline and polyaniline-clay nanocomposite-EVA: Preparation and properties," *Comp. Sci. Technol.*, vol. 69, no. 3/4, pp. 358–364, 2009.

[12] J. Kittur, B. Desai, R. Chaudhari, and P. K. Loharkar, "A comparative study of EMI shielding effectiveness of metals, metal coatings and carbon-based materials," *Proc. IOP Conf. Ser. Mater. Sci. Eng.*, vol. 810, no. 1, 2020, Art. no. 012019.

[13] M. H. Nisanci, F. de Paulis, D. Di Febo, and A. Orlandi, "Synthesis of composite materials with conductive aligned cylindrical inclusions," in *Proc. Prog. Electromagn. Res. Symp.*, 2012, pp. 27–30.

[14] A. Naseer et al., "Reinforcement of electromagnetic wave absorption characteristics in PVDF-PMMA nanocomposite by intercalation of carbon nanofibers," *Electron. Mater. Lett.*, vol. 15, pp. 201–207, 2019, doi: 10.1007/s13391-018-00104-9.

[15] K. Tserpes, V. Tzatzadakis, and J. Bachmann, "Electrical conductivity and electromagnetic shielding effectiveness of bio-composites," *J. Comp. Sci.*, vol. 4, no. 1, p. 28, 2020, doi: 10.3390/jcs4010028.

[16] M. I. C. Gomez, "Estudio del comportamiento de materiales cerámicos expuestos a un campo de microondas," Ph.D. dissertation, Microwave and Materials, Univ. of Nuevo Leon, Monterrey, Mexico, 2015.

[17] Freudenberg Sealing Technologies, "EMI shielding for thermoplastic housings," 2019. [Online]. Available: https://www.fst.com

[18] Y. Yang, M. C. Gupta, K. L. Dudley, and R. W. Lawrence, "A comparative study of EMI shielding properties of carbon nanofiber and multi-walled carbon nanotube filled polymer composites," *J. Nanosci. Nanotechnol.*, vol. 5, no. 6, pp. 927–931, 2005.

[19] Y. Yang, M. C. Gupta, K. L. Dudley, and R. W. Lawrence, "Novel carbon nanotube-polystyrene foam composites for electromagnetic interference shielding," *Nano Lett.*, vol. 5, no. 11, pp. 2131–2134, 2005.

[20] M. H. Al-Saleh and U. Sundararaj, "Electromagnetic interference shielding mechanisms of CNT/polymer composites," *Carbon*, vol. 47, no. 7, pp. 1738–1746, 2009.

[21] A. P. Singh et al., "Multiwalled carbon nanotube/cement composites with exceptional electromagnetic interference shielding properties," *Carbon*, vol. 56, pp. 86–96, 2013.

[22] Y. Li, H. Li, Z. Wang, and C. Jin, "Effect and mechanism analysis of functionalized multiwalled carbon nanotubes (MWCNTs) on C-S-H gel," *Cement Concrete Res.*, vol. 128, 2020, Art. no. 105955, doi: 10.1016/j.cemconres.2019.105955.

[23] I. W. Nam, S. M. Park, H. K. Lee, and L. Zheng, "Mechanical properties and piezoresistive sensing capabilities of FRP composites incorporating CNT fibers," *Comp. Struct.*, vol. 178, pp. 1–8, 2017, doi: 10.1016/j.compstruct.2017.07.008.

[24] B. Han, K. Zhang, and X. Yu, "Enhance the thermal storage of cement-based composites with phase change materials and carbon nanotubes," *J. Sol. Energy Eng.*, vol. 135, no. 2, 2013, Art. no. 024505, doi: 10.1115/1.4023181.

[25] *Standard Test Method for Measuring the Electromagnetic Shielding Effectiveness of Planar Materials*, ASTM International Std. D4935-18, 2018.

[26] A. Tamburrano, D. Desideri, A. Maschio, and M. Sabrina Sarto, "Coaxial waveguide methods for shielding effectiveness measurement of planar materials up to 18 GHz," *IEEE Trans. Electromagn. Compat.*, vol. 56, no. 6, pp. 1386–1395, Dec. 2014, doi: 10.1109/TEMC.2014.2329238.

[27] S. Gong, Z. H. Zhu, J. Li, and S. A. Meguid, "Modeling and characterization of carbon nanotube agglomeration effect on electrical conductivity of carbon nanotube polymer composites," *J. Appl. Phys.*, vol. 116, no. 19, 2014, Art. no. 194306, doi: 10.1063/1.4902175.

[28] I. Rodriguez-Pastor, H. Varela-Rizo, D. R. Bortz, G. Montes de Oca, I. Guinea, and I. Martin-Gullon, "Effects of processing and functionalization methods on nylon-6,6 nanocomposites with Helical-ribbon carbon nanofibers," *J. Appl. Polym. Sci.*, vol. 126, no. 4, pp. 1437–1448, 2012, doi: 10.1002/app.36758.

[29] B. Galindo, A. Benedito, F. Ramos, and E. Gimenez, "Microwave heating of polymers: Influence of carbon nanotubes dispersion on the microwave susceptor effectiveness," *Polym. Eng. Sci.*, vol. 56, no. 12, pp. 1321–1329, 2016, doi: 10.1002/pen.24365.

[30] S. Kuester et al., "Processing and characterization of conductive composites based on poly(styrene-b-ethylene-ran-butylene-b-styrene) (SEBS) and carbon additives: A comparative study of expanded graphite and carbon black," *Comp. B, Eng.*, vol. 84, pp. 236–247, 2016, doi: 10.1016/j.compositesb.2015.09.001.

[31] A. Aqel, K. M. M. A. El-Nour, R. A. A. Ammar, and A. Al-Warthan, "Carbon nanotubes, science and technology part (I) structure, synthesis and characterisation," *Arabian J. Chem.*, vol. 5, no. 1, pp. 1–23, 2012.

[32] P. Saini, "Electrical properties and electromagnetic interference shielding response of electrically conducting thermosetting nanocomposites," in *Thermoset Nanocomposites*. Weinheim, Germany: Wiley, 2013, pp. 211–237.

[33] P. Saini and M. Aror, "Microwave absorption and EMI shielding behavior of nanocomposites based on intrinsically conducting polymers, graphene and carbon nanotubes," in *New Polymers for Special Applications*. Rijeka, Croatia: InTech, 2012, pp. 73–112.

[34] S. Iijima, "Carbon nanotubes: Past, present, and future," *Phys. B, Condens. Matter*, vol. 323, no. 1–4, pp. 1–5, 2002, doi: 10.1016/S0921-4526(02)00869-4.

[35] R. H. Baughman, A. A. Zakhidov, and W. A. de Heer, "Carbon nanotubes–the route toward applications," *Science*, vol. 297, no. 5582, pp. 787–792, 2002, doi: 10.1126/science.1060928.

[36] J. E. Fischer et al., "Metallic resistivity in crystalline ropes of single-wall carbon nanotubes," *Phys. Rev. B, Condens. Matter.*, vol. 55, no. 8, pp. R4921–R4924, 1997.

[37] S. Iijima, "Helical microtubules of graphitic carbon," *Nature*, vol. 354, no. 6348, pp. 56–58, 1991.

[38] A. Oberlin, M. Endo, and T. Koyama, "Filamentous growth of carbon through benzene decomposition," *J. Cryst. Growth*, vol. 32, no. 3, pp. 335–349, 1976.

[39] P. Zhihua, P. Jingcui, P. Yanfeng, O. Yangyu, and N. Yantao, "Complex permittivity and microwave absorption properties of carbon nanotubes/polymer composite: A numerical study," *Phys. Lett. A*, vol. 372, no. 20, pp. 3714–3718, 2008, doi: 10.1016/j.physleta.2008.02.015.

[40] Z. Fan, G. Luo, Z. Zhang, L. Zhou, and F. Wei, "Electromagnetic and microwave absorbing properties of multi-walled carbon nanotubes/polymer composites," *Mater. Sci. Eng. B, Solid State Mater. Adv. Technol.*, vol. 132, no. 1/2, pp. 85–89, 2006, doi: 10.1016/j.mseb.2006.02.045.

[41] M. Wegrzyn, S. Juan, A. Benedito, and E. Giménez, "The influence of injection molding parameters on electrical properties of PC/ABS-MWCNT nanocomposites," *J. Appl. Polym. Sci.*, vol. 130, no. 3, pp. 2152–2158, 2013, doi: 10.1002/app.39412.
[42] T. Villmow, P. Pötschke, S. Pegel, L. Häussler, and B. Kretzschmar, "Influence of twin-screw extrusion conditions on the dispersion of multi-walled carbon nanotubes in a poly(lactic acid) matrix," *Polymer*, vol. 49, no. 16, pp. 3500–3509, 2008, doi: 10.1016/j.polymer.2008.06.010.
[43] B. P. Singh et al., "Designing of multiwalled carbon nanotubes reinforced low density polyethylene nanocomposites for suppression of electromagnetic radiation," *J. Nanoparticle Res.*, vol. 13, no. 12, pp. 7065–7074, 2011.
[44] C. Li, X.-J. Pang, and Z.-L. Yu, "Study on polycarbonate/multi walled carbon nanotubes composites produced by melt processing," *Mater. Sci. Eng., A*, vol. 457, pp. 287–291, 2007, doi: 10.1016/j.msea.2007.01.107.
[45] X. Zhang, T. Liu, T. V. Sreekumar, S. Kumar, X. Hu, and K. Smith, "Gel spinning of PVA/SWNT composite fiber," *Polymer*, vol. 45, no. 26, pp. 8801–8807, 2004, doi: 10.1016/j.polymer.2004.10.048.
[46] P. Pötschke, A. R. Bhattacharyya, A. Janke, and H. Goering, "Melt mixing of polycarbonate/multi-wall carbon nanotube composites," *Comp. Interfaces*, vol. 10, no. 4/5, pp. 389–404, 2003, doi: 10.1163/156855403771953650.
[47] MIL-STD-285, Attenuation measurements for enclosures, electromagnetic shielding, for electronic test purposes, method of, Pentagon, USA: DoD, Jun. 1956.
[48] "IEEE 299-2006," IEEE Standards Association, 2012. [Online]. Available: https://standards.ieee.org/ieee/299/3090/
[49] R. A. Weck, "Thin-film shielding for microcircuit applications and a useful laboratory tool for plane-wave shielding evaluation," *IEEE Trans. Electromagn. Compat.*, vol. EMC-10, no. 1, pp. 105–112, Mar. 1968.
[50] R. M. Simon and D. Stutz, "Test methods for shielding materials," *EMC Tech.*, vol. 2, pp. 39–48, 1983.
[51] A. R. Ondrejka and J. W. Adams, "Shielding effectiveness (SE) measurement techniques," in *Proc. IEEE Nat. Symp. Electromagn. Compat.*, 1984, pp. 249–253.
[52] R. D. Scheps, "Shielding effectiveness measurements using a dual TEM cell fixture," *EMC Tech.*, vol. 2, pp. 61–65, Jul.–Sep. 1983.
[53] P. F. Wilson and M. T. Ma, "Small aperture analysis of the dual TEM cell and an investigation of test object scattering in a single TEM cell," Tech. Note 1076, Nat. Bur. Stand., Boulder, CO, USA, Oct. 1984.
[54] A. L. Whitson and E. F. Vance, "Bolted lapped-joint EMP shields," Stanford Res. Inst. Int., Menlo Park, CA, USA, DNA 4472-F, Jun. 1977.
[55] S. A. Schelkunoff, *Electromagnetic Waves*. New York, NY, USA: Van Nostrand, 1943.
[56] M. S. Sarto and A. Tamburrano, "Innovative test method for the shielding effectiveness measurement of conductive thin films in a wide frequency range," *IEEE Trans. Electromagn. Compat.*, vol. 48, no. 2, pp. 331–341, May 2006, doi: 10.1109/TEMC.2006.874664.
[57] "*Vector star family of RF, µW, mmW VNAs MS4640A series*," Anritsu. [Online]. Available: https://www.anritsu.com/en-us/test-measurement/products/ms4640a-series
[58] T. W. Więckowski and J. M. Janukiewicz, "Methods for evaluating the shielding effectiveness of textiles," *Fibres Textiles*, vol. 14, no. 5, pp. 18–22, 2006.

Andrea Amaro (Student Member, IEEE) was born in Alicante, Spain, in 1998. She received the B.S. degree in electronics and telecommunications engineering in 2020 and the M.S. degree in electronics engineering in 2021 from the University of Valencia, Valencia, Spain, where she is currently working toward the Ph.D. degree in electronics engineering.

Since 2021, she has been working as a Researcher with the Electronics Engineering Department, University of Valencia. Her Ph.D. is related to the study of EMI shielding effectiveness in new alternative materials for mobility applications. She belongs to the EMC Society.

Adrian Suarez (Member, IEEE) received the B.S., M.S., and Ph.D. degrees in electronics engineering from the University of Valencia, Valencia, Spain, in 2013, 2014, and 2021, respectively.

From 2013 to 2015, he was a Research Assistant with the Design of Communication and Digital Systems Research Group, University of Valencia. Since 2015, he has been working as a Research Engineer with EMC Catedra University of Valencia-Würth Elektronik eiSos, Electronics Engineering Department, University of Valencia. Since 2017, he worked as an Adjunct Professor with the Electronics Engineering Department, University of Valencia. His research interests include the advanced characterization of shielding materials and the study of cable filtering materials based on conventional ceramics and nanocrystalline compositions.

Prof. Suarez collaborates in the P2715 of the Standard Development Committee of the IEEE EMC Society intended for write a guide for the characterization of the shielding effectiveness of planar materials.

Alessio Tamburrano (Senior Member, IEEE) received the Laurea degree (*summa cum laude*) in electrical engineering, the master's degree in electromagnetic compatibility and environmental impact of electromagnetic fields, and the Ph.D. degree in electrical engineering from the Sapienza University of Rome, Rome, Italy, in 2003, 2005, and 2007, respectively.

In 2022, he was appointed as a Full Professor of Electrotechnics with the Sapienza University of Rome. He is currently with the Department of Astronautical, Electrical and Energy Engineering (DIAEE), University of Rome "La Sapienza." His research activity has led to the publication of more than 100 articles in international journals and proceedings of international symposia. He is also the coauthor of 10 patents. His scientific production includes two chapters' contributions in books. His current research interests include modeling, design, and experimental characterization of nanostructured and multifunctional materials for electromagnetic applications; development of graphene-based highly sensitive piezoresistive paints/coatings and porous nanocomposites with strain sensing capabilities for structural health monitoring and wearable electronics applications; and modeling and simulation of the transmission-line performances and signal integrity of nanointerconnects made of single-wall carbon nanotube bundles, multiwall carbon nanotubes, and graphene nanoribbons for future high-speed electronics.

Dr. Tamburrano received several awards from IEEE. From 2013 to 2017, he served as the Chair of the Technical Committee of the IEEE EMC Society TC-11 "Nanotechnology and Advanced Materials." From 2010 to 2014, he was the Project Leader of the Joint Project Team 80004-9—Nanotechnologies—Vocabulary—Part 9: Electrotechnical products and systems of the International Electrotechnical Commission (IEC). Since 2016, he has been a Member of the Working Group P 2715—IEEE guides for the characterization of the shielding effectiveness of planar materials. He is also a Steering Committee Member of the Research Center on Nanotechnology applied to Engineering of Sapienza (CNIS).

Jose Torres (Senior Member, IEEE) received the B.S., M.S., and Ph.D. degrees in electronics engineering from the University of Valencia, Valencia, Spain, in 2000, 2000, and 2005, respectively.

From 2013 to 2015, he was a Research Assistant with the Design of Communication and Digital Systems Research Group, University of Valencia. Since 2015, he has been working as a Research Assistant with EMC Catedra University of Valencia-Würth Elektronik eiSos, Electronics Engineering Department, University of Valencia, Valencia. Since 2005, he worked as an Associate Professor with the Electronics Engineering Department, University of Valencia. He has been part of more than 20 national and international projects as a researcher and coordinator. He is the coauthor of more than 30 scientific papers and a reviewer of several IEEE journals. His research interests include signal integrity design, FPGA-based read-out systems for high-energy physics and IoT system development, and EMI management in embedded systems.

Dr. Torres collaborates in the Spanish Association of Telecommunications Engineers and he is the Co-Director of the EMC Catedra University of Valencia-Würth Elektronik eiSos.

Fabrizio Marra received the three-year degree in computer engineering, the master's degree in nanotechnology engineering, and the Ph.D. degree in materials engineering, technologies, and complex industrial systems from the Sapienza University of Rome, Rome, Italy, in 2009, 2012, and 2015, respectively.

During his Ph.D. degree, he was a Visiting Researcher with the Institute of Science and Technology of Polymers (CSIC-ICTP), Madrid, Spain. Since November 2016, he has been with the Department of Astronautics, Electrical and Energy Engineering (DIAEE), Sapienza University of Rome, and the Research Center on Nanotechnology Applied to Engineering CNIS, as the Technical Manager of the Rheology Laboratory and Electroreology. He is currently a Research Fellow with the Department of Astronautics, Electrical and Energy Engineering, Sapienza University of Rome, and CNIS. His scientific activity is mainly focused on the development of electromagnetic materials, absorbing radar materials, and deformation sensors.

Pedro A. Martinez (Member, IEEE) was born in Valencia, Spain, in 1979. He received the B.S. and M.S. degrees in electronics engineering in 2013 from the University of Valencia, Valencia, Spain, where he is currently working toward the Ph.D. degree in electronics engineering.

From 2012 to 2016, he was a Research Assistant with the Design of Communication and Digital Systems Research Group, University of Valencia. Since 2016, he has been working as a Research Assistant with EMC Catedra University of Valencia-Würth Elektronik eiSos, Electronics Engineering Department, University of Valencia, Valencia. Since 2018, he worked as an Adjunct Professor with the Electronics Engineering Department, University of Valencia. His research interests include the advanced characterization of shielding materials and the study of cable filtering materials based on conventional ceramics and nanocrystalline compositions.

Prof. Martinez collaborates in the IEEE EMC Society through the Technical Committee 4 for EMI Control.

Begoña Galindo received the Ph.D. degree in industrial engineering and production from the Polytechnical University of Valencia, Valencia, Spain.

Since 2005, she has been a Senior Researcher with the Compounding Department, AIMPLAS, Valencia, Spain. She is a flame retardant research group coordinator and has active participation in nanomaterials and plastronic research groups. She is the Principal Investigator of many regional, national, and European projects. She is currently working with the Leaders of Future and Sustainable Mobility Department, AIMPLAS. Moreover, she is coordinating the fire retardant research groups and the excellence science project in which low TRL developments are brought near to industrial level. As a result of the research activities ten scientific publications, four patents, and nine contribution to scientific seminars were submitted. Her research fields include nanocomposites, flame-retardants, long fiber reinforced thermoplastics, biopolymers, and conductive composites.

Neus Soriano received the Chemical Industrial Engineering degree from the Universidad Politécnica de Valencia, Valencia, Spain.

Since 2007, she has been working as a Technician with the Physical-Mechanical Laboratory, AIMPLAS, Valencia, Spain and as the Head of the laboratory since 2016. Since 2021, she has been a Characterization Group Leader. She has worked in the field of physical and mechanical test on plastics and composite materials, technical assistance in quality control of raw materials and finished products, validation of new materials, evaluation of causes of failure, behavior of products, and investigation in national and international projects focused in biotechnologies, biocomposites, composites, building application, automotive application, coatings, packaging, and innovation.

Jorge Victoria (Member, IEEE) received the Laurea degree in electrical engineering in 2005 from the University of Valencia, Valencia, Spain, where he is currently working toward the Industrial Ph.D. degree in electronics engineering.

From 2006 to 2012, he worked as EMC and Project Manager for Electromedical Devices at the research institute in Biomechanics of Valencia (IBV). Since 2013, he is the Division Manager for EMC Shielding Materials at Würth Elektronik eiSos. Since 2014, he is the Co-Director of the EMC Catedra University of Valencia-Würth Elektronik eiSos. His research interests include the advanced characterization of shielding materials to manage EMI interferences, specifically those based on magnetic sheets such as sintered ferrite sheets or noise suppression absorbers.

Mr. Victoria has collaborated in the IEEE EMC Society through the Special Committee 1 for Smart Grid.

Antonio Alcarria (Member, IEEE) was born in Cuenca, Spain, in 1992. He received the B.S. and M.S. degrees in electronics and telecommunications engineering in 2018 from the University of Valencia, Valencia, Spain, where he is currently working toward the Industrial Ph.D. degree in electronics engineering.

Since 2015, he has specialized in the Research, Design, and Development on the field of the Electromagnetic Compatibility working since 2015 with EMC Catedra University of Valencia-Würth Elektronik eiSos, a collaboration researching between Würth Elektronik and the University of Valencia. In November 2017, he also joined the main headquarter of Würth Elektronik as EMC Product Manager combining his main job in the company with the research in the EMC Catedra University of Valencia-Würth Elektronik eiSos. His research interests include the advanced characterization of shielding materials to manage EMI interferences, specifically those based on magnetic sheets such as sintered ferrite sheets or noise suppression absorbers.

4.2 Summary

The results presented in this chapter confirm that coaxial transmission line methods can be successfully adapted to operate in the microwave frequency range through miniaturization of the test fixture. The configuration used enabled accurate and repeatable shielding effectiveness measurements up to 18 GHz with small planar samples. This approach offers a practical alternative for materials that cannot be characterized with standard ASTM-based setups due to sample geometry constraints. However, the method remains restricted to flat and relatively rigid materials that can be shaped to fit the fixture. For more complex geometries or flexible composites, alternative measurement approaches are required. The following chapter introduces a non-standard method based on an Absorber Box configuration, aimed at addressing these challenges.

This chapter contributes directly to S.O.2 and S.O.4, by applying a derived method to the characterization of nanostructured materials and validating its performance in terms of sensitivity, repeatability, and traceability. Additionally, the analysis of the electromagnetic behavior across the frequency range and the physical rationale for the probe miniaturization support the S.O.5, by providing insights into the underlying mechanisms that govern the method's performance. The limitations encountered in coaxial configurations also support the motivation for exploring non-standardized approaches for cases where coaxial geometries are no longer feasible, paving the way for the method introduced in Chapter 5.

Chapter 5. Non-Standardized Shielding Characterization of Complex Planar Materials

This chapter presents the implementation of a non-standardized shielding effectiveness measurement method based on an Absorber Box *configuration. The approach is applied to fiber-reinforced nanocomposites with rigid and complex geometries, which cannot be reliably characterized using coaxial fixtures. The work was developed in collaboration with AIMPLAS within the framework of the SMART5G project.*

5.1 Scientific article II

Title: Shielding Effectiveness Measurement Method for Planar Nanomaterial Samples Based on CNT Materials up to 18 GHz

Authors: Andrea Amaro, Adrian Suarez, Jose Torres, Pedro A. Martinez, Roberto Herraiz, Antonio Alcarria, Adolfo Benedito, Rocio Ruiz, Pedro Galvez and Antonio Penades

Published in: Magnetochemistry 2023, 9(5), 114. Special Issue: Magnetic Materials, Thin Films and Nanostructures. 25 April 2023

DOI: 10.3390/magnetochemistry9050114

Impact factor (2023): JCR: 2.6

Quartile (2023): JCR: Q2 (20/44) (CHEMISTRY, INORGANIC & NUCLEAR)

Citations: 7 (WoS, accessed on 14 July 2025).

Description: Magnetochemistry (ISSN 2312-7481; CODEN: MAGNCZ) is a peer-reviewed, open-access journal covering all areas of magnetism and magnetic materials. It is published monthly online by MDPI since 2015, accepting research articles, short communications, and reviews. The journal focuses on fundamental and applied aspects of magnetochemistry, including molecular magnetism, spin crossover, magnetic nanoparticles, and magnetic resonance. The impact factor, quartile, and rank information were obtained from the Journal Citation Reports (JCR) and SCImago Journal Rank (SJR) databases, based on the 2023 publication year. Citation metrics have been consulted in the Web of Science database.

Synopsis:

The increasing demand for electromagnetic shielding materials compatible with high-frequency applications, particularly in the context of 5G communications, has motivated the development of multifunctional polymer-based composites reinforced with carbon nanotubes. These materials offer a compelling alternative to traditional metal-based shielding, as they enable the design of lightweight, corrosion-resistant, and easily processable components. However, as the complexity of the composite systems increases, particularly with the addition of structural reinforcements such as carbon or glass fibers, the fabrication and characterization of test specimens becomes more challenging. In particular, the sample geometries required by standard or modified coaxial test fixtures are often incompatible with rigid or fiber-reinforced compounds, due to difficulties in precise machining and geometric tolerances.

In this context, this chapter presents the evaluation of the electromagnetic shielding performance of a series of CNT-based composites, manufactured using acrylonitrile butadiene styrene (ABS) as the matrix material and incorporating different concentrations of multi-walled carbon nanotubes, as well as carbon and glass fiber reinforcements. To overcome the limitations of conventional measurement methods, a dedicated Absorber Box setup was developed. This system enables the characterization of shielding effectiveness over a frequency range of 700 MHz to 18 GHz using standard-size, flat samples, eliminating the need for complex shaping or edge conditioning. The measurement principle is based on a vertical transmission configuration with horn antennas and internal absorbers, offering a controlled environment with a dynamic range suitable for high-attenuation materials.

The study demonstrates that the shielding effectiveness improves with CNT concentration, reaching values above 80 dB at 7.125 GHz for the most heavily loaded sample. More importantly, the results confirm that the incorporation of carbon fiber reinforcement significantly enhances shielding performance even at lower filler contents, due to the intrinsic conductivity of the fibers and their synergistic interaction with the polymer matrix. The Absorber Box method proved to be a robust and repeatable technique for evaluating complex samples that cannot be assessed using traditional coaxial fixtures. The findings underscore the importance of selecting appropriate measurement methods based on material characteristics and reinforce the potential of hybrid composites as practical shielding solutions for next-generation electronic platforms.

magnetochemistry

MDPI

Article

Shielding Effectiveness Measurement Method for Planar Nanomaterial Samples Based on CNT Materials up to 18 GHz

Andrea Amaro [1,*], Adrian Suarez [1], Jose Torres [1], Pedro A. Martinez [1], Roberto Herraiz [1], Antonio Alcarria [2], Adolfo Benedito [3], Rocio Ruiz [3], Pedro Galvez [3] and Antonio Penades [3]

[1] Department of Electronic Engineering, University of Valencia, 46010 Burjassot, Spain; adrian.suarez@uv.es (A.S.); jose.torres@uv.es (J.T.); pedro.a.martinez@uv.es (P.A.M.); roberto.herraiz@uv.es (R.H.)
[2] Würth Elektronik eiSos GmbH & Co. KG, 74638 Waldenburg, Germany; antonio.alcarria@we-online.de
[3] AIMPLAS Technological Institute of Polymers, 46980 Valencia, Spain; abenedito@aimplas.es (A.B.)
* Correspondence: andrea.amaro@uv.es

Abstract: The study and measurement of the shielding effectiveness (SE) of planar materials is required to predict the suitability of a certain material to form an enclosed electromagnetic shield. One of the most widely used standards for measuring the SE of planar materials is ASMT D4935-18. It is based on a coaxial sample holder (CSH) that operates up to 1.5 GHz. Due to this standard's frequency limitations, new variants with higher frequency limits have been developed by decreasing the size of the CSH conductors and the samples. However, this method and its high-frequency variants require two types of samples with very specific geometries and sizes. This method is unsuitable for certain types of nanomaterials due to their complex mechanization at such undersized scales. This contribution proposes an alternative SE measurement method based on an absorber box that mitigates the problems presented by the ASTM D4935-18 standard. The SE of rigid nanomaterial samples based on several concentrations of multi-walled carbon nanotubes (MWCNT) and two different fiber reinforcements have been obtained.

Keywords: shielding effectiveness (SE); nanomaterials; absorber box; electromagnetic compatibility (EMC)

Citation: Amaro, A.; Suarez, A.; Torres, J.; Martinez, P.A.; Herraiz, R.; Alcarria, A.; Benedito, A.; Ruiz, R.; Galvez, P.; Penades, A. Shielding Effectiveness Measurement Method for Planar Nanomaterial Samples Based on CNT Materials up to 18 GHz. *Magnetochemistry* **2023**, *9*, 114. https://doi.org/10.3390/magnetochemistry9050114

Academic Editor: Cătălin-Daniel Constantinescu

Received: 24 March 2023
Revised: 21 April 2023
Accepted: 23 April 2023
Published: 25 April 2023

1. Introduction

The fast-paced advancements in electronic devices, information technology, wearable devices, and 5G technology have significantly increased electromagnetic interference (EMI) and radiation pollution [1]. This has required developing new materials with advanced shielding capabilities to reduce the effects of EMI. Developing this kind of material aims to increase the security of sensitive devices or systems that can be susceptible to EMI. Moreover, new advanced materials must ensure the protection of human health to reduce the risk of problems derived from exposure to electromagnetic radiation. Consequently, there is a high demand for advanced materials that can significantly address the challenges posed by EMI.

The investigation of lightweight EMI shielding materials will allow the possibility of increasing safety in 5G communications. When it comes to shielding materials, one of the most determining parameters for the application of the material is shielding effectiveness (SE). The SE indicates the attenuation intensity experimented by an electromagnetic wave traveling through a medium, A, after interacting with a medium, B (shield).

Magnetic materials, which are the main ones responsible for magnetic losses, achieve electromagnetic wave (EMW) absorption through magnetic hysteresis loss, eddy current effects, and ferromagnetic resonance [2–4]. Ferrites are widely used as EMW absorbers due to their high magnetic permeability, saturation magnetization (Ms), and resistivity (Ω), as well as a significant flexibility that allows the modification of their chemical composition to

adapt their magnetic properties to specific applications [5–7]. A recent study evaluated the efficiency of magnetostatic protection using nanostructured permalloy shielding coatings, demonstrating their potential for enhancing the shielding efficiency of electronic devices achieving a maximum SE value of 29 dB [8]. On the other hand, carbonaceous materials (e.g., carbon nanotubes (CNT), MXenes, or graphene foams) are excellent candidates for enhancing the absorption of the incident EMW due to their interesting electromagnetic and molecular properties, such as a unique combination of high conductivity and low density [9,10]. Specifically, multi-walled carbon nanotubes (MWCNTs) possess a shielding effect against EMI owing to their conductivity and unique internal porous structure and morphology. Consequently, they are an excellent and cost-effective choice for the primary material in composites. Moreover, the availability of specific heteroatomic groups in MWCNTs makes them suitable for convenient modification in subsequent applications. The combination of high conductivity and the presence of numerous internal interfaces because of either their porous structure or molecular arrangement enhances the dielectric loss through interfacial polarization. This also introduces an additional absorption mechanism based on multiple reflections, consisting of the continuous reflection of the incident wave in the different interfaces of the particle; thus, enhancing the attenuation of the EMW reflections [9,11]. The dispersion of carbonaceous particles in a polymer matrix, either thermoplastic or thermosetting, entails the improvement of the SE capabilities of the matrix [12] This allows the obtaining of specific compounds for lightweight applications overcoming the limitations of metals in terms of high density and corrosion susceptibility. Increasing the content of carbonaceous particles was found to have a positive effect on the SE of the resulting compound, achieving a maximum absorption of −38 dB in the X-band with 5% wt MWCNTs [13] and −66 dB for a polystyrene (PS) compound containing 20% wt MWCNT obtained via compression molding [14].

However, further increasing the content of carbon fillers also entails the increment of the compound viscosity and, therefore, hinders its processability, as noted in [15]. Fiber-reinforced polymer (FRP) composite materials are characterized by their heterogeneity and anisotropy, which imparts to them the property of not exhibiting plastic deformation. FRP composites have found widespread use in a diverse range of contemporary applications, such as space, aviation, and automotive. Carbon-fiber-reinforced polymer (CFRP) and glass-fiber-reinforced polymer (GFRP) composite materials, among other fiber-reinforced materials, have gained increasing popularity due to their outstanding strength and low specific weight properties, leading them to replace conventional materials in various applications [16]. The use of CFRP is a prominent alternative to address the manufacturing problems derived from the use of particle-based composites [17]. Although recent studies have demonstrated the feasibility of using woven prepreg laminates to produce shielding effectiveness of more than 100 dB at low frequencies (<1 GHz) [18], the specific contribution of each type of shielding mechanism and the effect of the typology of the fibers at higher frequencies remains an open question. Suitable compositions and orientation of fibers made desired properties and functional characteristics of some GFRP composites equal to steel, had higher stiffness than aluminum, and the specific gravity was one-quarter of the steel [19]. Martinez et al. performed SE measurements in the frequency range of 300 kHz–8 GHz on GF composites in combination with different conductive materials, such as MWCNT and copper mesh, reporting an attenuation of approximately −40 dB up to 1.5 GHz for the copper mesh case [20]. Another study investigated the EMI shielding performance of carbon-nanomaterial-embedded fiber-reinforced polymer composites, revealing that the EMI shielding effectiveness of the composites was significantly improved with the addition of carbon nanomaterials. A sample with 3% CNT-GNP CFRP composition demonstrated an EMI shielding effectiveness higher than 15 dB [21].

To evaluate the suitability of these novel shielding materials for integration into a 5G system or other high-frequency applications, it is necessary to perform a characterization of their SE. Due to the wide variety of applications and shapes that a shielding material can adopt, this is generally characterized as a planar material. Depending on the frequency

range where the material will operate, there are various measurement methods to determine their shielding effectiveness. Currently, the most widely used standard for measuring the effectiveness of shielding of planar materials is the ASTM D4935-18 standard [22]. However, this standard is limited in frequency to 1.5 GHz, making it significantly restricted when considering 5G technology that operates at much higher frequencies. Alternative measurement methods based on free-space measurements, such as the IEEE 299 standard, are available but are hindered by the complexity of measurement due to the dimensions of the material sample required and the infrastructure required to perform the measurements [23]. Considering these limitations, alternative measurement methods derived from existing standards are currently being developed to address these issues.

In this work, the proposed measurement method is based on an absorbing box that overcomes the limitations that standard methods present. This method eliminates the sample size and mechanization issue, as it does not require a sample that is either too large or too small. Additionally, it makes it possible to measure in a frequency range that goes further than the region defined by the method presented in the ASTM D4935-18 standard. Furthermore, this method mitigates the problems of surrounding influences as measurements are taken within a controlled, absorbing environment. The results of EMI shielding effectiveness of the developed samples are reported in the frequency range of 700 MHz–18 GHz, covering the sub-6 GHz band of the 5G spectrum and part of the mmWave band.

This manuscript is organized as follows. First, Section 2 describes the manufacturing process of the five samples and their most relevant characteristics. Section 3 illustrates the main planar material measurement methods. This section also describes the current standard methods, their limitations, and the non-standardized measurement techniques. In this section, it is described the measurement setup to determine the SE of the different samples. Subsequently, the obtained results are presented in Section 4. This section also discusses the performance of the samples in the entire frequency range in terms of the attenuation that they provide. Finally, the main conclusions obtained in this research are summarized in Section 5.

2. Material Characterization

2.1. Material Selection

Before thermoplastics were extended, thermosets were widely used for various applications. However, as the industry evolves, thermosets have some serious limitations. When heating a thermoset once, it becomes irreversibly hardened when cured due to heating. Once cured, a thermoset plastic cannot be modified in shape by applying heat or pressure because the curing process has set a permanent chemical bond. The only way to break that chemical bond is by exposing it to a high-temperature source where the thermoset plastic is burned off. Hence the recyclability is zero compared to thermoplastic polymers, which can be repeatedly heated and remolded into desired shapes or forms [24].

Acrylonitrile butadiene styrene (ABS) is an amorphous thermoplastic copolymer built by polymerizing styrene and acrylonitrile in the presence of polybutadiene. The combination of the three confers to ABS a wide range of characteristics, such as impact resistance, toughness, heat resistance, or weather and chemical resistance [24]. ABS is widely used in the plastic industry for modern processes such as plastic injection molding for end products such as protective housings, stiff packaging, and structurally robust parts, as well as in the production of polymer blends, such as polycarbonate + ABS or polyamide + ABS, and can be regularly found in the automotive sector [25–27]. Additionally, the use of ABS has also been reported for EMI shielding applications throughout the manufacturing of ABS/MWCNT compounds, due to its processability and dimensional stability [28,29]. Raw ABS 118HF pellets supplied by Elix Polymers are used in this study in the production of seven samples containing different MWCNT concentrations and reinforcements. These samples are summarized in Table 1. A CNT Masterbatch from Nanocyl, the Plasticyl ABS1501, is used to manufacture Sample 7.

Table 1. List of samples.

Sample ID	Description	Particle Type	Particle Percentage
1	ABS	NA [1]	NA
2	ABS + 5% CNT	MWCNT	5%
3	ABS + 10% CNT	MWCNT	10%
4	CF LFP ABS + 3% CNT	MWCNT	3%
5	GF LFP ABS + 3% CNT	MWCNT	3%
6	2 × CF LFP ABS + 3% CNT	MWCNT	3%
7	MB [2] ABS + 15% CNT	MWCNT	15%

[1] NA: Not applicable. [2] MB: Masterbatch

2.2. Samples Manufacturing

The samples studied to determine their SE to prevent EMI has been manufactured following a two-step process encompassing the production of the raw thermoplastic compounds and the subsequent obtention of the testing samples. The compounding stage included using an extruder setup with ABS/CNT pellets and a thermoplastic pultrusion line for LFP production. Finally, the samples underwent compression molding to produce the final rectangular specimens.

2.2.1. Compounding

The initial stage consists of obtaining the raw compounds used in manufacturing the testing samples. These initial compounds carry diverse concentrations of multi-walled carbon nanotube (MWCNT) particles. Furthermore, a sample consisting of 100% raw ABS (Sample 1) allowed the definition of a minimum reference value of EMI shielding. The compounds are obtained following three different and independent techniques.

The compounds used in the manufacturing of Samples 2 to 5 are produced by means of a PRISM 16 L/D 25 twin screw extruder and located at the compounding facilities at AIMPLAS (Figure 1a). In this process, ABS pellets and particles are fed together into the extruder via a specific hopper. During the extrusion process, the raw materials are mixed due to the effect of temperature and the shearing forces exerted by the twin screws. Taking into consideration 240 °C as the processing temperature of the ABS matrix used, a flat temperature profile of 260 °C is settled to process the compounds to ensure good processability of the materials (Table 2). Then, at the end of the extruder, a continuous filament with a pre-defined diameter is obtained and cooled down. Finally, a cutting unit located at the end of the setup generates the ABS/CNT pellets with the desired length.

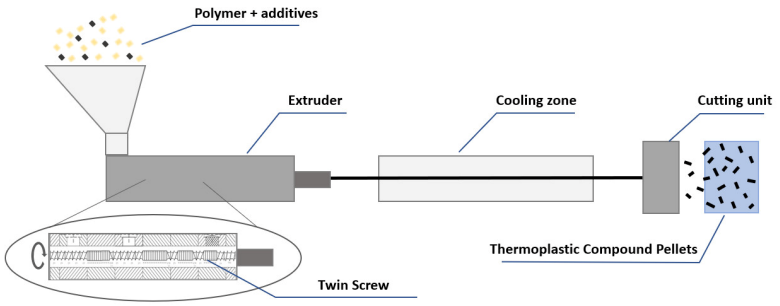

(**a**)

Figure 1. *Cont.*

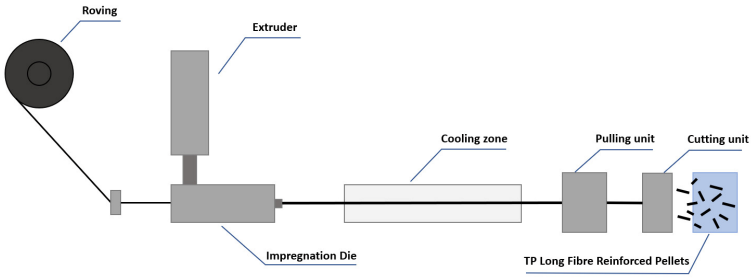

(**b**)

Figure 1. Compounding process. (**a**) Schematic of the extruder setup. (**b**) Schematic of the LFP production line.

Table 2. Extrusion parameters.

EXTRUSION PARAMETERS										
FEEDER	**EXTRUSION ZONE**		**TEMPERATURE PROFILE**							
SET POINT (Kg/h)	**SCREW (RPM)**	**PRESSURE (bar)**	**ZONE 1 (°C)**	**ZONE 2 (°C)**	**ZONE 3 (°C)**	**ZONE 4 (°C)**	**ZONE 5 (°C)**	**ZONE 6 (°C)**	**ZONE 7 (°C)**	**ZONE 8 (°C)**
1	200	8.2	260	260	260	260	260	260	260	260

Long fiber pellets (LFP) are produced in a thermoplastic pultrusion line developed by AIMPLAS, allowing Ø4 mm unidirectional threads of glass or carbon fiber impregnated by the ABS/CNT compounds previously developed (Figure 1b). In this process, the pellets produced in the previous step are fed to the same extruder described previously in order to melt the polymer and facilitate the subsequent impregnation of the fiber. A temperature profile of 270 °C is used to process the ABS/CNT compound in the extruder to ensure good processability and further fiber impregnation. The resulting melted polymer matrix compound is then transferred to the impregnation die to impregnate the fiber thread effectively. The continuous thread of thermoplastic impregnated fiber leaving the impregnation die at a rate of 600 g/h is cooled down and cut into 12 mm pellets reinforced with oriented and continuous either carbon or glass fiber. The resulting carbon and glass LFP are used to manufacture Samples 4 and 5, respectively.

2.2.2. Compression Molding

Following the production of the pellets, rectangular specimens of dimensions 210 mm × 297 mm × 2 mm are obtained (Figure 2) via compression molding using a CUYMA PH1000 hot press. In this process, the pellets obtained in Section 2.2.1 are placed in a mold of pre-defined dimensions and located between two rigid and hot plates. The effect of the temperature and pressure upon the closure of the mold induced the melting of the pellets and obtaining testing samples with the required dimensions (Figure 3). For all specimens, the temperature is kept constant at 250 °C through the entire compression cycle, which accounted for an initial force of 60 kN for 5 min, followed by an increase in the force to 100 kN and holding for 10 min (Table 3).

Seven testing samples are produced, one per each type of compound. An additional specimen is produced with the same formulation as used for the manufacturing of Sample 6. Coupling these two specimens together (Sample 7) would shed light on the relationship between the increase in the thickness by a factor of 2 and the EMI shielding.

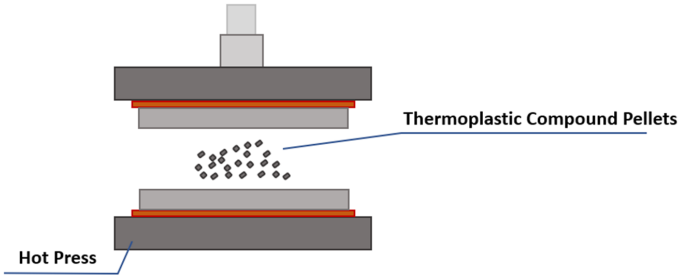

Figure 2. Schematic of the hot press molding process.

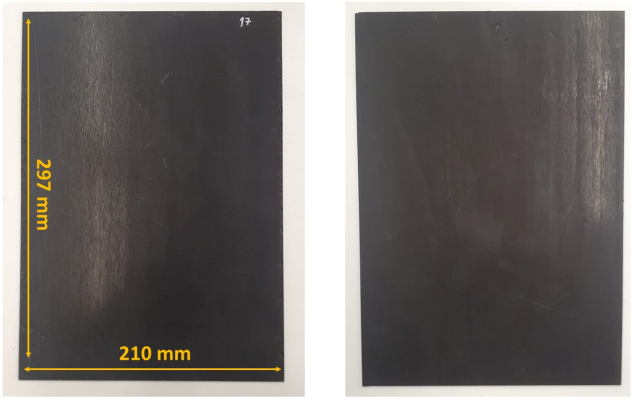

(**a**) (**b**)

Figure 3. CF LFP ABS + 3% CNT sample. (**a**) Front side. (**b**) Back side.

Table 3. Hot press molding parameters.

Time (min)	Pressure (kN)	Temperature (°C)
5	60	250
10	100	250

2.3. Dispersion Analysis

Following the preparation of the samples, an analysis of the dispersion of the EMI shielding particles in the polymeric matrix is deemed necessary to assess the quality of the manufacturing process. Scanning electron microscopy (SEM) imaging is performed using a Hitachi S-4800 Scanning Electron Microscope which allowed the characterization of the surface of Samples 2, 4, and 7, generated in Section 2.2 (Figure 4). The selected samples are representative of each of the three manufacturing processes and materials described previously.

CNTs appear as thin and elongated structures and are homogeneously distributed across the three samples, indicating a high-quality manufacturing process. Sample 7 contains the highest concentration of CNTs after visual assessment, confirming the nominal specifications of this sample (Figure 4a,b). It is worth noting that the combined effect of the low apparent density of the CNTs (~0.23 g/cm^3) and the high weight percentage of CNTs (15%) contained by this sample, results in a dense network of CNT that hinders the visualization of the polymeric matrix.

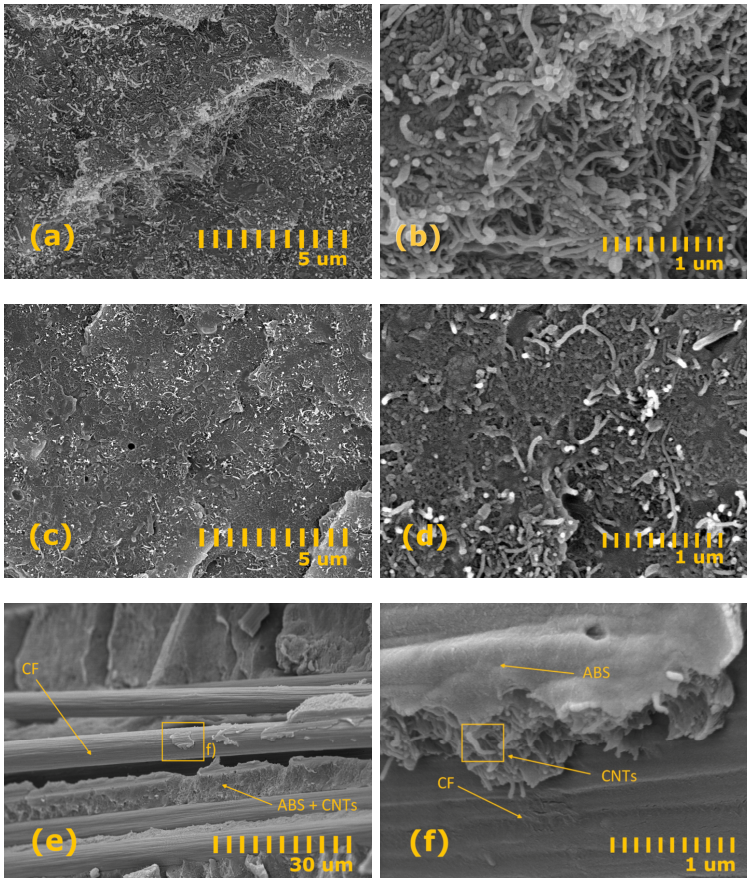

Figure 4. SEM images of three of the developed samples. General view (**left**). Detailed view (**right**). (**a**,**b**) MB ABS + 15% CNT (**c**,**d**) ABS + 5%CNT (**e**,**f**) CF LFP ABS + 3% CNT.

As the concentration of CNT decreases (Samples 2 and 4), the polymeric matrix is rendered visible, and the network of CNT becomes less dense (Figure 4c,d). Additionally, the correct impregnation of the carbon fibers by the polymer matrix can be observed in Figure 4e, ruling out the delamination of the fibers produced by the sample preparation.

Regarding the CNT distribution, it can be observed that a similar distribution is obtained across the samples included in Figure 4. This effect indicates a high level of reproducibility of the manufacturing process. Following a visual examination, empty spaces and aggregates are not appreciated, and CNTs are homogeneously dispersed in the polymer matrix.

3. Planar Material Measurement Methods

The current standard method that defines the measurement procedure to determine the shielding effectiveness of planar materials is the ASTM 4935-18. Nevertheless, the frequency region of this measurement method is limited in frequency (up to 1.5 GHz). Other measurement techniques used to analyze the performance of planar materials are based on the IEEE 299 standard. Due to the wide variety of applications that need to be shielded by using housing with a specific size and shape, planar materials are generally characterized, considering different field conditions. Thereby, depending on the frequency range and the sample features, different measurement techniques may be used to cover the

entire frequency range of interest. The 5G operates in a wide range of frequencies. Currently, two different frequency ranges are available for the 5G technology, FR1 and FR2. The bands in the FR1 spectrum are envisaged for the operation of traditional cellular communication, whereas FR2 bands aim to provide short-range very high data rate capability. The 5G FR1 range covers frequencies up to 7.125 GHz, and FR2 encompasses frequencies above 24.5 GHz.

3.1. Standard Measurement Methods

The main techniques for the measurement of the SE of planar materials are based on using mono-mode coaxial TEM cells, according to the standard ASTM D4935-18, or the use of emitting and receiving antennas as in the IEEE 299 standard. The first method has a frequency limit of about 1.5 GHz; the last one applies for higher frequencies, but it requires large sheet samples, which is a disadvantage when dealing with novel materials that rely on rare raw materials. The cost of the shielding particles can be very high, making unfeasible the manufacturing of large-scale samples. Consequently, measuring these materials using a method that requires covering the entire door of an anechoic chamber becomes impractical.

The ASTM D4935-18 is the standard test method for measuring the electromagnetic shielding effectiveness of planar materials. This method allows measuring planar samples in a narrow frequency range from 30 MHz to 1.5 GHz. The technique measures the insertion loss (IL) that results when introducing test samples in a coaxial two-conductor transmission line holder, supporting transverse electromagnetic (TEM) propagation mode. The procedure requires two types of specimens with the same thickness to make SE measurements: the reference and the load specimens (Figure 5). The difference between the measurements of the load and the reference specimen provides the measurement of the SE, caused by the reflection and absorption of the material between the two flanks of the coaxial probe. The upper-frequency limit that can be measured with this method depends on the cut-off frequency for the transverse electric propagation mode of the coaxial cell holder. At frequencies higher than the cut-off, higher-order modes other than TEM can propagate, changing the field distribution inside the cell and causing resonances in the measured results, which have an adverse effect on the accuracy of the measured results. Therefore, the main disadvantage of the fixture is the narrow frequency band of operation, which is limited, considering the operating frequencies of current electronic devices and systems.

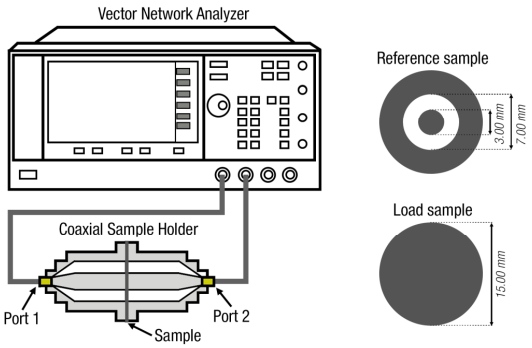

Figure 5. Measurement test setup based on the ASTM D4935-18 procedure and sample geometries and dimensions.

The IEEE 299 standard defines how to measure the effectiveness of electromagnetic shielding enclosures. This method is carried out by placing a sample of the material under test between two antennas connected to a vector network analyzer equipment (VNA) that provides the emitting signal to one of the antennas and receives the field measured by the receiving antenna (Figure 6). Thereby, it is possible to obtain the shielding effectiveness

of the material under test by analyzing the S-parameters obtained through a reference measurement (without the material sample) and a load measurement (by placing the material between the two antennas). The reference can be taken in free space or through an open aperture in an anechoic chamber wall. The SE is obtained by taking the difference between the received field strength (in dB units) with the sample absent and with the sample present. The nature of the illuminating field varies with frequency and the type of antenna used.

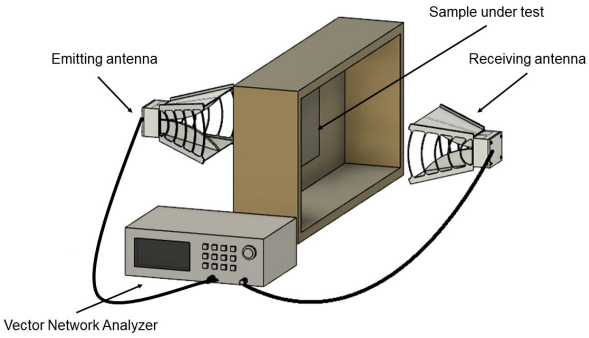

Figure 6. Measurement test setup based on the IEEE 299 standard procedure.

To these limitations is added the high influence between the characteristics of the anechoic chamber as well as the proper location/orientation of the antennas and the sample in the space.

3.2. Non-Standardized Measurement Methods

Due to the increase in operating frequencies and the evolution of 5G towards FR2, it is important to develop non-standardized measurement methods through setups, fixtures, and techniques compatible with the operating frequencies of 5G technologies and the samples manufactured.

From the standards, some derivative methods can be highlighted: nested reverberation chambers [30], vibrating intrinsic reverberation chambers [31], TEM cell methods [32], ASTM D4935-18 high-frequency variants [33–35], or absorber box methods [36,37]. The last one proposes an alternative to free space measurements in an anechoic chamber, where the sample size is significantly reduced, and no complex sample preparation is required. Moreover, the equipment and the sample size determine the cutoff frequency, so the method is considerably adaptable to the type of material to be measured. This alternative also eliminates the main problems that the other techniques present, making this method suitable for this study.

As some bibliographic sources indicate, extending the upper-frequency limit of the ASTM D4935-18 standard could be possible. Some institutions have modified this standard coaxial cell holder to perform SE measurements at higher frequencies and on smaller-size materials under test [34,35]. Basically, as the cut-off frequency, and consequently the upper-frequency limit, depends on cell dimensions, new versions of coaxial sample holders can be designed and fabricated, reducing the inner radius of the outer conductor and the radius of the center one.

On the other hand, the measurements based on the IEEE 299 standard are another interesting line of research since they can be performed with RF antennas (inside an anechoic chamber), extending the frequency region defined by the ASTM D4935-18 standard. The upper frequency for IEEE 299 methods is limited by the chamber leakage and the need for the sample to be large enough to minimize edge diffraction effects. Nevertheless, test-to-test variations arise from normal differences between instruments, from discrepancies between transmitting and receiving antennas, including their positions, and primarily from differ-

ences between test techniques. Most of the methods based on free space require sample dimensions too large, in addition to being strongly conditioned by the environmental conditions and the directivity of the antennas. Consequently, the proposed alternative method is based on an EMI absorber box lined with absorbent material and two antennas: one transmitter and one receiver.

3.3. Proposed Shielding Effectiveness Measurement System

The proposed measurement method is an adaptation of one of the methods included in the P2715 standard, a guide for the characterization of the shielding effectiveness of planar materials. This method provides the SE of planar materials, adapting to the specific requirements of the study. The main advantage is that the sample machining is simple, which represents a significant breakthrough when dealing with rigid and delicate materials that cannot be machined with very specific geometries or tiny dimensions. Furthermore, no electrical connection to the sample is required, which allows the measurement of samples with low conductivity, contrary to the measurement method proposed in the ASTM D4935 standard. These facts mean that a wide range of measurements can be made with reasonable speed due to the easiness of the measurement procedure. Another notable advantage is the elimination of frequency limitation, making it a suitable method for measurements in the frequency range where 5G technology operates.

The scheme of the proposed prototype is shown in Figure 7. The receiving antenna embedded in the absorber and the receiving antenna are commercial 700 MHz to 18 GHz A-Info LB-7180 ridged waveguide horns. The dimensions of the cavity are 300 × 500 mm, thus, adapting to the rectangular shape of the horn antennas [38]. In one of the sides of the box, a hole has been drilled where an SMA-type connector is placed and connected to the transmitting antenna inside the cavity. The laminated absorber is arranged inside the cavity of the absorber box cut to fit the geometry and dimensions of the antenna. The absorber material is a commercial series made from polyurethane foam that is treated with carbon and assembled in a laminate construction to generate a controlled conductivity gradient. The upper layers above the emitting antenna have a square opening of 100 × 100 mm where the sample is placed to measure the SE of the sample. Assuming no contact exists between the equipment and the sample, two more sheets of absorbent material are placed on top of the sample to mitigate diffraction losses due to the edge effect and to flatten the sample in case it has a concave or convex shape due to the manufacturing process. These top layers of absorbers have an opening of the same dimensions as the sample layer to illuminate the sample as uniformly as possible.

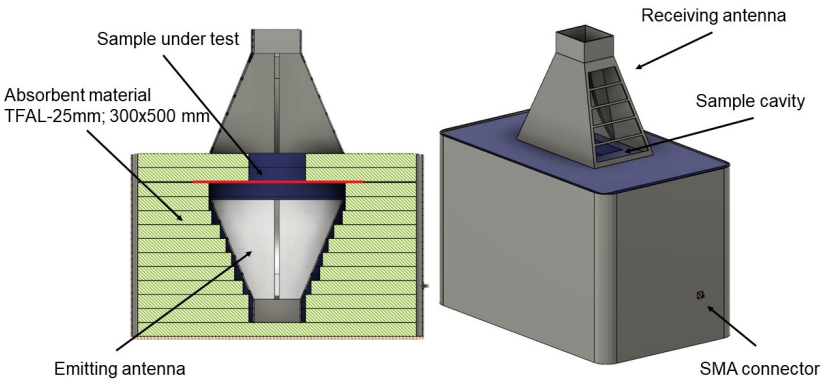

Figure 7. Cross-sectional view of the prototype system.

The selected size of the developed samples is 210 × 297 mm. These dimensions correspond to a fairly standard size for sample prototyping, although it is possible to perform measurements with samples up to 300 × 500 mm, which corresponds to the maximum dimensions of the cavity. Furthermore, with this size, the samples aim to be large enough to reduce the edge effect previously mentioned, but at the same time, small enough to ensure that production is simple and cost-effective.

The antennas are connected to port 1 (emitting channel) and port 2 (receiving channel) of a VNA measuring equipment through an SMA-type connector and two cables Megaphase KB18-S1S1-48 SMA. The frequency range of the final system is 700 MHz–18 GHz, limited by the maximum and minimum operating frequencies of the antennas.

The procedure to obtain the shielding effectiveness of the different samples is based on measuring the scattering parameter S_{21} by taking the transmission ratio through the system without any sample ($S_{21,ref}$), and with the sample present in the cavity ($S_{21,sample}$). Subsequently, the SE is calculated according to Equation 1:

$$SE\ (dB) = S_{21,sample} - S_{21,ref} \quad (1)$$

The prototype and the final measurement setup are shown in Figure 8, where the receiving horn antenna is situated above a material under test and connected to the VNA equipment.

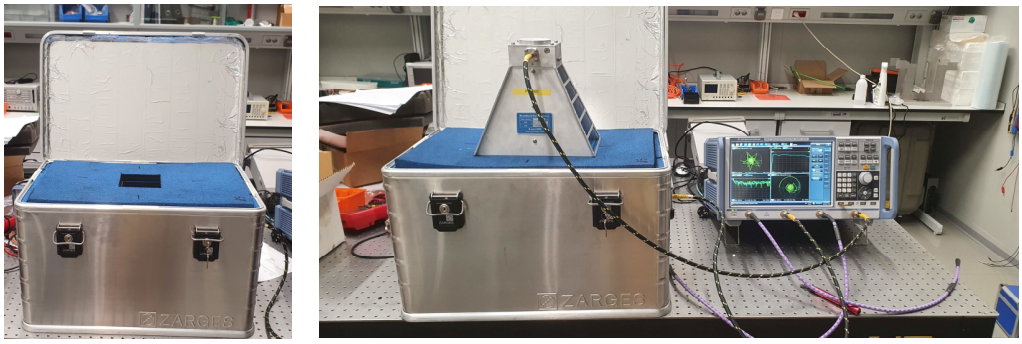

(**a**) (**b**)

Figure 8. Experimental measurement setup. (**a**) Sample window layer. (**b**) Experimental setup performing a sample measurement.

To characterize the system, the measurement of the dynamic range of the proposed method has been carried out. The SE of the cavity without a sample has been compared with the SE resulting from placing a perfect electric conductor (PEC) with the maximum size of the cavity (300 × 500 mm) to avoid the effect of diffraction at the edges. In this case, the sample is an aluminum sheet with a thickness of t = 2 mm. Figure 9 shows the resulting dynamic range of the system, which is approximately -100 dB and is expected to be suitable to measure the SE of the developed materials according to the values obtained in previous studies of composites with similar characteristics [20,39].

The most notable features of the measurement method used to evaluate the developed samples are summarized in Table 4.

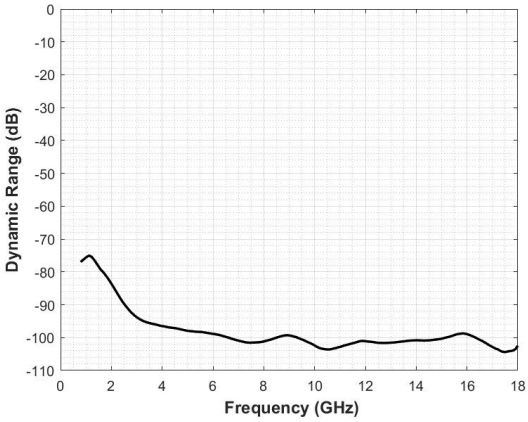

Figure 9. Measured dynamic range of the system with a 2 mm thick aluminum sample.

Table 4. Hot press molding parameters.

Measured Parameter	Unit of Measure	Cavity Dimensions	Sample Size	Frequency Range	Measured Dynamic Range
Shielding effectiveness	dB	300 × 500 mm	210 × 297 mm	700 MHz–18 GHz	−100 dB

4. Results and Discussion

This section is focused on showing the results corresponding to the measurement of seven sample composites under test. Firstly, it is compared the different composite samples based on ABS (samples 1, 2, 3, and 7) to analyze how the increase in the concentration of CNT is turned into an improvement of the SE parameter. Subsequently, the influence of the reinforcement material used to manufacture the composite is studied by comparing the samples based on glass fiber and carbon fiber (samples 4 and 5). Finally, the effect of introducing a thicker carbon fiber reinforcement in the composite is analyzed (samples 4 and 6).

Figure 10 shows the results obtained in terms of SE of different composites with an ABS matrix without fiber reinforcement and three different concentrations of %w CNT. The ABS trace represents the outcome of the SE measurement conducted on the ABS matrix without any filler material. This particular measurement is used as a reference to compare the SE values obtained from the other samples. It can be observed how this trace does not provide considerable attenuation but the increase in CNT filler leads to a rise in the SE provided by the material. If we take the value of 7.125 GHz as a reference, which corresponds to the upper limit of the FR1 band in the 5G spectrum, a value of −24.75 dB is obtained for the trace with a concentration of 5w%CNT. For the sample with twice the weight concentration of CNT, the SE value increases to −39.65 dB. In the last case, for the 15w%CNT sample at the reference frequency, the SE value obtained is −81.30 dB.

Below the reference frequency, the behavior of the traces is slightly different. The red trace corresponding to sample 2 shows a linear behavior, whereas the traces corresponding to the samples with the highest CNT concentration (samples 3 and 7) show an increase in SE as the frequency increases. On the other hand, starting at approximately 14 GHz, it can be observed that the red trace (sample 2) continues to exhibit a flat behavior, whereas the blue trace (sample 3) continues to decrease. However, the black trace (sample 7) shows a change in slope, taking an ascending trend. This fact leaves the door open for further study at higher frequencies to determine if, at a given frequency, the sample with the highest concentration of CNT may not necessarily present the greatest attenuation.

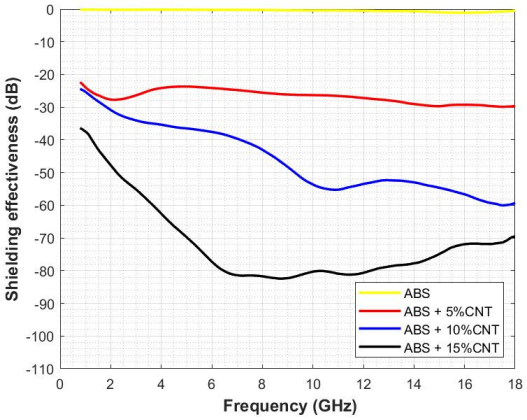

Figure 10. Comparison of ABS polymer samples with three different w%CNT concentrations.

It has been observed that to achieve higher levels of attenuation, it is necessary to increase the concentration of CNT. However, this presents a challenge during the machining process as the addition of CNT increases the viscosity of the composite. To address this issue, two compounds have been developed with the addition of different reinforcements, one based on CF and the other based on GF. These reinforcements provide rigidity to the material, thereby improving its mechanical properties.

Figure 11 shows the shielding effectiveness provided by the CF reinforcement sample comparing it with the GF reinforcement sample (samples 4 and 5, respectively) with a 3w%CNT. It can be observed that the CF sample exhibits considerably higher attenuation compared to the GF sample when the same %w filler is introduced. Quantitatively comparing the results, for the selected reference frequency of 7.125 GHz, it can be observed that the SE value of the CF sample is −60.03 dB. In contrast, the SE value obtained for the GF sample is −14.24 dB, which significantly differs from the CF sample, even though the weight percentage of CNT is the same for both samples. This is attributed to the nature of the fiber reinforcements, as carbon fiber alone exhibits a certain level of shielding depending on the fiber density due to the highly conductive nature of carbon fibers, whereas fiberglass does not cause significant attenuation.

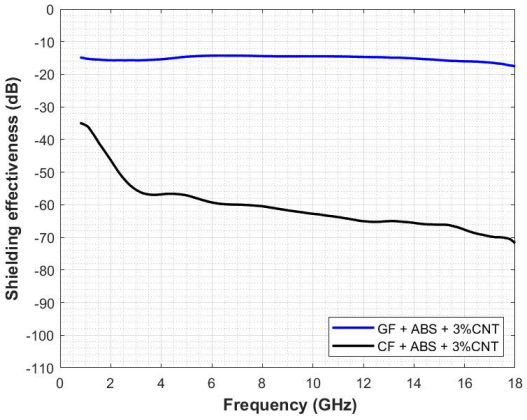

Figure 11. Carbon-fiber- and glass-fiber-reinforced polymers.

Although GF does not provide a significant attenuation by itself, these two compounds have been compared due to the fact that GF provides some advantages in terms of cost, production, and machining. GF is generally more affordable because the materials used to produce it are widely available. Additionally, the manufacturing of GF is simpler and requires fewer processing steps. On the other hand, this type of reinforcement is easier to manipulate and has a longer lifespan than CF reinforcement. Therefore, the type of reinforcement chosen will depend on the final application of the composite and the required level of attenuation.

Figure 12 shows the influence of the sample thickness in the measurement of the SE. To achieve this, a CF reinforcement sample (sample 4) with a thickness of t = 2 mm and 3w%CNT filling is compared with two stacked sheets of the sample (sample 6). On the other hand, the red trace shows the measurement result of the two overlapping sheets. These observations suggest that the sample thickness significantly affects the shielding capability of the material. Below the reference frequency, the behavior of the traces is similar up to approximately 3.5 GHz, where the two traces diverge. It can be observed how the CF sample (black trace) presents considerable attenuation, particularly from 4 GHz. From this point up to 7.125 GHz, the black trace (sample 2) shows a linear behavior with a slightly decreasing slope, whereas the red trace (sample 6) shows a more abrupt decrease until the reference frequency, where it flattens out. Comparing the results for the selected frequency of 7.125 GHz, it can be observed that the SE value of the single-layer CF sample is −60.03 dB, whereas the SE value of the double-layer CF sample shows an increase of 21.29 dB, reaching a SE value of −81.32 dB. Moreover, it is noted that the red trace shows an increase in slope starting at approximately 16 GHz. This phenomenon may be attributed to multiple reflections that occur between the two sheets of material.

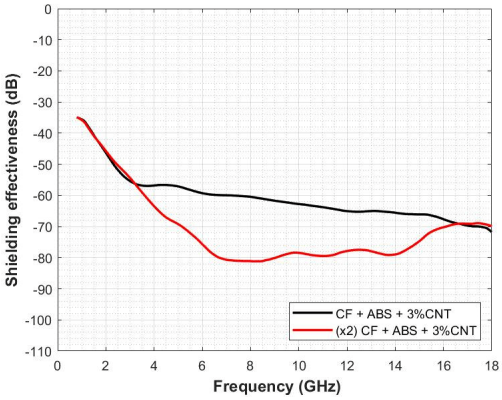

Figure 12. Carbon-fiber-reinforced polymers. Comparison of one sample (black trace) and two superposed samples (red trace).

The following Table 5 provides a summary of the most representative results for each of the seven samples in three different frequency ranges. This table shows the maximum and minimum SE values in decibels.

The ability to detect these variations is essential for optimizing the performance of shielding materials in a given application. By identifying the frequency ranges in which a material provides the most significant attenuation in terms of attenuation, it is possible to design more effective shielding systems. These results demonstrate how this method is capable of detecting variations in the shielding performance of the material across different frequency ranges.

Table 5. Summary of the most representative results in three different frequency ranges.

Sample ID	Frequency Ranges					
	700 MHz to 6 GHz		6 GHz to 12 GHz		12 GHz to 18 GHz	
	Min SE (dB)	Max SE (dB)	Min SE (dB)	Max SE (dB)	Min SE (dB)	Max SE (dB)
1	−0.12	−0.25	−0.21	−0.54	−0.43	−1.30
2	−21.87	−28.62	−24.28	−27.36	−27.17	−30.11
3	−24.16	−37.41	−37.41	−56.35	−51.81	−60.44
4	−34.92	−59.89	−59.78	−65.40	−63.56	−71.76
5	−14.25	−15.89	−14.19	−14.67	−14.60	−17.62
6	−34.78	−77.53	−77.23	−82.61	−68.19	−80.49
7	−36.24	−77.99	−77.99	−83.84	−69.58	−80.95

5. Conclusions

The proposed measurement methodology shows significant advantages, including the simplicity of the sample machining, which means that very specific geometries or tiny dimensions are not required. This method allows the measurement of samples with low conductivity, contrary to the measurement method proposed in the ASTM D4935 standard. The sample insertion and removal process can be completed within a matter of seconds, which supposes that a wide range of measurements can be made with reasonable speed due to the easiness of the measurement procedure. The measured dynamic range is approximately −100 dB, allowing us to analyze the samples developed in this study in the frequency range where 5G technology operates.

On the other hand, EMI shielding effectiveness in the 700 MHz–18 GHz frequency range has been studied. Two types of materials have been compared, depending on the presence of fiber reinforcement. It has been observed the performance of the materials studied in a wider frequency spectrum than specified by ASTM4935-18 standard and controlling the surrounding effects by using the absorber box method.

Some of the samples analyzed have demonstrated to provide a significant attenuation. For those composites based on a polymer matrix with different concentrations of CNT, a value of −81.30 dB has been obtained for the frequency of 7.125 GHz for the 15w%CNT composite, which is a very significant SE value considering the nature of these materials. Whilst it is true that an increased volume fraction of filler may lead to a decrease in the mechanical performance of the host matrix by means of deterioration of its inherent morphology, it is necessary to incorporate a higher filler content in order to achieve higher SE. It is desirable to employ CNT/polymer composites at low filler loadings to produce cost-effective and versatile conductive composites.

The inclusion of a carbon fiber reinforcement has proven to be an effective strategy for achieving significant attenuation in composite materials, providing higher attenuation than the GF-reinforced composite with the same CNT concentration. This approach offers an advantage over using a high percentage of filler, which may lead to undesirable mechanical properties. This is due to the highly conductive nature of carbon fibers, which can effectively attenuate electromagnetic radiation. Furthermore, using CF reinforcement can also provide additional benefits such as increased stiffness and strength, as well as reduced weight. This, in turn, makes these materials an excellent alternative to replace traditional shielding materials.

It has to be highlighted that these types of characterizations are very relevant from a technological and industrial point of view. Specifically, for those sectors related to 5G technology, since the use of EMI shielding based on plastic materials has many advantages, such as manufacturing cost reduction.

Author Contributions: Conceptualization, A.S., J.T., A.B. and R.R.; Methodology, A.A. (Andrea Amaro), P.A.M. and A.A. (Antonio Alcarria); Validation, A.S., J.T. and P.A.M.; Formal analysis, A.A. (Andrea Amaro), R.H. and A.A. (Antonio Alcarria); Investigation, A.A. (Andrea Amaro), A.S. and R.H.; Resources, A.B., R.R., P.G. and A.P.; Writing—original draft, A.A. (Andrea Amaro), A.S., R.H.,

P.G. and A.P.; Writing—review & editing, J.T., P.A.M, A.B. and R.R.; Project administration, J.T.; Funding acquisition, J.T. All authors have read and agreed to the published version of the manuscript.

Funding: The project with reference PLEC2021-007994 has been funded by MCIN/AEI/10.13039/501100011033 and by the European Union NextGenerationEU/PRTR.

Institutional Review Board Statement: Not applicable.

Informed Consent Statement: Not applicable.

Data Availability Statement: Not applicable.

Conflicts of Interest: The authors declare no conflict of interest.

References

1. Martinez, P.A.; Navarro, E.A.; Victoria, J.; Suarez, A.; Torres, J.; Alcarria, A.; Perez, J.; Amaro, A.; Menendez, A.; Soret, J. Design and Study of a Wide-Band Printed Circuit Board Near-Field Probe. *Electronics* **2021**, *10*, 2201. [CrossRef]
2. Ibrahim, I.R.; Matori, K.A.; Ismail, I.; Awang, Z.; Rusly, S.N.A.; Nazlan, R.; Mohd Idris, F.; Muhammad Zulkimi, M.M.; Abdullah, N.H.; Mustaffa, M.S.; et al. A Study on Microwave Absorption Properties of Carbon Black and Ni0.6Zn0.4Fe2O4 Nanocomposites by Tuning the Matching-Absorbing Layer Structures. *Sci. Rep.* **2020**, *10*, 3135. [CrossRef] [PubMed]
3. Zhao, B.; Deng, J.; Zhang, R.; Liang, L.; Fan, B.; Bai, Z.; Shao, G.; Park, C.B. Recent Advances on the Electromagnetic Wave Absorption Properties of Ni Based Materials. *Eng. Sci.* **2018**, *3*, 5–40. [CrossRef]
4. Victoria, J.; Suarez, A.; Torres, J.; Martinez, P.; Alcarria, A.; Martos, J.; Garcia-Olcina, R.; Soret, J.; Muetsch, S.; Gerfer, A. Transmission Attenuation Power Ratio Analysis of Flexible Electromagnetic Absorber Sheets Combined with a Metal Layer. *Materials* **2018**, *11*, 1612. [CrossRef]
5. Houbi, A.; Aldashevich, Z.A.; Atassi, Y.; Bagasharova Telmanovna, Z.; Saule, M.; Kubanych, K. Microwave Absorbing Properties of Ferrites and Their Composites: A Review. *J. Magn. Magn. Mater.* **2021**, *529*, 167839. [CrossRef]
6. Suarez, A.; Victoria, J.; Torres, J.; Martinez, P.A.; Alcarria, A.; Perez, J.; Garcia-Olcina, R.; Soret, J.; Muetsch, S.; Gerfer, A. Performance Study of Split Ferrite Cores Designed for EMI Suppression on Cables. *Electronics* **2020**, *9*, 1992. [CrossRef]
7. Suarez, A.; Victoria, J.; Alcarria, A.; Torres, J.; Martinez, P.; Martos, J.; Soret, J.; Garcia-Olcina, R.; Muetsch, S. Characterization of Different Cable Ferrite Materials to Reduce the Electromagnetic Noise in the 2–150 KHz Frequency Range. *Materials* **2018**, *11*, 174. [CrossRef]
8. Zubar, T.; Grabchikov, S.; Kotelnikova, A.; Kaniukov, E.; Kutuzau, M.; Leistner, K.; Nielsch, K.; Vershinina, T.; Tishkevich, D.; Kanafyev, O.; et al. Efficiency of Magnetostatic Protection Using Nanostructured Permalloy Shielding Coatings Depending on Their Microstructure. *Nanomaterials* **2021**, *11*, 634. [CrossRef]
9. Iqbal, A.; Kwon, J.; Kim, M.-K.; Koo, C.M. MXenes for Electromagnetic Interference Shielding: Experimental and Theoretical Perspectives. *Mater. Today Adv.* **2021**, *9*, 100124. [CrossRef]
10. Qin, M.; Zhang, L.; Wu, H. Dielectric Loss Mechanism in Electromagnetic Wave Absorbing Materials. *Adv. Sci.* **2022**, *9*, 2105553. [CrossRef]
11. Wu, N.; Hu, Q.; Wei, R.; Mai, X.; Naik, N.; Pan, D.; Guo, Z.; Shi, Z. Review on the Electromagnetic Interference Shielding Properties of Carbon Based Materials and Their Novel Composites: Recent Progress, Challenges and Prospects. *Carbon* **2021**, *176*, 88–105. [CrossRef]
12. Wang, L.; Qiu, H.; Song, P.; Zhang, Y.; Lu, Y.; Liang, C.; Kong, J.; Chen, L.; Gu, J. 3D Ti3C2Tx MXene/C Hybrid Foam/Epoxy Nanocomposites with Superior Electromagnetic Interference Shielding Performances and Robust Mechanical Properties. *Compos. Part A Appl. Sci. Manuf.* **2019**, *123*, 293–300. [CrossRef]
13. Sachdev, V.K.; Sharma, S.K.; Tomar, M.; Gupta, V.; Tandon, R.P. EMI Shielding of MWCNT/ABS Nanocomposites in Contrast to Graphite/ABS Composites and MWCNT/PS Nanocomposites. *RSC Adv.* **2016**, *6*, 45049–45058. [CrossRef]
14. Arjmand, M.; Apperley, T.; Okoniewski, M.; Sundararaj, U. Comparative Study of Electromagnetic Interference Shielding Properties of Injection Molded versus Compression Molded Multi-Walled Carbon Nanotube/Polystyrene Composites. *Carbon* **2012**, *50*, 5126–5134. [CrossRef]
15. Chung, D.D.L. Electromagnetic Interference Shielding Effectiveness of Carbon Materials. *Carbon* **2001**, *39*, 279–285. [CrossRef]
16. Altin Karataş, M.; Gökkaya, H. A Review on Machinability of Carbon Fiber Reinforced Polymer (CFRP) and Glass Fiber Reinforced Polymer (GFRP) Composite Materials. *Def. Technol.* **2018**, *14*, 318–326. [CrossRef]
17. Martins, L.C.; Pontes, A.J. Fiber Reinforced Thermoplastics Compounds for Electromagnetic Interference Shielding Applications. *J. Reinf. Plast. Compos.* **2022**, *41*, 206–214. [CrossRef]
18. Munalli, D.; Dimitrakis, G.; Chronopoulos, D.; Greedy, S.; Long, A. Electromagnetic Shielding Effectiveness of Carbon Fibre Reinforced Composites. *Compos. Part B Eng.* **2019**, *173*, 106906. [CrossRef]
19. Awan, G.H.; Ali, L.; Ghauri, K.M.; Ramzan, E.; Ehsan, E. Effect of various forms of glass fiber reinforcements on tensile properties of polyester matrix composite. *J. Fac. Eng. Technol.* **2010**, *16*, 33–39.

20. Martinez, P.A.; Victoria, J.; Torres, J.; Suarez, A.; Alcarria, A.; Amaro, A.; Galindo-Galiana, B.; Losada-Fernandez, C.; Ramirez-Monsell, V.; Lopez-Rius, B. Analysis of EMI Shielding Effectiveness for Plastic Fiber Composites in the 5G Sub-6 GHz Band. In Proceedings of the 2021 Joint IEEE International Symposium on Electromagnetic Compatibility Signal and Power Integrity, and EMC Europe, EMC/SI/PI/EMC Europe 2021, Raleigh, NC, USA, 26 July–13 August 2021.
21. *ASTM D4935-18*; Standard Test Method for Measuring the Electromagnetic Shielding Effectiveness of Planar Materials. ASTM International: West Conshohocken, PA, USA, 2018. [CrossRef]
22. *IEEE Std 299-2006 (Revision of IEEE Std 299-1997)*; IEEE Standard Method for Measuring the Effectiveness of Electromagnetic Shielding Enclosures. IEEE: Piscataway, NJ, USA, 2007; pp. 1–52. [CrossRef]
23. Chanda, M.; Roy, S.K. *Plastics Technology Handbook*; CRC Press: Boca Raton, FL, USA, 2006; ISBN 9780429124020.
24. Harper, C.A. (Ed.) *Handbook of Plastic Processes*; Wiley: New York, NY, USA, 2006; ISBN 9780471662556.
25. Moore, J.D. Acrylonitrile-Butadiene-Styrene (ABS)—A Review. *Composites* **1973**, *4*, 118–130. [CrossRef]
26. Pradeep, S.A.; Iyer, R.K.; Kazan, H.; Pilla, S. Automotive Applications of Plastics: Past, Present, and Future. In *Applied Plastics Engineering Handbook*; Elsevier: Amsterdam, The Netherlands, 2017; pp. 651–673.
27. Kapoor, S.; Goyal, M.; Jindal, P. Effect of Functionalized Multi-Walled Carbon Nanotubes on Thermal and Mechanical Properties of Acrylonitrile Butadiene Styrene Nanocomposite. *J. Polym. Res.* **2020**, *27*, 40. [CrossRef]
28. Shen, H.Y.; Jiao, Q.Z.; Zhao, Y.; Li, H.S.; Sun, Z. Electrical Conductivity and Electromagnetic Interference Shielding Effectiveness of Multiwalled Carbon Nanotubes Filled ABS Composites. *Adv. Mater. Res.* **2011**, *194–196*, 1554–1557. [CrossRef]
29. Holloway, C.L.; Hill, D.A.; Ladbury, J.; Koepke, G.; Garzia, R. Shielding Effectiveness Measurements of Materials Using Nested Reverberation Chambers. *IEEE Trans. Electromagn. Compat.* **2003**, *45*, 350–356. [CrossRef]
30. Hara, M.; Yoshikai, T.; Takahashi, Y.; Vogt-Ardatjew, R.; Leferink, F. Numerical Analysis of Vibrating Intrinsic Reverberation Chamber between Various Shielding Effectiveness Measurement Techniques. In Proceedings of the 2020 International Symposium on Electromagnetic Compatibility—EMC EUROPE, Rome, Italy, 23–25 September 2020; pp. 1–6.
31. Pocai, M.; Dotto, I.; Festa, D. Fabrics SE Measurements in a Reverberation Chamber by an Apertured TEM Cell and by a Small Nested Reverberation Chamber. In Proceedings of the 2011 IEEE International Symposium on Electromagnetic Compatibility, Long Beach, CA, USA, 14–19 August 2011; pp. 693–698.
32. Tamburrano, A.; Desideri, D.; Maschio, A.; Sabrina Sarto, M. Coaxial Waveguide Methods for Shielding Effectiveness Measurement of Planar Materials Up to 18 GHz. *IEEE Trans. Electromagn. Compat.* **2014**, *56*, 1386–1395. [CrossRef]
33. Sarto, M.S.; Tamburrano, A. Innovative Test Method for the Shielding Effectiveness Measurement of Conductive Thin Films in a Wide Frequency Range. *IEEE Trans. Electromagn. Compat.* **2006**, *48*, 331–341. [CrossRef]
34. Tamburrano, A.; Sarto, M.S. Electromagnetic Characterization of Innovative Shielding Materials in the Frequency Range up to 8 Gigahertz. In Proceedings of the 2004 International Symposium on Electromagnetic Compatibility (IEEE Cat. No.04CH37559), Silicon Valley, CA, USA, 9–13 August 2004; pp. 551–556.
35. Marvin, A.C.; Dawson, L.; Flintoft, I.D.; Dawson, J.F. A Method for the Measurement of Shielding Effectiveness of Planar Samples Requiring No Sample Edge Preparation or Contact. *IEEE Trans. Electromagn. Compat.* **2009**, *51*, 255–262. [CrossRef]
36. Austin, A.N.; Dawson, J.F.; Flintoft, I.D.; Marvin, A.C. Analysis of the Shielding Properties of Metalised Nonwoven Materials. In Proceedings of the 2013 International Symposium on Electromagnetic Compatibility, Brugge, Belgium, 2–6 September 2013; pp. 526–531.
37. LB-7180 0.7-18GHz Broadband Horn Antenna Technical Specification. Available online: http://www.ainfoinc.com.cn/en/p_ant_h_brd.asp (accessed on 10 April 2023).
38. Amaro, A.; Suarez, A.; Tamburrano, A.; Torres, J.; Marra, F.; Martinez, P.A.; Galindo, B.; Soriano, N.; Victoria, J.; Alcarria, A. EMI Shielding Effectiveness Study for Innovative Carbon Nanotube Materials in the 5G Frequency Region. *IEEE Trans. Electromagn. Compat.* **2023**, *65*, 177–185. [CrossRef]
39. Boroujeni, A.Y.; Tehrani, M.; Manteghi, M.; Zhou, Z.; Al-Haik, M. Electromagnetic Shielding Effectiveness of a Hybrid Carbon Nanotube/Glass Fiber Reinforced Polymer Composite. *J. Eng. Mater. Technol.* **2016**, *138*, 041001. [CrossRef]

5.2 Summary

The results presented in this chapter demonstrate that the Absorber Box method is a reliable and flexible alternative for the shielding effectiveness characterization of structural composite materials. Unlike coaxial or waveguide-based approaches, the configuration enables testing of large and rigid samples that are representative of real-world application formats. The ability to evaluate industrially produced laminates reinforces the applicability of the method in realistic EMC scenarios. These findings motivate the further refinement and validation of the Absorber Box setup, which is explored in the next chapter through the development of a simulation model to analyze field behavior and benchmark experimental results.

This work fulfills S.O.3 and S.O.4, by implementing and validating a non-standardized measurement method and demonstrating its suitability for complex composite materials. The robustness of the setup also supports its subsequent extension into numerical modeling, which is addressed in Chapter 6.

Chapter 6. Improved Absorber Box Method with Simulation-Based Validation

This chapter presents an enhanced version of the Absorber Box *method, supported by a finite element simulation model developed to analyze field behavior and validate measurement results. The work involves the characterization of shielding properties of advanced materials from Würth Elektronik, exploring physical effects such as diffraction and cavity interactions that influence shielding performance, particularly at lower frequencies.*

6.1 Scientific article III

Title: Determination of Electromagnetic Shielding Effectiveness Using an Enhanced Absorber Box Method: Theoretical, Simulation, and Experimental Approaches

Authors: Andrea Amaro, Jose Torres, Adrian Suarez, Roberto Herraiz, Pedro A. Martinez, Jesus Soret, Raimundo Garcia-Olcina, Antonio Alcarria

Published in: Measurement Science and Technology IOP Publishing, 36(7). 25 June 2025

DOI: 10.1088/1361-6501/ade55a

Impact factor (2024): JCR: 3.4

Quartile (2024): JCR: Q1 (37/175) (ENGINEERING, MULTIDISCIPLINARY)

Citations: 0 (WoS, accessed on 14 July 2025).

Description: Measurement Science and Technology (ISSN: 0957-0233; eISSN: 1361-6501) is a peer-reviewed scientific journal published monthly by IOP Publishing. Established in 1923, it focuses on the theory, practice, and application of measurement in physics, chemistry, engineering, and the environmental and life sciences. The journal emphasizes the novelty of reported methods, their characterization, and performance demonstration through examples or applications.

Synopsis:

Accurate measurement of shielding effectiveness is critical for evaluating the performance of materials designed to suppress electromagnetic interference in high-frequency applications. However, conventional standardized methods often present practical and technical limitations when applied to emerging shielding solutions. Frequency constraints, sample geometry requirements, and the need for complex facilities can hinder their application, especially in the characterization of novel materials used in advanced sectors such as telecommunications, automotive electronics, and aerospace systems.

This chapter presents the development, optimization, and validation of an enhanced Absorber Box method for measuring shielding effectiveness. Unlike previous studies focused solely on applying existing techniques, this work proposes a custom-built measurement system, specifically designed to improve field uniformity, reduce diffraction effects, and allow reliable characterization across a wide frequency range, from 700 MHz to 18 GHz. The system features a fully enclosed metallic box with optimized absorber placement and antenna configuration, enabling reproducible measurements without the need for large anechoic chambers or precise sample machining.

To assess the behavior and limitations of the system, a complete simulation model was implemented using the finite element method. This digital twin allowed the evaluation of electromagnetic field distribution, the influence of sample size, and the optimization of antenna positioning. The simulations were validated experimentally by comparing measured transmission parameters and shielding effectiveness values for a range of materials with different electromagnetic properties. The results showed strong agreement between simulated and measured data, confirming the reliability of the model and the robustness of the proposed setup.

The study also investigates the influence of sample size and edge diffraction on shielding effectiveness measurements, showing that under certain conditions, geometric effects can significantly distort the results. Based on this analysis, optimal sample dimensions and frequency thresholds are established to ensure reliable characterization.

This contribution provides not only a functional and validated measurement methodology, but also an in-depth theoretical and simulation understanding of its operating principles. The method represents a flexible and precise alternative to conventional techniques and is especially valuable for the evaluation of planar materials in research, development, and pre-certification stages.

OPEN ACCESS
IOP Publishing
Measurement Science and Technology
Meas. Sci. Technol. **36** (2025) 076003 (14pp)
https://doi.org/10.1088/1361-6501/ade55a

Determination of electromagnetic shielding effectiveness using an enhanced Absorber Box method: theoretical, simulation, and experimental approaches

Andrea Amaro[1,*], Jose Torres[1], Adrian Suarez[1], Roberto Herraiz[1], Pedro A Martinez[1], Jesús Soret[1], Raimundo Garcia-Olcina[1] and Antonio Alcarria[2]

[1] Department of Electronic Engineering, University of Valencia, 46100 Valencia, Spain
[2] EMC Shielding & Grounding Team, Würth Elektronik eiSos, 74638 Waldenburg, Germany

E-mail: andrea.amaro@uv.es

Received 9 April 2025, revised 3 June 2025
Accepted for publication 17 June 2025
Published 25 June 2025

Abstract

Accurate characterization of shielding effectiveness (SE) is essential for evaluating electromagnetic interference shielding materials in high-frequency applications such as 5G communications, automotive, radar, and aerospace. Standardized methods like ASTM D4935-18 and IEEE 299-2006 have frequency limitations, precise sample preparation, and demand complex experimental setups that can hinder practical implementation. This study presents an advanced characterization of an optimized Absorber Box methodology that enhances SE measurement accuracy, extends the frequency range beyond 1.5 GHz, and minimizes edge diffraction effects. The proposed approach provides a controlled testing environment in a more compact setup compared to anechoic chambers, facilitating practical implementation without compromising precision. The system's reliability is validated through numerical simulations using finite element method analysis. Experimental results confirm the method's ability to differentiate materials with different SE, demonstrating strong agreement between simulated and measured data. This approach offers a flexible and robust alternative to conventional SE measurement techniques, making it particularly advantageous for high-frequency shielding material characterization.

Keywords: electromagnetic shielding, Absorber Box, finite element method, shielding effectiveness, EMI characterization

* Author to whom any correspondence should be addressed.

1. Introduction

The characterization of electromagnetic shielding materials has become a fundamental aspect of electromagnetic compatibility (EMC) research due to the growing complexity of electronic systems and the increasing prevalence of high-frequency electromagnetic interference (EMI) [1, 2].

The rapid expansion of 5G technology, which operates across both the sub-6 GHz and millimeter-wave frequency bands, has significantly heightened concerns about EMI, as wireless communication, automotive radar, aerospace electronics, and industrial applications demand robust shielding solutions [3, 4]. Effective electromagnetic shielding is critical for ensuring system reliability, reducing signal degradation, and preventing interference between components in densely packed electronic environments. Given these challenges, accurate measurement techniques are essential for evaluating the shielding effectiveness (SE) of materials, particularly at high frequencies where standard methods face significant limitations [5].

Standardized methods for measuring SE, such as ASTM D4935-18 and IEEE 299-2006, provide well-established frameworks for evaluating electromagnetic shielding performance [6, 7]. However, these methods present limitations that can hinder their applicability in specific measurement scenarios. The assumptions and conditions under which these standards were originally developed may not always align with the characteristics of emerging shielding materials or novel application contexts.

As shielding technologies continue to evolve, these constraints highlight the need for alternative methodologies that offer greater flexibility and adaptability to modern measurement requirements.

One of the main constraints of ASTM D4935-18 is its restricted frequency range, which is inherently limited by the coaxial transmission line geometry to frequencies below approximately 1.5 GHz. This frequency limit renders ASTM D4935-18 inadequate for assessing materials intended for millimeter-wave 5G systems, where adapted measurement techniques are required to evaluate frequency-dependent shielding materials [8]. Furthermore, this method needs precise circular sample geometries, typically of rigid or uniform composition, which are incompatible with flexible, non-homogeneous, or nanostructured materials frequently encountered in novel EMI shielding solutions.

On the other hand, IEEE 299-2006 offers broader frequency coverage through free-space measurement techniques, but its implementation introduces significant practical challenges. The method requires large planar samples or shielding enclosures and typically requires specialized anechoic chambers, limiting its accessibility for researchers without such infrastructure. Moreover, although sometimes applied to individual material samples, this standard is primarily intended to evaluate complete shielding enclosures, reducing its suitability for early-stage material screening or miniaturized applications.

In both cases, traditional techniques often face limitations when dealing with specific sample geometries, especially when these are difficult to implement with certain materials, due to limited material availability or budget constraints, which are common in developing advanced shielding materials. All these factors underscore the need for compact, cost-effective, and versatile alternatives, such as the improved Absorber Box methodology proposed in this study, which maintains measurement accuracy while adapting to research aligned with current industrial realities.

Many modern materials, such as nanocomposites, flexible shielding films, and metamaterials, do not conform to the strict geometrical and dimensional requirements imposed by the standards. These materials often exhibit non-uniform compositions, unconventional thicknesses, or structural characteristics that hinder their compatibility with traditional testing setups [9–11]. In response, alternative SE measurement techniques have emerged, offering more flexible and adaptable approaches that accommodate a wider variety of material configurations [12]. These alternatives enable the accurate characterization of novel shielding solutions while addressing the geometric and environmental constraints that standard methods may impose [13–16].

Among these emerging approaches, Absorber Box-based methodologies have proven to be a promising alternative for SE measurement [17]. By providing a controlled electromagnetic environment, Absorber Box effectively reduces external interferences, minimizes environmental variability, and offers greater flexibility in sample preparation. These characteristics make them particularly well-suited for evaluating shielding materials across a broad frequency spectrum while maintaining measurement reliability and reproducibility [16, 18, 19]. These systems are particularly advantageous when characterizing materials in the gigahertz frequency range, where conventional techniques struggle with precision due to their inherent design limitations.

However, despite their advantages, traditional Absorber Box methods present certain limitations. One of the most significant challenges encountered in these setups is the edge diffraction effect, a phenomenon that occurs when electromagnetic waves interact with the boundaries of the sample of the material under test (MUT), leading to diffraction, scattering, and potential leakage of energy [20, 21]. The impact of this effect depends on factors such as the wavelength of the incident wave, the size and shape of the sample, and the configuration of the Absorber Box. At frequencies where wavelengths become comparable to the sample dimensions, edge diffraction effects can introduce measurement inaccuracies, leading to over or underestimation of its shielding performance.

This study presents a comprehensive study of an enhanced Absorber Box methodology incorporating modifications designed to improve measurement accuracy and optimize key parameters, such as antenna distance and sample size, to minimize diffraction effects. By refining the sample holder configuration and ensuring a more uniform electromagnetic field distribution within the measurement cavity, this approach enhances the precision of SE evaluations over a broader frequency spectrum. Additionally, it extends the measurement capabilities beyond 1.5 GHz, addressing high-frequency

requirements for emerging EMI shielding applications. The system features a custom-fabricated, fully enclosed metallic structure without structural slots or seams, eliminating leakage paths and improving field confinement. Internally, multilayer microwave absorbers are placed to suppress internal reflections and stabilize wave propagation. The design also allows modular and reproducible antenna placement, supporting consistent measurement geometry without physical modifications. These improvements directly address the main limitations of standardized methods such as ASTM D4935-18, which is restricted in frequency and geometry, and IEEE 299-2006, which requires large anechoic chambers and full enclosure testing. To validate the proposed approach, ANSYS HFSS, a widely used 3D finite element method (FEM) analysis tool, is employed to create a digital twin of the measurement system, enabling predictive analysis and iterative optimization. Numerical simulations provide a detailed assessment of electromagnetic wave interactions with shielding materials, facilitating the identification of potential sources of error before experimental testing. By comparing simulated results with experimental data, this study ensures measurement accuracy and reliability while refining key system parameters for enhanced precision.

The manuscript is structured as follows: first, the experimental methodology is described, detailing the modifications introduced to enhance measurement accuracy and minimize the edge diffraction effect. Next, the simulation framework developed using FEM analysis is outlined, illustrating how computational modeling is used to refine the measurement setup and predict shielding behavior. Subsequently, experimental results are presented and compared with simulation predictions, demonstrating the effectiveness of the proposed method in characterizing high-frequency shielding materials. Finally, the conclusions summarize the key findings of the study, emphasizing the broader implications of the enhanced measurement approach in the field of electromagnetic shielding, highlighting, the capability of the absorber-based system to measure materials with different SE levels and differentiate them with precision and reliability.

2. Measurement method

Ensuring accurate and reproducible evaluation of SE requires a well-defined measurement setup that minimizes external interferences and maintains consistency across experiments. This study employs a structured enclosure to achieve these objectives, providing a controlled environment for electromagnetic characterization.

The measurement system is enclosed within a 50 $\times$ 50 $\times$ 50 cm metal enclosure. This design provides flexibility in experimental configurations, allowing for precise control over the distance between antennas and accommodating larger samples. The cubic geometry ensures a directional electromagnetic field distribution within the cavity, minimizing measurement inconsistencies that may arise from asymmetric boundary conditions. Furthermore, the enclosure's dimensions enhance the system's versatility, enabling compatibility with a broader range of materials and facilitating more comprehensive evaluations of SE. These design considerations contribute to a controlled and reproducible measurement environment, improving accuracy in electromagnetic characterization.

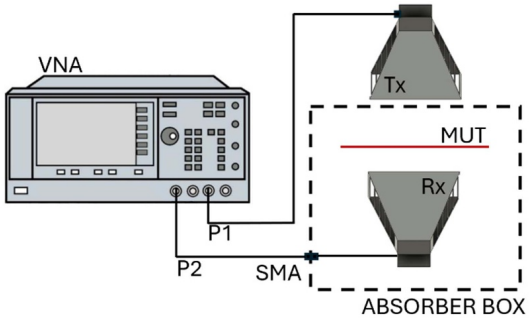

Figure 1. Schematic of the Absorber Box measurement setup.

2.1. Evaluation of the new approach: Absorber Box method

This study proposes a substantial improvement over the previous design of the measurement box by modifying its dimensions to 50 $\times$ 50 $\times$ 50 cm. In conventional designs, the presence of slots in the structure of the box can generate slot-antenna effects, leading to electromagnetic field leakage and affecting measurement accuracy [22]. In the current version, the enclosure was fabricated by a specialized metalworking company using folded aluminum panels with welded edges, resulting in a continuous metallic surface with no structural slots. A single SMA port was included for the receiving antenna cable, carefully sized to minimize leakage. This optimization of the cavity dimensions promotes a more homogeneous distribution of the electromagnetic field inside, allowing for directional signal propagation and reducing unwanted reflections that could affect the measurement.

The measurement procedure is carried out using a 26.5 GHz Keysight P9375A vector network analyzer (VNA). For the experimental setup shown in figure 1, port 1 of the VNA is connected to the transmitting antenna, located outside the box. The receiving antenna, positioned inside the cavity, is connected to a coaxial cable with an SMA connector that passes through the box via a drilled hole, establishing the connection with port 2 of the VNA. This configuration enables accurate characterization of the samples, ensuring reliable and reproducible measurements.

Multilayer foam absorbent materials with a thickness of 25 mm and dimensions of 50 $\times$ 50 cm have been used to minimize internal reflections and ensure that electromagnetic waves are properly attenuated within the box. These absorbers, based on carbon-loaded polyurethane foam (TFAL-Series), are laminated to produce a graded conductivity profile suitable for broadband operation [23]. They have been cut and arranged to match the geometry of the receiving antenna. Additionally, by adjusting the number of absorber layers placed inside the cavity, the effective distance between the antennas can

be modified, allowing different configurations to be studied without altering the physical structure of the box.

Subsequently, the SE (dB) of the sample is calculated according to equation (1):

$$\mathrm{SE\ (dB)} = \mathrm{S21_{sample}} - \mathrm{S21_{ref}} \tag{1}$$

where $\mathrm{S21_{ref}}$ is the transmission parameter of the air measured between the two antennas without any sample, and $\mathrm{S21_{sample}}$ is the transmission parameter of the sample placed between the antennas.

Thanks to this optimized design, the proposed system enables accurate measurements while avoiding errors caused by signal dispersion or external interference. One of its key advantages is that it eliminates the need for an anechoic chamber, allowing measurements to be performed in a compact space without requiring large-scale setups. Additionally, this system does not necessitate large material samples, as measurements can be conducted with samples only a few centimeters in size. This is particularly beneficial for evaluating expensive or difficult-to-manufacture materials, where minimizing sample size in testing stages is essential for cost efficiency and practicality. The reduced space requirements and the simplicity of the experimental configuration also contribute to a lower overall measurement cost, as the setup can be deployed in standard laboratory environments without the need for specialized infrastructure. Compared to traditional methods, the enhanced Absorber Box offers a portable and accessible alternative that enables rapid and repeatable evaluations, making it suitable for iterative testing, early-stage material screening, or comparative studies across a wide frequency range.

This approach represents a significant advancement in the characterization of materials and electromagnetic devices, providing a robust and reproducible method for evaluating electromagnetic properties in a controlled measurement environment. Furthermore, this system allows easy and efficient sample measurement, facilitating its use in various research and development applications.

The final experimental system is shown in figure 2, where the emitting horn antenna is situated above a MUT and connected to the VNA equipment.

2.2. Characterization of the Absorber Box method

To ensure the reliability and reproducibility of the measurements in the experimental system, preliminary tests of the S_{21} parameter in air were carried out by varying the separation between the transmitting and receiving antenna. Distances of 5 cm, 10 cm, 15 cm and 22 cm were tested, the results of which are presented in figure 3.

The analysis of the data obtained reveals that there is a relationship between the transmission coefficient S_{21} and the distance between the antennas following a behavior that, under far-field conditions, is described by the Friis transmission equation [24]:

$$P_\mathrm{r} = P_\mathrm{t}\left(\frac{\lambda}{4\pi d}\right)^2 G_\mathrm{t}G_\mathrm{r} \tag{2}$$

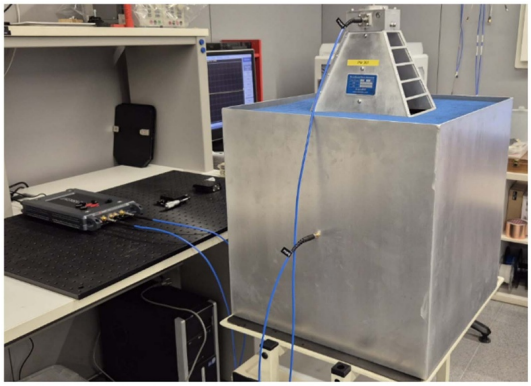

Figure 2. Configuration of the real experimental system: Absorber Box.

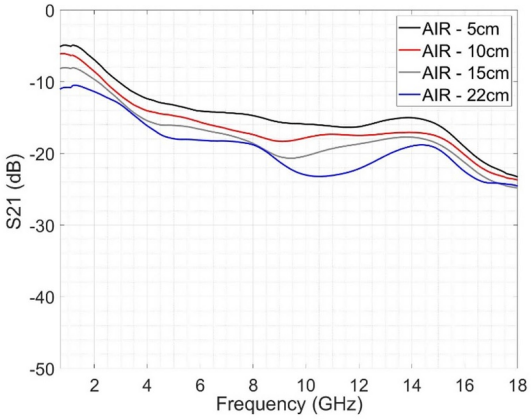

Figure 3. Air S_{21} parameter between the antennas varying the distance.

$$S_{21} = 10\log_{10}\left(\frac{P_\mathrm{r}}{P_\mathrm{t}}\right) = 10\log_{10}\left[\left(\frac{\lambda}{4\pi d}\right)^2 G_\mathrm{t}G_\mathrm{r}\right] \tag{3}$$

where P_r represents the received power, P_t is the transmitted power, λ is the wavelength, d is the separation between antennas, and G_t and G_r are the gains of the transmitting and receiving antennas, respectively. This equation highlights the inverse square dependence of received power on distance, which explains the observed attenuation trend in the experimental data.

However, in our case, the antenna separations place the system in a regime where the far-field condition, typically defined as $d \gg 2D^2/\lambda$, is not satisfied, preventing the direct application of the Friis equation, which assumes far-field propagation. Nevertheless, while near-field effects such as reflections and diffraction could introduce additional complexities, these are mitigated by the absorbers used inside the cavity and the sample size, an aspect that is analyzed in detail later in this

work. The use of absorbing materials within the cavity represents a controlled environment, minimizing reflected waves and multipath propagation, which could otherwise affect the near-field measurement accuracy.

Therefore, since the theoretical model cannot be directly applied in this case, we adopt a balanced approach that combines experimental reference measurements and numerical simulations. Specifically, we use the S_{21} measurement of the air between the two antennas as an experimental reference, which serves as a baseline for comparison. Additionally, a simulation model of the system will be developed in ANSYS HFSS to validate the measurement setup and ensure consistency between experimental results and theoretical expectations within the considered distance regime.

As shown in figure 3, the measured S_{21} parameter decreases as the antenna separation increases, following the theoretical free-space path loss model. Notably, the attenuation becomes more pronounced for distances greater than 10 cm, particularly at frequencies above 6 GHz, where the signal reduction is significant. This behavior is consistent with the wavelength dependence, as higher frequencies correspond to shorter wavelengths, leading to increased propagation losses. Additionally, at larger distances, diffraction effects and multipath interference become more relevant, causing fluctuations in the received signal and compromising measurement stability.

Based on these results, a distance of 5 cm was established as the optimum condition for the measurements in this study. This configuration provides an adequate balance between efficiency in signal transmission and reduction of external disturbances, thus minimizing the introduction of systematic errors in the characterization of the samples. In this way, a controlled and reproducible experimental framework is guaranteed, which allows for obtaining reliable and representative results in analyzing the S_{21} parameter.

Once the optimal measurement distance was established, an analysis was conducted to evaluate the influence of sample size on SE. For this purpose, copper foil (EMC shielding tape) with a thickness of 0.04 mm was used, varying its dimensions as shown in figure 4. This analysis aims to determine how different sample sizes affect the measured attenuation across the frequency range, ensuring that the SE characterization remains consistent and reliable.

The results obtained from the measurement of samples of different copper foil sizes with the Absorber Box measurement method are presented in figure 5. The results reveal a clear dependence of the SE on the dimensions of the sample. Specifically, larger samples show higher attenuation levels across the entire frequency range, with values below -40 dB, even the largest samples showing attenuations below -80 dB. In contrast, as the sample size decreases, the SE performance is quite affected, decreasing to values of -10 dB for the smallest sample of 12×12 cm. This trend is particularly evident at lower frequencies, where the differences in SE become more pronounced.

One of the main factors influencing electromagnetic shielding measurements is the edge diffraction effect. In this phenomenon, an incident wave interacts with the boundaries of a conductive sample, leading to energy leakage beyond the geometric shadow region. When an electromagnetic wave encounters a discontinuity, such as the sharp edges of a conductive sheet, part of the energy is scattered in different directions, contributing to diffraction losses. The extent of diffraction depends on the relationship between the sample size (L) and the wavelength (λ):

1. If $L \gg \lambda$: the diffraction effect is less significant.
2. If $L \ll \lambda$: the diffraction effect is more significant.

In our specific case, the frequency range spans from 700 MHz to 18 GHz, corresponding to wavelengths ranging from approximately 42.8 cm (at 700 MHz) to 1.67 cm (at 18 GHz). Since the sample dimensions in our setup are on the

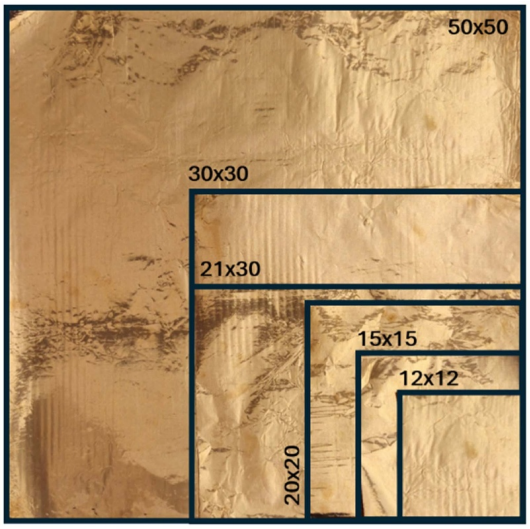

Figure 4. Copper foil (EMC shielding tape) samples of various dimensions.

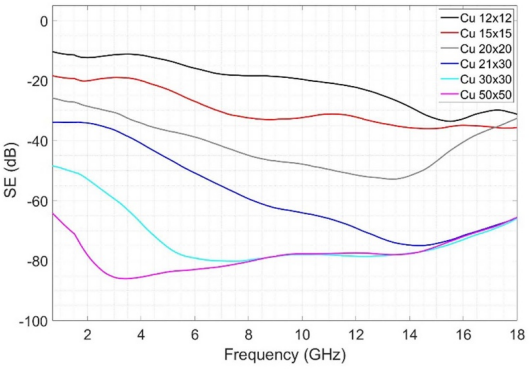

Figure 5. SE of the copper foil, varying the sample size.

order of tens of centimeters, diffraction effects are more pronounced at lower frequencies where $L \ll \lambda$, leading to significant energy leakage beyond the geometric shadow region. As the frequency increases ($L \gg \lambda$), the diffraction effect becomes less significant, improving measurement accuracy. This behavior underscores the need for an optimized measurement configuration to mitigate diffraction-related errors, particularly in the lower-frequency range.

From an analytical perspective, the diffraction coefficient D_{UTD} quantifies the fraction of the electromagnetic wave that bends around the edges of a conducting sheet. This coefficient is derived from the uniform theory of diffraction (UTD), which extends the geometrical theory of diffraction to provide a more accurate description of wave propagation near discontinuities.

The diffraction coefficient is expressed as:

$$D = \frac{\mathrm{e}^{\frac{j\pi}{4}} \sin\frac{\pi}{n}}{n(2\pi k)^{1/2}\sin\beta}\left[\left(\cos\frac{\pi}{n} - \cos\frac{\theta-\alpha}{n}\right)^{-1} \mp \left(\cos\frac{\pi}{n} - \cos\frac{\theta+\alpha+\pi}{n}\right)^{-1}\right] \tag{4}$$

where $k = \frac{2\pi f}{c}$ is the wavenumber, $n = \frac{\pi}{\alpha}$ is the wedge parameter determined by the internal angle α, θ represents the incident wave angle, and β is the diffraction angle [25–27].

In the specific case of the experimental setup considered, where the incident wave is normal to the sample ($\theta = 0°$), the diffraction wave propagates perpendicularly to the plane ($\beta = 90°$), and the distance between the antennas and the sheet is small compared to the sample size ($r_1 \approx r_2 \ll L$), the diffraction effect is primarily governed by the sample dimensions rather than the distance between the antennas [28]. Under these conditions, the diffraction coefficient simplifies to:

$$D_{\mathrm{UTD}} \approx \frac{\mathrm{e}^{\frac{-j\pi}{4}}}{\sqrt{2\pi kL}}. \tag{5}$$

This expression reveals two fundamental characteristics of the diffraction process. First, as the size of the sheet increases, the diffraction effect diminishes since a larger sheet obstructs wave propagation more effectively, reducing the amount of energy diffracted beyond the geometric shadow region. Second, at lower frequencies, diffraction losses become more pronounced as longer wavelengths interact more significantly with obstacles and tend to bend around edges more easily. Consequently, at higher frequencies, the diffraction effect is less significant, which increases the shielding performance of the sample. This relationship underscores the importance of considering diffraction effects when evaluating SE, particularly for finite-sized samples, as they can introduce measurement uncertainties that may lead to overestimating transmission losses if not properly accounted for.

From an experimental standpoint, as illustrated in figure 5, edge diffraction effects significantly influence the SE of the samples. In smaller samples, the interaction between the incident electromagnetic waves and the sample boundaries enhances diffraction, increasing wave leakage and consequently reducing the overall shielding performance. This effect is particularly noticeable at lower frequencies, where the wavelength is comparable to the characteristic dimensions of the sample, leading to a greater contribution of diffracted energy to the transmitted field. A key observation is that the SE curves for the 50 × 50 cm and 30 × 30 cm samples converge in the 7–8 GHz frequency range, indicating that diffraction effects become negligible beyond a specific sample size and shielding performance stabilizes. In this range, the wavelength becomes small compared to the sample size, reducing the relative influence of edge diffraction. In this frequency band, the shielding behavior stabilizes, and the attenuation is mainly governed by the material's intrinsic properties, rather than by geometric constraints. This suggests that increasing the sample size beyond this point does not significantly enhance SE, as the measured attenuation is primarily governed by the intrinsic properties of the material rather than by geometric constraints. Furthermore, larger samples exhibit a smoother attenuation trend across the frequency range, whereas smaller samples present more pronounced variations. This indicates that edge diffraction not only reduces SE but also introduces fluctuations in the measured values. These variations may affect the accuracy of the characterization, underscoring the importance of selecting an appropriate sample size to obtain reliable and reproducible results.

These findings highlight the necessity of optimizing sample dimensions to achieve meaningful SE measurements. The sample size should be large enough to minimize diffraction-related losses while ensuring that the measured SE corresponds to the material's inherent behavior. To achieve representative results, it is advisable to use sample dimensions larger than the dominant wavelengths within the analyzed frequency range. This minimizes edge diffraction effects and ensures a more accurate evaluation of the shielding performance.

Based on these results, it is concluded that, for this system, the optimal sample size corresponds to the maximum cavity dimensions, 50 × 50 cm. However, due to practical limitations related to the standard dimensions of commercially available materials, 30 × 30 cm samples will be used in this study. Given that the SE traces for 30 × 30 cm and 50 × 50 cm converge at 7–8 GHz, these frequencies will be considered as the threshold above which diffraction effects no longer influence the SE values. By focusing the analysis on frequencies above this limit, a more precise characterization of the SE can be achieved, ensuring that the measured values reflect the intrinsic properties of the material rather than being affected by edge-related phenomena.

3. Simulation model definition

In this study, a FEM simulation model was developed to validate the behavior of the real system. The primary objective of the model is to serve as a 'digital twin' of the physical setup, allowing for a detailed analysis of the system's performance under various conditions. By recreating the real-world configuration as accurately as possible, this model allows for detailed simulations that predict the system's behavior and assist in optimizing its design.

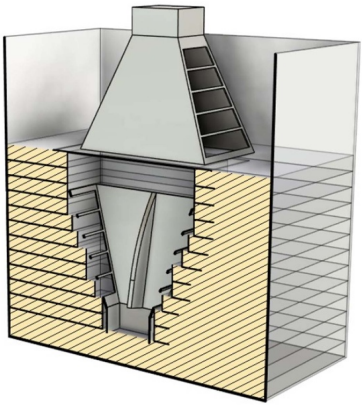

Figure 6. 3D model of the Absorber Box method with a sample under test.

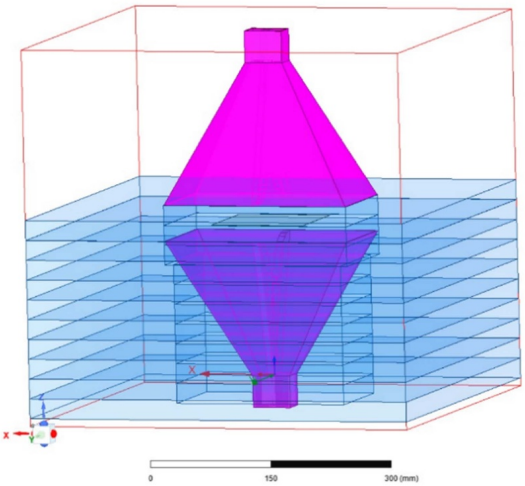

Figure 7. Simulation model of the Absorber Box method.

The FEM simulation is created using the software ANSYS HFSS Electronics Desktop. The experimental measurement setup has been replicated to assess the scattering parameter S_{21} of the developed system. To accurately simulate the full-scale system, broadband antennas were carefully designed and validated to replicate the performance of real antennas within the frequency range of 0.7–18 GHz. These antennas are excited using wave ports to ensure precise electromagnetic field excitation. The mesh density was optimized in both the antennas and the sample under test to achieve reliable and convergent simulation results. Additionally, the electromagnetic properties of the microwave-absorbing material used to line the interior of the enclosure were obtained directly from the manufacturer, ensuring accurate modeling of wave absorption characteristics. The enclosure walls were modeled using perfect electric conductor boundary conditions, while impedance boundaries were applied to the absorbers based on their frequency-dependent electromagnetic properties. Radiation boundaries were also included in selected regions to minimize reflections and simulate open-field propagation. The proposed system of the simulation model is shown in figure 6:

To validate the accuracy of the simulation model, a comparative approach was implemented using theoretical SE calculations. Instead of relying solely on experimental data, reference values were generated using analytical models based on well-established electromagnetic shielding theory [29, 30]. This approach assesses whether the simulation model can reliably reproduce theoretical predictions.

The validation process involved defining hypothetical materials with known values of permittivity (ε_r), permeability (μ_r), and conductivity (σ).

The SE for these materials was initially computed using analytical formulas, considering both reflection loss (SE_R) and absorption loss (SE_A) [31],

$$SE_R = 20\log\left|\frac{Z_m + Z_0}{4Z_m}\right| \tag{6}$$

$$Z_m = \sqrt{\frac{j\omega\mu}{\sigma + j\omega\varepsilon}} \tag{7}$$

$$SE_A = 8.686\alpha d \tag{8}$$

$$\alpha = R_e\left(\sqrt{j\omega\mu(\sigma + j\omega\varepsilon)}\right) \tag{9}$$

where Z_0 is the impedance of free space, typically 377 Ω, Z_m is the intrinsic impedance of the material, α is the attenuation constant and d is the thickness of the shielding material.

The total SE can be expressed as:

$$SE_{total} = SE_R + SE_A. \tag{10}$$

The developed simulation model for the SE analysis of the Absorber Box method is shown in figure 7:

After obtaining theoretical SE values, the same material parameters were implemented in the simulation environment, ensuring that boundary conditions and material properties were consistent with the analytical model. As established in previous sections, the simulations were conducted using 30 × 30 cm samples, based on the conclusions drawn earlier regarding optimal sample dimensions.

Figure 8 illustrates the general trend of SE values between the two approaches: theoretical and simulated. The trends are well-aligned, particularly at mid-frequencies and the minor deviations observed at higher frequencies suggest potential

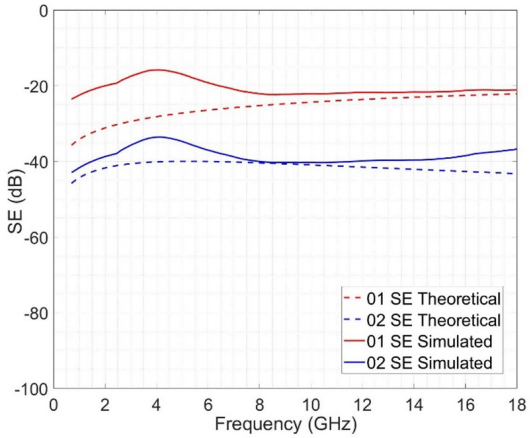

Figure 8. Comparison of theoretical and simulated S_{21} parameters for materials with different conductivities.

Table 1. Comparison of the theoretical and simulated values of the hypothetical materials.

ID	Theoretical value @1 GHz	Simulated value @1 GHz	Theoretical value @10 GHz	Simulated value @10 GHz
01	–34.17 dB	–22.34 dB	–24.33 dB	–22.11 dB
02	–44.32 dB	–41.51 dB	–40.92 dB	–40.27 dB

numerical approximations or limitations in wave interactions within the simulation environment. The discrepancies between theoretical and simulated SE values become more pronounced at lower frequencies, particularly below 7–8 GHz. This effect can be attributed to the findings presented in figure 5, which demonstrate that the SE of smaller samples is significantly affected by diffraction effects in this frequency range. Additionally, the simulation model has intrinsic limitations that become more evident at lower frequencies, where the cavity dimensions influence the accuracy of the computed SE values.

The results of the simulations are compared with the theoretical calculations to evaluate their agreement in table 1.

The results confirm that the simulation model can replicate the shielding behavior predicted by theoretical models, particularly at mid and high frequencies, where both approaches exhibit great agreement. At lower frequencies, the simulated SE values tend to underestimate the theoretical predictions. Despite these differences, the overall correlation between theoretical and simulated values supports the reliability of the simulation model. It is worth noting that the strong agreement observed at higher frequencies, where the wavelength is comparable to or smaller than the structural features of the system, validates the accuracy of the simulation geometry, material modeling and boundary conditions. This consistency confirms that the digital twin developed using FEM can be used not only to interpret experimental results, but also to optimize the design of future measurement setups and to pre-assess the performance of new materials under similar conditions. Therefore, the simulation model serves as a robust predictive tool, extending the applicability of the Absorber Box methodology to a wider range of configurations and frequency bands.

4. Results and discussion

This section presents the results of the transmission and SE assessment, along with the analysis of the electric field distribution in the tested materials. Initially, the measurement system and numerical model are validated through a comparative analysis of the S_{21} scattering parameter in free space. Subsequently, the SE of various materials is quantified to establish their attenuation characteristics.

Furthermore, the E-field distribution is analyzed to provide deeper insight into the interaction between electromagnetic waves and the shielding materials. This evaluation enables the identification of localized variations in field intensity, offering a more comprehensive understanding of attenuation efficiency and shielding performance across different materials.

4.1. Transmission and SE results

The first step in validating the system involved analyzing the accuracy of the reference measurement ($S21_{\text{air}}$), which serves as a baseline for comparison with the tested materials. This measurement is crucial, as a considerable discrepancy between the experimental and simulated values in the absence of a sample could indicate errors in the system setup or equipment calibration. The comparison of $S21_{\text{air}}$ presented in figure 9 exhibited a strong correlation between the simulation model

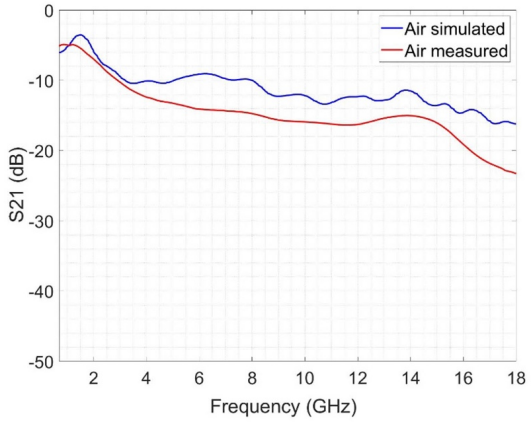

Figure 9. Comparison of the S_{21} parameter of the air obtained by FEM simulation and experimentally measured.

and the experimental data, with both following similar trends and closely matching the measured traces across the analyzed frequency range.

While a significant agreement is observed, some differences between the simulation and experimental results are expected due to the inherent complexity of accurately replicating all elements of the physical setup in a numerical model. To further investigate these variations and enhance the understanding of the measurement system, a more detailed analysis is conducted using an alternative material.

Figure 10 presents a comparative analysis of two graphs: the first illustrates the measured S_{21} parameter for a dielectric material ($\sigma = 0$, $\mu \approx 1$ and $\varepsilon \approx 19$). In contrast, the second depicts the SE, calculated as the difference between the material's S_{21} measurement and the air reference. It is observed that the agreement between measured and simulated traces is less pronounced in the S_{21} graph (figure 10(a)), primarily due to approximations in the simulation model. These discrepancies stem from the inherent tolerances in the characterization of the absorber material, as well as the complexity associated with accurately replicating the antenna model, particularly in terms of radiation pattern and gain. However, when the air reference is subtracted (figure 10(b)), the resulting SE traces exhibit a significantly improved correspondence between measured and simulated data. Given that SE is the key parameter for evaluating electromagnetic shielding performance, the strong agreement in the SE graph provides validation for the accuracy and reliability of the simulation model across the analyzed frequency range.

In figure 10(a), the agreement between simulation and experiment is strongest below 4 GHz, with the traces closely matching, particularly at 2.7 GHz, where both take a value of -10.23 dB. However, as frequency increases, the measured transmission tends to be lower than the simulated data, with the most significant discrepancies occurring above 12 GHz. The largest error is found at the 18 GHz frequency, where the difference between the measured and simulated traces is

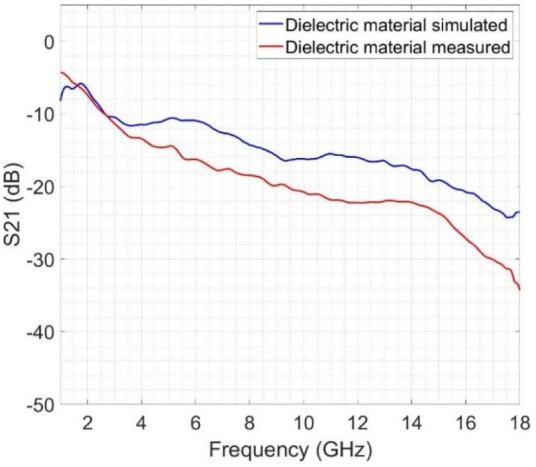

(a)

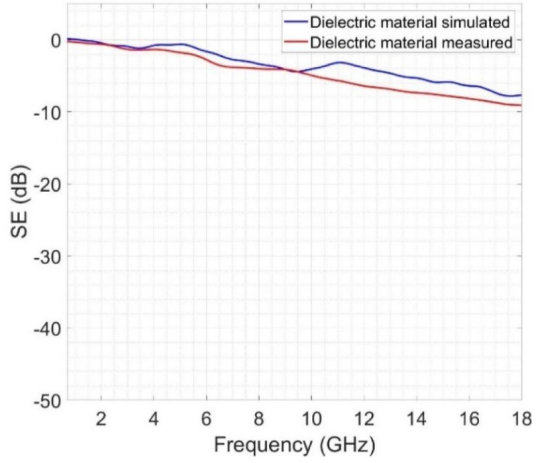

(b)

Figure 10. Comparison of the measurements of a dielectric material obtained by FEM simulation and experimentally measured. (a) S_{21} (dB); (b) SE (dB).

-10.8 dB, primarily attributed to variations in the dielectric properties of the real sample, additional losses introduced by the experimental setup, or simplifications in the antenna radiation pattern and cable transitions not fully captured in the model. On the other hand, in figure 10(b), the agreement between the two traces is more pronounced at lower frequencies, particularly below 4 GHz. In this case, the largest error is found at the 11.1 GHz frequency, being 2.5 dB, likely associated with residual cavity effects or small imperfections in the absorber performance at higher frequencies.

After confirming the agreement between simulated and experimental results, measurements were conducted on a set of selected materials with different attenuation levels (figure 11).

Table 2. Sample description.

Sample ID	Description	Dimensions (mm)
Composite material	Glass fiber reinforced composite with 3%wt of carbon nanotubes	30 × 30 × 21
Dielectric material	High-performance dielectric material	30 × 30 × 6.0
Shielding textile	Conductive shielding fabric	30 × 30 × 0.1
Absorber sheet 01	Flexible electromagnetic absorber sheet	30 × 30 × 1.0
Absorber sheet 02	Flexible electromagnetic absorber sheet	30 × 30 × 2.0
Thermal-shielding material 01	Thermally and electromagnetic shielding material	30 × 30 × 1.0
Thermal-shielding material 02	Thermally and electromagnetic shielding material	30 × 30 × 3.0

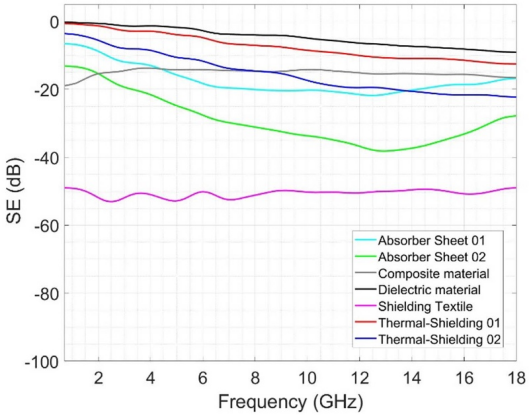

Figure 11. Experimental SE results for the different samples, measured using the Absorber Box method.

The materials were chosen to represent a wide range of SE, from low to high attenuation, ensuring a comprehensive evaluation of the Absorber Box measurement system under various shielding conditions. The analyzed samples included a glass fiber-reinforced composite with 3%wt carbon nanotubes, a high-performance dielectric material, a conductive shielding fabric, a flexible electromagnetic absorber sheet in two different thicknesses, and a thermally and electromagnetically shielding material, also tested in two thicknesses. Each of these materials exhibits distinct electromagnetic properties and various levels of attenuation. All of the samples are described in table 2.

The glass fiber-reinforced composite with 3%wt carbon nanotubes is expected to provide moderate attenuation, as the conductive fillers within the insulating matrix contribute to partial electromagnetic wave absorption and reflection. The high-performance dielectric material, being non-conductive, is anticipated to exhibit minimal SE, primarily affecting wave propagation rather than absorption or reflection. The flexible electromagnetic absorber sheets, tested in two different thicknesses, are specifically engineered for absorption, with greater attenuation expected for the thicker variant. Similarly, the thermal–electromagnetic shielding materials, also evaluated in two thicknesses, combine thermal insulation with electromagnetic shielding, with the thicker sample expected to provide enhanced attenuation. The conductive shielding fabric is designed for lightweight EMI protection, offering higher attenuation than the other materials due to its conductive nature. By analyzing these materials, this study aims to evaluate the Absorber Box's ability to differentiate between varying shielding capabilities and validate its performance across a diverse set of shielding materials.

Experimental results indicated that materials with higher conductivity exhibited significantly greater SE values, with attenuation levels exceeding −50 dB across the measured frequency range. In contrast, materials with lower conductivity provided a more moderate or negligible reduction in EMI. The most notable trend is observed in the shielding textile, which consistently maintains the highest attenuation, with SE values below −50 dB across the entire frequency range, confirming its efficiency as an EMI shielding material primarily due to strong reflection mechanisms.

The glass fiber-reinforced composite with 3%wt carbon nanotubes shows a gradual decrease in SE with increasing frequency, ranging from approximately −10 dB at low frequencies to nearly −30 dB at higher frequencies. This suggests that while the presence of carbon nanotubes enhances shielding performance, the material does not act as a perfect barrier, likely due to its composite structure and partial conductivity. In contrast, the dielectric material demonstrates negligible SE, remaining close to 0 dB in the low frequency range, reinforcing its expected role in wave propagation rather than attenuation.

A frequency-dependent behavior is evident in the flexible electromagnetic absorber sheets, where Absorber Sheet 02 (thicker variant) outperforms Absorber Sheet 01, particularly above 8 GHz, where their SE values diverge more significantly. This suggests that absorption mechanisms in these materials become more effective at higher frequencies. A similar frequency-dependent trend is observed in the thermal–electromagnetic shielding materials, where Thermal-Shielding 02 exhibits slightly higher attenuation than Thermal-Shielding 01, particularly in the mid-frequency range (6–12 GHz). However, both thermal shielding materials show less attenuation compared to the absorber sheets, indicating a combined but less dominant shielding mechanism. An interesting behavior is seen in the composite material and thermal-shielding traces, which show a clear dip in attenuation around 8–12 GHz, suggesting possible resonance effects or

Table 3. SE values of the different samples.

Sample ID	SE value @1 GHz	SE value @10 GHz
Composite material	−18.51 dB	−14.19 dB
Dielectric material	−0.31 dB	−4.92 dB
Shielding textile	−49.10 dB	−50.23 dB
Absorber sheet 01	−6.74 dB	−20.26 dB
Absorber sheet 02	−13.29 dB	−33.67 dB
Thermal-shielding material 01	−0.71 dB	−8.51 dB
Thermal-shielding material 02	−3.81 dB	−17.39 dB

frequency-dependent interactions within their structures. In contrast, the shielding textile remains nearly constant, suggesting a broadband shielding response with minimal frequency-dependent variations.

Table 3 summarizes the shielding effectiveness values of all tested materials at 1 GHz and 10 GHz.

Overall, these results emphasize the strong reflective shielding capabilities of conductive textiles, the frequency-dependent nature of absorbers, and the limitations of dielectric and composite materials in providing significant shielding. The findings highlight the importance of selecting shielding materials based on the specific frequency range and required attenuation levels for EMI protection applications. Furthermore, the absorber-based measurement system demonstrates high resolution in distinguishing SE variations across different materials and frequency ranges. Its ability to precisely discern differences in attenuation mechanisms reinforces its reliability for comprehensive SE characterization in diverse shielding applications.

4.2. Electric field distribution results

To further validate the accuracy of the measurement system, simulations were performed to analyze the distribution of the electric field within the Absorber Box method. These simulations provide a detailed analysis of the wave propagation behavior, allowing for a better understanding of how electromagnetic waves interact with the system components, including the antennas, the absorbing materials, and the samples.

Figure 12 pretends to evaluate the impact of the absorbing material on minimizing the influence of unwanted effects in the characterization of SE in the AIR reference measurement. A comparison of the *E*-field distribution in AIR is presented, with and without the presence of the absorbing material, at a frequency of 10 GHz. This frequency has been selected as a reference throughout the study to maintain consistency with previous results. Figure 12(a) illustrates the reference measurement without the absorbing material. In this setup, significant variability is observed due to reflections and disturbances caused by the environment and the measurement system configuration. These unwanted interferences affect the accuracy of the measurement and can introduce inconsistencies in SE characterization, leading to unreliable results. In contrast, figure 12(b) shows the reference measurement

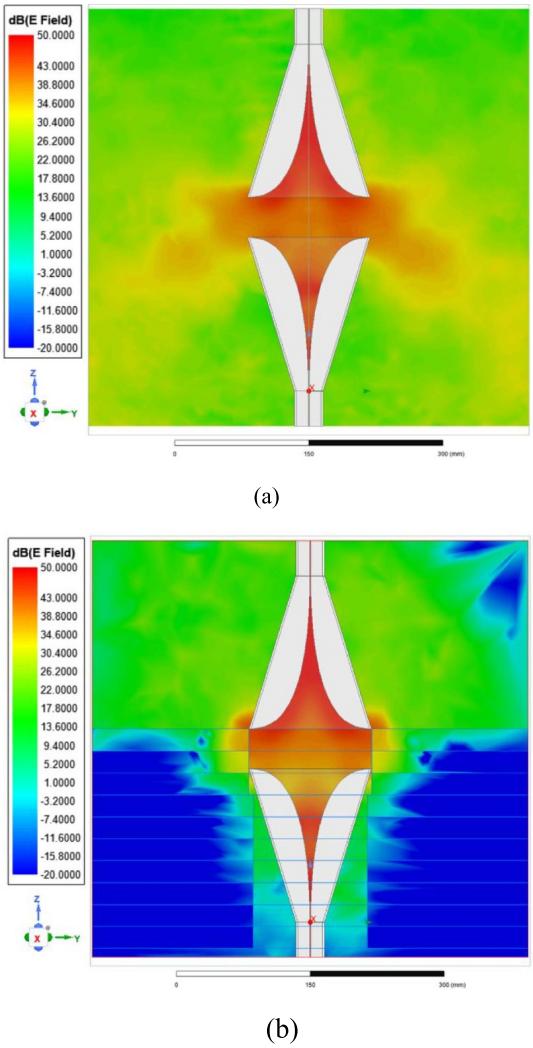

Figure 12. Analysis of the *E*-field distribution in dB. (a) The reference AIR measurement without the absorbing material; (b) the reference AIR measurement with the absorbing material.

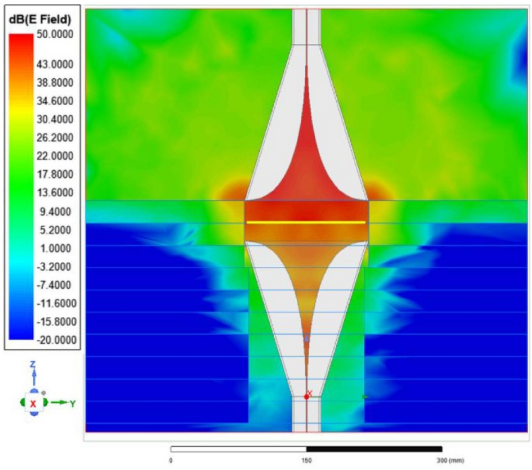

(a)

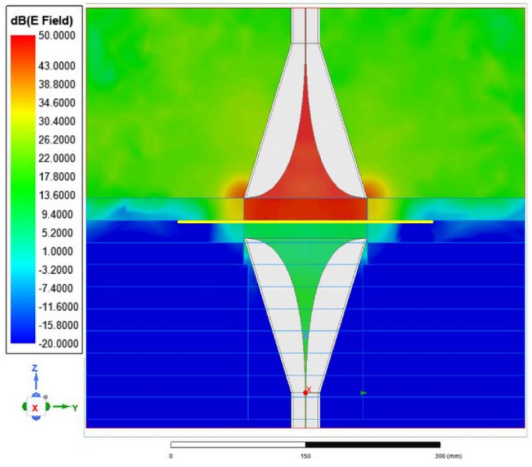

(b)

Figure 13. Analysis of the *E*-field distribution. (a) The 12 × 12 cm MUT; (b) the 30 × 30 cm MUT.

of air with the absorbing material placed inside the cavity. The absorbing material creates a controlled electromagnetic propagation channel, significantly reducing unwanted effects associated with antenna interference. The presence of the absorbing material minimizes signal distortions and effectively mitigates environmental reflections, leading to a more stable and accurate measurement of the SE baseline.

These results justify the use of the absorbing material in the measurement system, as its inclusion enables a more precise evaluation of the material's effect on electromagnetic radiation attenuation, thereby ensuring a controlled and repeatable testing environment.

On the other hand, figure 13 investigates the influence of sample size on SE characterization by comparing two samples of the previously mentioned material 02, with dimensions of 12 × 12 cm and 30 × 30 cm, respectively. This comparison allows for a clearer understanding of how the size of the sample affects the transmission of electromagnetic. Figure 13(a) depicts the field distribution for the 12 × 12 cm sample. In this case, the electromagnetic field manages to leak into the receiving antenna due to pronounced edge diffraction effects. This phenomenon results in a decrease in the measured attenuation, leading to an underestimation of the material's SE. The relatively small sample size allows a considerable portion of the incident field to bypass the material, reducing its apparent shielding performance. By contrast, figure 13(b) presents the field distribution for the 30 × 30 cm sample. With the increased sample size, the unwanted transmission through the edges is significantly reduced, ensuring a more accurate evaluation of the material. The larger sample better confines the electromagnetic field, minimizing diffraction effects and yielding a more representative measurement of the SE.

These findings align with the results presented in figure 5, which demonstrate the impact of sample size on SE measurements. As the sample size increases, edge diffraction decreases, leading to a more accurate representation of the material's intrinsic electromagnetic behavior. This analysis confirms the necessity of using appropriately sized samples to ensure reliable SE measurements and to minimize errors caused by geometric effects unrelated to the material's inherent shielding properties.

5. Conclusions

This study validated the accuracy and effectiveness of an enhanced Absorber Box method for measuring SE in electromagnetic applications. Through a combined approach of experimental, theoretical and simulation analysis, the proposed system demonstrated reliable measurements across a broad frequency range, addressing several limitations of existing standardized methods. The experimental and simulated results exhibited strong overall agreement, supporting the reliability of the proposed model. However, minor discrepancies were identified in specific spectral regions that can be attributed to the interaction between sample geometry and the electromagnetic field distribution within the Absorber Box, as well as localized interference and resonance effects.

A key finding of this study was the significant influence of sample size on SE measurements. It was observed that smaller samples exhibited stronger edge diffraction effects, which could lead to an underestimation of the material's true attenuation capabilities. Conversely, appropriately sized samples minimized these diffraction effects, resulting in more precise and representative measurements.

Additionally, the inclusion of absorbing material within the measurement box significantly enhanced system accuracy by reducing unwanted interferences and minimizing internal reflections. This optimized design enabled the effective characterization of a wide range of shielding materials. The experimental results confirmed the system's capability to differentiate materials with varying attenuation levels, demonstrating

its precision and reliability in distinguishing SE across different materials and frequency ranges. The ability to accurately measure materials with different shielding performances reinforces the robustness of this method as a practical alternative to conventional SE measurement techniques.

In conclusion, the proposed method represents an efficient and flexible alternative for the characterization of electromagnetic shielding materials. Its combination of accuracy, ease of implementation, and compatibility with diverse materials makes it a valuable tool for applications in telecommunications, automotive, aerospace, and other sectors where EMI is a critical concern. Future research may focus on optimizing the box geometry and analyzing materials with more complex properties to further enhance the system's precision and applicability.

Data availability statement

No new data were created or analysed in this study.

Acknowledgments

This study forms part of the Advanced Materials programme and was supported by MCIN with funding from European Union NextGenerationEU (PRTR-C17.I1) and by Generalitat Valenciana (MFA/2022/060).

References

[1] Min Koo C, Sambyal P, Iqbal A, Shahzad F and Hong J 2021 Electromagnetic interference and shielding *Two-Dimensional Materials for Electromagnetic Shielding* (Wiley) pp 1–24

[2] Vance E F and Graf W 1988 The role of shielding in interference control *IEEE Trans. Electromagn. Compat.* **30** 294–7

[3] Futatsumori S and Hiraga N 2024 Electromagnetic interference issues of aircraft radio altimeters due to Sub-6 band 5G mobile communications systems in Japan *2024 IEEE Joint Int. Symp. on Electromagnetic Compatibility, Signal & Power Integrity: EMC Japan/Asia-Pacific Int. Symp. on Electromagnetic Compatibility (EMC Japan/APEMC Okinawa)* (IEEE) pp 45–48

[4] Son H and Chong Y 2019 Analysis of the interference effects of 5G system on automotive collision avoidance radars *2019 Int. Conf. on Information and Communication Technology Convergence (ICTC)* (IEEE) pp 1463–6

[5] Gallardo B P, de Francisco P G, Romero S F, Rebate I M, Somolinos D R and Martinez D P 2021 Limitations in the shielding effectiveness measurement methods for carbon fiber composites *IEEE Electromagn. Compat. Mag.* **10** 52–61

[6] ASTM standard (ASTM D4935-18) 2018 *Test Method for Measuring the Electromagnetic Shielding Effectiveness of Planar Materials* (https://doi.org/10.1520/D4935-18)

[7] Anon 2007 IEEE standard method for measuring the effectiveness of electromagnetic shielding enclosures *IEEE Std 299-2006 (Revision of IEEE Std 299-1997)* pp 1–52

[8] Micheli D, Delfini A, Pastore R, Marchetti M, Diana R and Gradoni G 2017 Absorption cross section of building materials at mm wavelength in a reverberation chamber *Meas. Sci. Technol.* **28** 024001

[9] David N A, Wild P M and Djilali N 2012 Parametric study of a polymer-coated fibre-optic humidity sensor *Meas. Sci. Technol.* **23** 035103

[10] Bakli H, Moualhi M and Makhlouf M 2022 High-sensitivity electrical properties measurement of graphene-based composites using interferometric near-field microwave technique *Meas. Sci. Technol.* **33** 045012

[11] Qiu L, Ding S, Wang D and Han B 2023 Self-sensing GFRP-reinforced concrete beams containing carbon nanotube-nano carbon black composite fillers *Meas. Sci. Technol.* **34** 084003

[12] Chang T, Zhang X, Yang C, Sun Z and Cui H-L 2017 Measurement of complex terahertz dielectric properties of polymers using an improved free-space technique *Meas. Sci. Technol.* **28** 045002

[13] Amaro A, Suarez A, Tamburrano A, Torres J, Marra F, Martinez P A, Galindo B, Soriano N, Victoria J and Alcarria A 2023 EMI shielding effectiveness study for innovative carbon nanotube materials in the 5G frequency region *IEEE Trans. Electromagn. Compat.* **65** 177–85

[14] Martinez P A, Victoria J, Torres J, Suarez A, Alcarria A, Amaro A, Galindo-Galiana B, Losada-Fernandez C, Ramirez-Monsell V and Lopez-Rius B 2021 Analysis of EMI shielding effectiveness for plastic fiber composites in the 5G sub-6 GHz band *2021 Joint IEEE Int. Symp. on Electromagnetic Compatibility Signal and Power Integrity, and EMC Europe, EMC/SI/PI/EMC Europe 2021*

[15] Barjola A, Herráiz R, Amaro A, Torres J, Suárez A and Giménez E 2024 $Ti_3C_2T_x$ electromagnetic shielding performance: investigating environmental influences and structural changes *Adv. Electron. Mater.* **10** 2400024

[16] Zapata A S, Dawson J F, Ariën Y, Catrysse J, Pissoort D and Marvin A C 2023 An overview of the IEEE P2715 guide for the characterization of the shielding effectiveness of planar materials *IEEE Electromagn. Compat. Mag.* **12** 78–88

[17] 2023 *IEEE Std 2715™ Guide for the Characterization of the Shielding Effectiveness of Planar Materials* IEEE Standard

[18] Marvin A C, Dawson L, Flintoft I D and Dawson J F 2009 A method for the measurement of shielding effectiveness of planar samples requiring no sample edge preparation or contact *IEEE Trans. Electromagn. Compat.* **51** 255–62

[19] Amaro A, Suarez A, Torres J, Martinez P A, Herraiz R, Alcarria A, Benedito A, Ruiz R, Galvez P and Penades A 2023 Shielding effectiveness measurement method for planar nanomaterial samples based on CNT materials up to 18 GHz *Magnetochemistry* **9** 114

[20] Brown T W C and Khalily M 2018 Integrated shield edge diffraction model for narrow obstructing objects *IEEE Trans. Antennas Propag.* **66** 6588–95

[21] Kang J-S, Kim J-H and Park J-I Reduction of edge diffraction effects of MUT holder using EM absorber in W-band free-space material measurements

[22] Yingpeng F, Zhengwei D, Gong K and Guoding L 2003 Analysis on shielding effectiveness of metallic enclosures with slot *Asia-Pacific Conf. on Environmental*

Electromagnetics, 2003. CEEM 2003. Proc. (IEEE) pp 43–46
[23] Anon datablad-TFAL series. Electromagnetic Absorber Datasheet
[24] Balanis C A Antenna theory analysis and design third edition
[25] Paknys R 2016 Uniform theory of diffraction *Applied Frequency-Domain Electromagnetics* (Wiley) pp 268–316
[26] Kandimalla D, De A and Sanyal S 2015 A novel UTD-type diffraction coefficient for a straight edge in a curved screen *IEEE Trans. Antennas Propag.* **63** 1172–7
[27] Keller J B Geometrical theory of diffraction*
[28] Kouyoumjian R G and Pathak P H 1974 A uniform geometrical theory of diffraction for an edge in a perfectly conducting surface *Proc. IEEE* **62** 1448–61
[29] Schelkunoff S A 1943 *Electromagnetic Waves* (D Van Nostrand)
[30] McDowell A J and Hubing T H 2014 Analysis and comparison of plane wave shielding effectiveness decompositions *IEEE Trans. Electromagn. Compat.* **56** 1711–4
[31] Ott H W 2009 *Electromagnetic Compatibility Engineering* (Wiley)

6.2 Summary

This chapter illustrates the advantages of incorporating numerical simulation into the evaluation of shielding effectiveness using the Absorber Box method. The development of a validated digital twin enables deeper analysis of field propagation and material response, strengthening the physical interpretation of experimental results. The collaboration with Würth Elektronik provided access to new shielding materials, the characterization of which confirmed the method's applicability to real industrial products. These outcomes reinforce the Absorber Box configuration as a versatile tool for both measurement and simulation-driven EMI assessment, closing the methodological cycle addressed throughout this thesis.

This work fulfills S.O.6 and S.O.7, by developing a numerical model of the measurement system and validating its reliability and consistency with theoretical expectations. The comparison between simulation and theoretical calculations directly supports S.O.5, by establishing the analytical basis used for benchmarking the results. Moreover, the combined use of experimental and simulation tools reinforces the general methodological framework proposed in this thesis, thereby contributing to the fulfillment of S.O.8.

Chapter 7. Conclusions and technological transfer

This final chapter presents the general and specific conclusions drawn from this doctoral thesis. Additionally, this chapter presents the transfer of results and knowledge derived from this Ph.D. study to the industry.

7.1 Conclusions

This doctoral thesis was undertaken with the objective of developing, implementing, and validating alternative methods for measuring shielding effectiveness in planar materials. The work was motivated by the limitations of standardized methodologies when applied to materials for emerging communication applications, complex sample geometries, or extended frequency ranges, as increasingly required in complex electromagnetic compatibility scenarios.

The research has been articulated around two main methodological strategies: the adaptation of standardized coaxial transmission line methods, and the implementation of a non-standardized measurement configuration based on an Absorber Box. These approaches have been progressively developed, refined, and validated throughout the different chapters, offering solutions tailored to specific material constraints and measurement needs.

Chapters 3 and 4 addressed the first line of work, focused on coaxial probe methods derived from the ASTM D4935-18 standard. In Chapter 3, a coaxial configuration was adapted to allow the characterization of fiber-reinforced composite samples in the sub-6 GHz range. The study demonstrated that, even within the assumptions of the standard, adaptations are required when the geometry and physical nature of the samples deviate from ideal cases. In Chapter 4, a miniaturized version of the coaxial probe was implemented in collaboration with the University of Rome “La Sapienza”, allowing single-mode measurements up to 18 GHz. The reduced size of the fixture enabled the characterization of small samples while preserving repeatability and sensitivity, making it suitable for high-frequency shielding analysis.

The second methodological direction was addressed in Chapters 5 and 6, through the development of a measurement setup based on an Absorber Box configuration. Chapter 5 introduced the physical implementation of the method, designed to evaluate large, rigid,

or structurally reinforced samples that are incompatible with coaxial geometries. The configuration was applied to a set of composite laminates provided by AIMPLAS in the framework of the SMART5G project. The project's focus on enabling technologies for high-frequency communications offered a relevant and realistic scenario for validating the applicability of the method in the context of future 5G electronic systems.

Chapter 6 extended this approach by introducing numerical simulation into the measurement workflow. A finite element model of the Absorber Box was developed using ANSYS HFSS to replicate the physical setup and simulate the electromagnetic field distribution across the sample. This allowed for a detailed study of wave propagation, diffraction phenomena, and measurement sensitivity, particularly in the low-frequency region where cavity effects become more relevant. The agreement between simulated and measured results provided validation for the model and reinforced the physical consistency of the proposed methodology.

Beyond the experimental and simulation developments, this thesis has made a broader methodological contribution by bridging the gap between standardized procedures and real-world requirements. The work demonstrates that measurement methods can be extended and adapted without compromising the results, as long as they are properly validated through experiments and simulations. This is particularly relevant in the context of technologies such as 5G, autonomous systems, and high-density electronics, where the diversity of materials and designs continues to grow, and where reliable EMC characterization becomes increasingly critical.

Additionally, the collaborative nature of this research has played a key role in the success of the work. The partnerships established with AIMPLAS, Würth Elektronik, and the University of Rome "La Sapienza" enabled access to advanced materials, industrial measurement challenges, and complementary expertise. The integration of this thesis within the SMART5G strategic project framework has provided a technologically relevant environment in which to develop and validate the proposed methods. These collaborations have also facilitated the transfer of results into technical documentation and application notes, contributing to the broader impact of the work beyond the academic domain.

In summary, this thesis contributes to the advancement of measurement methodologies for electromagnetic shielding by proposing and validating practical alternatives to conventional standards. The methods developed here are versatile and adaptable to a wide range of materials and testing scenarios. They form the basis for ongoing research and development in the field of shielding effectiveness, supporting the transition of academic knowledge into industry-relevant solutions.

7.2 Technological transfer

The knowledge generated through this research has been transferred beyond the academic context through the implementation of experimental measurement setups, the development of measurement guides, and the integration of selected findings and material results into industrial documentation (Figure 7.1). This section summarizes the main actions derived from the research, structured around three dimensions: infrastructure development, methodological dissemination, and user guides for the industry.

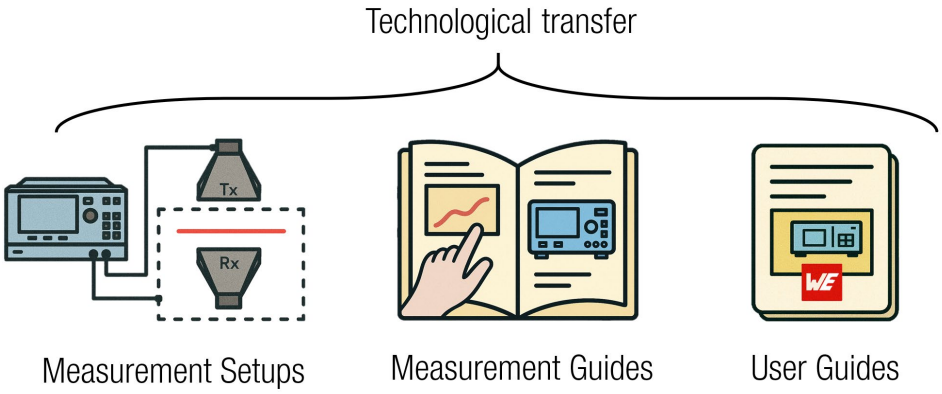

Figure 7.1 *Technological transfer strategy*

7.2.1 Measurement Setups

As part of this work, two complete experimental measurement setups have been designed, implemented, and validated to characterize the shielding effectiveness of planar materials. The first corresponds to the adaptation of the coaxial transmission line method, initially derived from ASTM D4935-18, and implemented in two configurations. The first is designed for sub-6 GHz applications and was used to characterize fiber-reinforced composite samples. The second is a miniaturized fixture developed in the University of Rome “La Sapienza”, allowing single-mode operation up to 18 GHz. Both setups were optimized for use with planar samples and integrated into laboratory environments for routine material testing.

The second configuration corresponds to the Absorber Box method (Figure 7.2). This setup was designed to evaluate materials that are incompatible with coaxial geometries due to size, rigidity, or structural complexity. The method enables shielding effectiveness measurements under quasi-free-space conditions and has been validated through both experimental procedures and simulations. The Absorber Box system is currently in use for evaluating industrial planar materials and has proven to be reliable and scalable.

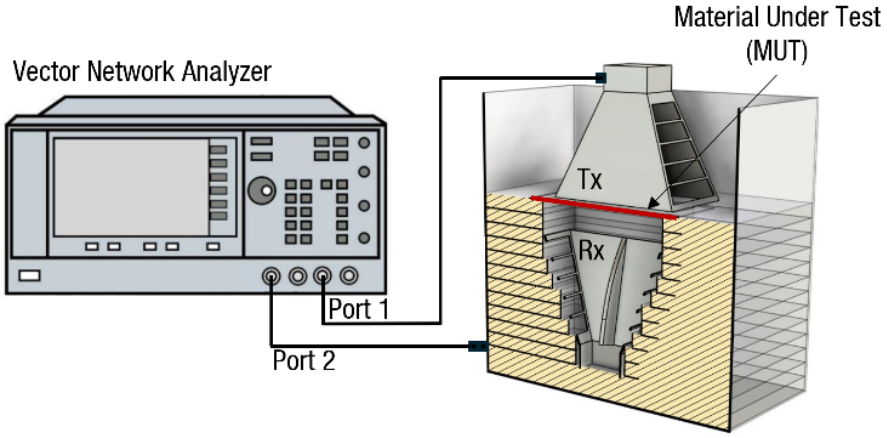

Figure 7.2 Absorber Box schematic measurement setup

7.2.2 Contribution to IEEE 2715-2023 standard document

The experimental methodologies developed during this thesis have contributed to the definition of internal testing procedures and the practical interpretation of existing guidelines. Notably, the measurements conducted as part of this work were included in the IEEE P2715 standard (*Guide for the Characterization of the Shielding Effectiveness of Planar Materials*) [3], as part of a multi-laboratory round robin exercise involving several international institutions. The Universitat de València, through the contributions of this doctoral research, is explicitly represented in the comparative results shown in the standard (Figure 7.3), alongside institutions such as Sapienza University of Rome.

The coaxial and absorber-based configurations explored in this thesis have been aligned with the principles established in that guide, while also extending their application to new materials and measurement conditions. The outcomes of this work have been presented at national conferences (VII Spanish EMC Conference) and in peer-reviewed publications, contributing to ongoing discussions on the evolution of measurement standards and the need for new measurement methods in high-frequency characterization.

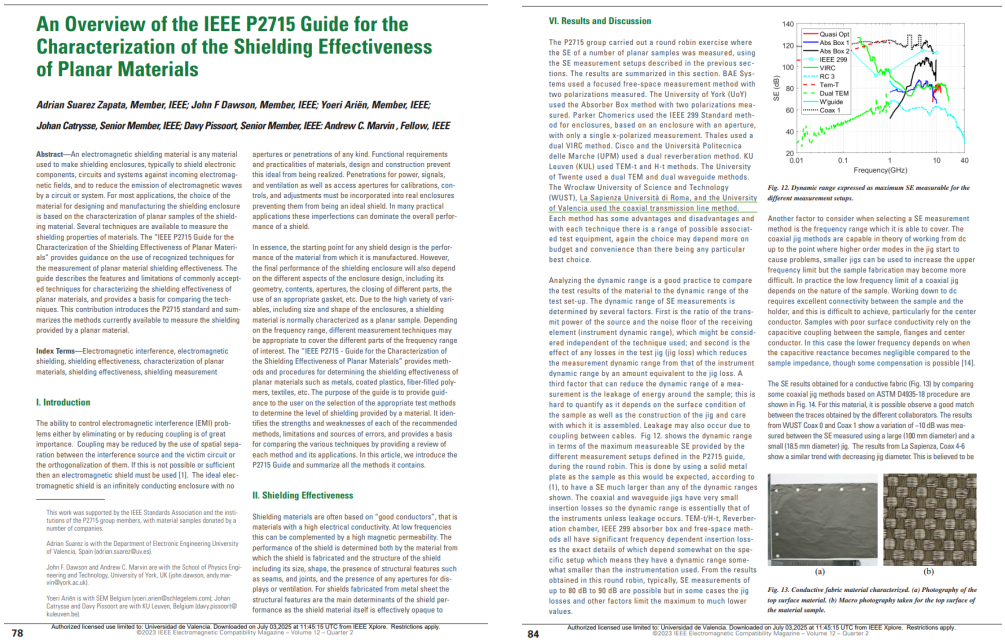

An Overview of the IEEE P2715 Guide for the Characterization of the Shielding Effectiveness of Planar Materials

Adrian Suarez Zapata, Member, IEEE; John F Dawson, Member, IEEE; Yoeri Ariën, Member, IEEE; Johan Catrysse, Senior Member, IEEE; Davy Pissoort, Senior Member, IEEE; Andrew C. Marvin , Fellow, IEEE

Abstract—An electromagnetic shielding material is any material used to make shielding enclosures, typically to shield electronic components, circuits and systems against incoming electromagnetic fields, and to reduce the emission of electromagnetic waves by a circuit or system. For most applications, the choice of the material for designing and manufacturing the shielding enclosure is based on the characterization of planar samples of the shielding material. Several techniques are available to measure the shielding properties of materials. The "IEEE P2715 Guide for the Characterization of the Shielding Effectiveness of Planar Materials" provides guidance on the use of recognized techniques for the measurement of planar material shielding effectiveness. The guide describes the features and limitations of commonly accepted techniques for characterizing the shielding effectiveness of planar materials, and provides a basis for comparing the techniques. This contribution introduces the P2715 standard and summarizes the methods currently available to measure the shielding provided by a planar material.

Index Terms—Electromagnetic interference, electromagnetic shielding, shielding effectiveness, characterization of planar materials, shielding effectiveness, shielding measurement

I. Introduction

The ability to control electromagnetic interference (EMI) problems either by eliminating or by reducing coupling is of great importance. Coupling may be reduced by the use of spatial separation between the interference source and the victim circuit or the orthogonalization of them. If this is not possible or sufficient then an electromagnetic shield must be used [1]. The ideal electromagnetic shield is an infinitely conducting enclosure with no apertures or penetrations of any kind. Functional requirements and practicalities of materials, design and construction prevent this ideal from being realized. Penetrations for power, signals, and ventilation as well as access apertures for calibrations, controls, and adjustments must be incorporated into real enclosures preventing them from being an ideal shield. In many practical applications these imperfections can dominate the overall performance of a shield.

In essence, the starting point for any shield design is the performance of the material from which it is manufactured. However, the final performance of the shielding enclosure will also depend on the different aspects of the enclosure design, including its geometry, contents, apertures, the closing of different parts, the use of an appropriate gasket, etc. Due to the high variety of variables, including size and shape of the enclosures, a shielding material is normally characterized as a planar sample. Depending on the frequency range, different measurement techniques may be appropriate to cover the different parts of the frequency range of interest. The "IEEE P2715 - Guide for the Characterization of the Shielding Effectiveness of Planar Materials" provides methods and procedures for determining the shielding effectiveness of planar materials such as metals, coated plastics, fiber-filled polymers, textiles, etc. The purpose of the guide is to provide guidance to the user on the selection of the appropriate test methods to determine the level of shielding provided by a material. It identifies the strengths and weaknesses of each of the recommended methods, limitations and sources of errors, and provides a basis for comparing the various techniques by providing a review of each method and its applications. In this article, we introduce the P2715 Guide and summarize all the methods it contains.

II. Shielding Effectiveness

Shielding materials are often based on "good conductors", that is materials with a high electrical conductivity. At low frequencies this can be complemented by a high magnetic permeability. The performance of the shield is determined both by the material from which the shield is fabricated and the structure of the shield including its size, shape, the presence of structural features such as seams, and joints, and the presence of any apertures for displays or ventilation. For shields fabricated from metal sheet the structural features are the main determinants of the shield performance as the shield material itself is effectively opaque to

This work was supported by the IEEE Standards Association and the institutions of the P2715 group members, with material samples donated by a number of companies.

Adrian Suarez is with the Department of Electronic Engineering University of Valencia, Spain (adrian.suarez@uv.es).

John F. Dawson and Andrew C. Marvin are with the School of Physics Engineering and Technology, University of York, UK (john.dawson, andy.marvin@york.ac.uk).

Yoeri Ariën is with SEM Belgium (yoeri.arien@schlegelemi.com); Johan Catrysse and Davy Pissoort are with KU Leuven, Belgium (davy.pissoort@kuleuven.be).

VI. Results and Discussion

The P2715 group carried out a round robin exercise where the SE of a number of planar samples was measured, using the SE measurement setups described in the previous sections. The results are summarized in this section. BAE Systems used a focused free-space measurement method with two polarizations measured. The University of York (UoY) used the Absorber Box method with two polarizations measured. Parker Chomerics used the IEEE 299 Standard method for enclosures, based on an enclosure with an aperture, with only a single x-polarized measurement. Thales used a dual VIRC method. Cisco and the Università Politecnica delle Marche (UPM) used a dual reverberation method. KU Leuven (KUL) used TEM-t and H-t methods. The University of Twente used a dual TEM and dual waveguide methods. The Wroclaw University of Science and Technology (WUST), La Sapienza Università di Roma, and the University of Valencia used the coaxial transmission line method. Each method has some advantages and disadvantages and with each technique there is a range of possible associated test equipment, again the choice may depend more on budget and convenience than there being any particular best choice.

Analyzing the dynamic range is a good practice to compare the test results of the material to the dynamic range of the test set-up. The dynamic range of SE measurements is determined by several factors. First is the ratio of the transmit power of the source and the noise floor of the receiving element (instrument dynamic range), which might be considered independent of the technique used; and second is the effect of any losses in the test jig (jig loss) which reduces the measurement dynamic range from that of the instrument dynamic range by an amount equivalent to the jig loss. A third factor that can reduce the dynamic range of a measurement is the leakage of energy around the sample; this is hard to quantify as it depends on the surface condition of the sample as well as the construction of the jig and care with which it is assembled. Leakage may also occur due to coupling between cables. Fig 12. shows the dynamic range in terms of the maximum measureable SE provided by the different measurement setups defined in the P2715 guide, during the round robin. This is done by using a solid metal plate as the sample as this would be expected, according to (1), to have a SE much larger than any of the dynamic ranges shown. The coaxial and waveguide jigs have very small insertion losses so the dynamic range is essentially that of the instruments unless leakage occurs. TEM-t/H-t, Reverberation chamber, IEEE 299 absorber box and free-space methods all have significant frequency dependent insertion losses the exact details of which depend somewhat on the specific setup which means they have a dynamic range somewhat smaller than the instrumentation used. From the results obtained in this round robin, typically, SE measurements of up to 80 dB to 90 dB are possible but in some cases the jig losses and other factors limit the maximum to much lower values.

Fig. 12. Dynamic range expressed as maximum SE measurable for the different measurement setups.

Another factor to consider when selecting a SE measurement method is the frequency range which it is able to cover. The coaxial jig methods are capable in theory of working from dc up to the point where higher order modes in the jig start to cause problems, smaller jigs can be used to increase the upper frequency limit but the sample fabrication may become more difficult. In practice the low frequency limit of a coaxial jig depends on the nature of the sample. Working down to dc requires excellent connectivity between the sample and the holder, and this is difficult to achieve, particularly for the center conductor. Samples with poor surface conductivity rely on the capacitive coupling between the sample, flanges and center conductor. In this case the lower frequency depends on when the capacitive reactance becomes negligible compared to the sample impedance, though some compensation is possible [14].

The SE results obtained for a conductive fabric (Fig. 13) by comparing some coaxial jig methods based on ASTM D4935-18 procedure are shown in Fig. 14. For this material, it is possible observe a good match between the traces obtained by the different collaborators. The results from WUST Coax B and Coax 1 show a variation of ~10 dB was measured between the SE measured using a large (100 mm diameter) and a small (18.5 mm diameter) jig. The results from La Sapienza, Coax 4-6 show a similar trend with decreasing jig diameter. This is believed to be

Fig. 13. Conductive fabric material characterized. (a) Photography of the top surface material. (b) Macro photography taken for the top surface of the material sample.

Figure 7.3 Extract from the IEEE P2715 standard (DOI: 10.1109/IEEESTD.2023.10115252)

7.2.3 Technical dissemination through User Guides

Some of the results generated in this thesis are being prepared for inclusion in technical User Guides aimed at designers and engineers working in the field of electromagnetic compatibility. In particular, shielding effectiveness values obtained from the characterization of the WE-EMIP product, will be featured in a User Guide issued by Würth Elektronik (Figure 7.4). This document is intended to support product selection and design processes by providing validated measurement data obtained under controlled conditions using the Absorber Box method.

The inclusion of these results in industrial documentation not only strengthens the technical foundation of commercial design tools, but also exemplifies the effective transfer of experimental knowledge from academic research to practical engineering contexts. This form of dissemination contributes to closing the gap between laboratory-scale developments and real-world EMC applications, reinforcing the societal and technological relevance of the research.

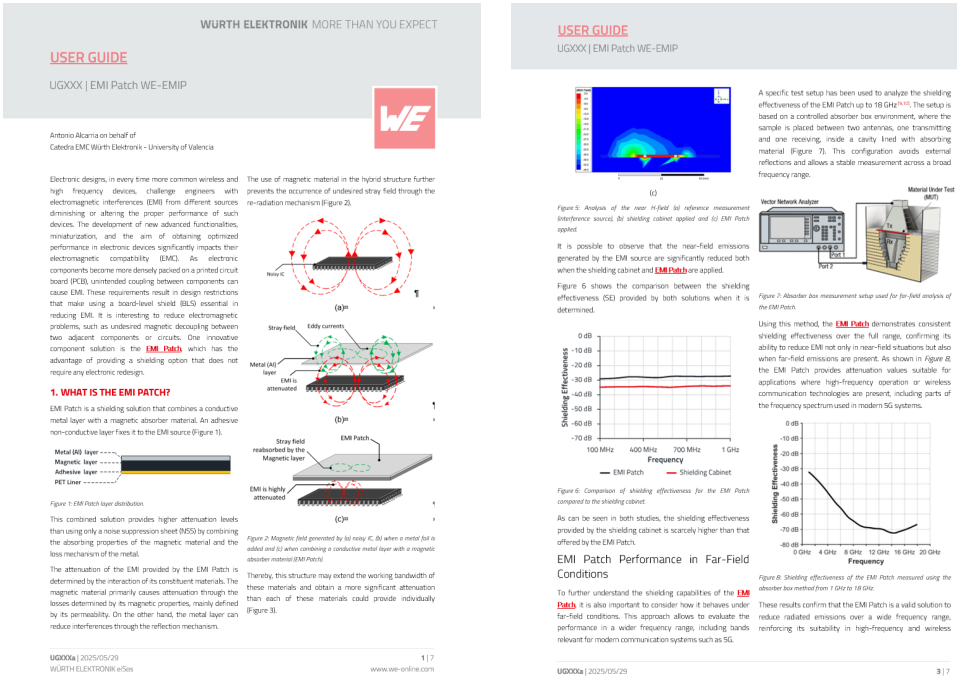

WÜRTH ELEKTRONIK MORE THAN YOU EXPECT

USER GUIDE

UGXXX | EMI Patch WE-EMIP

Antonio Alcarria on behalf of
Catedra EMC Würth Elektronik - University of Valencia

Electronic designs, in every time more common wireless and high frequency devices, challenge engineers with electromagnetic interferences (EMI) from different sources diminishing or altering the proper performance of such devices. The development of new advanced functionalities, miniaturization, and the aim of obtaining optimized performance in electronic devices significantly impacts their electromagnetic compatibility (EMC). As electronic components become more densely packed on a printed circuit board (PCB), unintended coupling between components can cause EMI. These requirements result in design restrictions that make using a board-level shield (BLS) essential in reducing EMI. It is interesting to reduce electromagnetic problems, such as undesired magnetic decoupling between two adjacent components or circuits. One innovative component solution is the **EMI Patch**, which has the advantage of providing a shielding option that does not require any electronic redesign.

1. WHAT IS THE EMI PATCH?

EMI Patch is a shielding solution that combines a conductive metal layer with a magnetic absorber material. An adhesive non-conductive layer fixes it to the EMI source (Figure 1).

Figure 1: EMI Patch layer distribution.

This combined solution provides higher attenuation levels than using only a noise suppression sheet (NSS) by combining the absorbing properties of the magnetic material and the loss mechanism of the metal.

The attenuation of the EMI provided by the EMI Patch is determined by the interaction of its constituent materials. The magnetic material primarily causes attenuation through the losses determined by its magnetic properties, mainly defined by its permeability. On the other hand, the metal layer can reduce interferences through the reflection mechanism.

The use of magnetic material in the hybrid structure further prevents the occurrence of undesired stray field through the re-radiation mechanism (Figure 2).

Figure 2: Magnetic field generated by (a) noisy IC, (b) when a metal foil is added and (c) when combining a conductive metal layer with a magnetic absorber material (EMI Patch).

Thereby, this structure may extend the working bandwidth of these materials and obtain a more significant attenuation than each of these materials could provide individually (Figure 3).

(c)

Figure 5: Analysis of the near H-field (a) reference measurement (interference source), (b) shielding cabinet applied and (c) EMI Patch applied.

It is possible to observe that the near-field emissions generated by the EMI source are significantly reduced both when the shielding cabinet and **EMI Patch** are applied.

Figure 6 shows the comparison between the shielding effectiveness (SE) provided by both solutions when it is determined.

Figure 6: Comparison of shielding effectiveness for the EMI Patch compared to the shielding cabinet.

As can be seen in both studies, the shielding effectiveness provided by the shielding cabinet is scarcely higher than that offered by the EMI Patch.

EMI Patch Performance in Far-Field Conditions

To further understand the shielding capabilities of the **EMI Patch**, it is also important to consider how it behaves under far-field conditions. This approach allows to evaluate the performance in a wider frequency range, including bands relevant for modern communication systems such as 5G.

A specific test setup has been used to analyze the shielding effectiveness of the EMI Patch up to 18 GHz[8,9]. The setup is based on a controlled absorber box environment, where the sample is placed between two antennas, one transmitting and one receiving, inside a cavity lined with absorbing material (Figure 7). This configuration avoids external reflections and allows a stable measurement across a broad frequency range.

Figure 7: Absorber box measurement setup used for far-field analysis of the EMI Patch.

Using this method, the **EMI Patch** demonstrates consistent shielding effectiveness over the full range, confirming its ability to reduce EMI not only in near-field situations but also when far-field emissions are present. As shown in *Figure 8*, the EMI Patch provides attenuation values suitable for applications where high-frequency operation or wireless communication technologies are present, including parts of the frequency spectrum used in modern 5G systems.

Figure 8: Shielding effectiveness of the EMI Patch measured using the absorber box method from 1 GHz to 18 GHz.

These results confirm that the EMI Patch is a valid solution to reduce radiated emissions over a wide frequency range, reinforcing its suitability in high-frequency and wireless

Figure 7.4 User Guide of the WE-EMIP

REFERENCES

[1] "Standard Test Method for Measuring the Electromagnetic Shielding Effectiveness of Planar Materials 1", doi: 10.1520/D4935-18.

[2] "IEEE Standard Method for Measuring the Effectiveness of Electromagnetic Shielding Enclosures," *IEEE Std 299-2006 (Revision of IEEE Std 299-1997)*, pp. 1–52, 2007, doi: 10.1109/IEEESTD.2007.323387.

[3] "IEEE Guide for the Characterization of the Shielding Effectiveness of Planar Materials," Feb. 15, 2023, *IEEE, Piscataway, NJ, USA*. doi: 10.1109/IEEESTD.2023.10115252.

[4] H. W. Ott, *Electromagnetic Compatibility Engineering*. Wiley, 2009. doi: 10.1002/9780470508510.

[5] C. R. Paul, *Introduction to Electromagnetic Compatibility*, 2nd ed. Hoboken, NJ: Wiley, 2005. doi: 10.1002/0471758159.

[6] S. B. Kondawar and P. R. Modak, *Theory of EMI shielding*. 2020. doi: 10.1016/B978-0-12-817590-3.00002-6.

[7] J. M. Palmer, "The measurement of transmission, absorption, emission, and reflection," *Handbook of optics*, vol. 2, pp. 21–25, 1995.

[8] J. W. Gooch and J. K. Daher, "Fundamentals of Electromagnetic Shielding," in *Electromagnetic Shielding and Corrosion Protection for Aerospace Vehicles*, New York, NY: Springer New York, 2007, pp. 17–24. doi: 10.1007/978-0-387-46096-3_3.

[9] B. S. Guru and H. R. Hiziroglu, *Electromagnetic Field Theory Fundamentals*. Cambridge University Press, 2009. [Online]. Available: https://books.google.es/books?id=qzNdDtZUPXMC

[10] J. Kittur, B. Desai, R. Chaudhari, and P. K. Loharkar, "A comparative study of EMI shielding effectiveness of metals, metal coatings and carbon-based materials," *IOP Conf Ser Mater Sci Eng*, vol. 810, no. 1, p. 012019, Mar. 2020, doi: 10.1088/1757-899X/810/1/012019.

[11] Y. Yao *et al.*, "Polymer-based lightweight materials for electromagnetic interference shielding: a review," *J Mater Sci*, vol. 56, no. 11, pp. 6549–6580, Apr. 2021, doi: 10.1007/s10853-020-05635-x.

[12] J.-M. Thomassin, C. Jérôme, T. Pardoen, C. Bailly, I. Huynen, and C. Detrembleur, "Polymer/carbon based composites as electromagnetic interference (EMI) shielding materials," *Materials Science and Engineering: R: Reports*, vol. 74, no. 7, pp. 211–232, Jul. 2013, doi: 10.1016/j.mser.2013.06.001.

[13] N. A. D'Souza, L. K. Sahu, A. Ranade, W. Strauss, and A. Hernandez-Luna, "Polymer Nanocomposites in Processing," in *Handbook of Plastic Processes*, John Wiley & Sons, Ltd, 2006, ch. 12, pp. 681–736. doi: https://doi.org/10.1002/0471786586.ch12.

[14] H. Y. Shen, Q. Z. Jiao, Y. Zhao, H. S. Li, and Z. Sun, "Electrical Conductivity and Electromagnetic Interference Shielding Effectiveness of Multiwalled Carbon Nanotubes Filled ABS Composites," *Adv Mat Res*, vol. 194–196, pp. 1554–1557, Feb. 2011, doi: 10.4028/www.scientific.net/AMR.194-196.1554.

[15] M. Arjmand, T. Apperley, M. Okoniewski, and U. Sundararaj, "Comparative study of electromagnetic interference shielding properties of injection molded versus compression molded multi-walled carbon nanotube/polystyrene composites," *Carbon N Y*, vol. 50, no. 14, pp. 5126–5134, Nov. 2012, doi: 10.1016/j.carbon.2012.06.053.

[16] İ. ARAZ, "The measurement of shielding effectiveness for small-in-size ferrite-based flat materials," *TURKISH JOURNAL OF ELECTRICAL ENGINEERING & COMPUTER SCIENCES*, vol. 26, no. 6, pp. 2997–3007, Nov. 2018, doi: 10.3906/elk-1803-162.

[17] R. Valenzuela, "Novel Applications of Ferrites," *Physics Research International*, vol. 2012, pp. 1–9, Mar. 2012, doi: 10.1155/2012/591839.

[18] A. Houbi, Z. A. Aldashevich, Y. Atassi, Z. Bagasharova Telmanovna, M. Saule, and K. Kubanych, "Microwave absorbing properties of ferrites and their composites: A review," *J Magn Magn Mater*, vol. 529, p. 167839, Jul. 2021, doi: 10.1016/j.jmmm.2021.167839.

[19] M. Altin Karataş and H. Gökkaya, "A review on machinability of carbon fiber reinforced polymer (CFRP) and glass fiber reinforced polymer (GFRP) composite materials," *Defence Technology*, vol. 14, no. 4, pp. 318–326, Aug. 2018, doi: 10.1016/j.dt.2018.02.001.

[20] A. Y. Boroujeni, M. Tehrani, M. Manteghi, Z. Zhou, and M. Al-Haik, "Electromagnetic Shielding Effectiveness of a Hybrid Carbon Nanotube/Glass Fiber Reinforced Polymer Composite," *J Eng Mater Technol*, vol. 138, no. 4, Oct. 2016, doi: 10.1115/1.4033576.

[21] D. Jang, B.-J. Kim, and I.-W. Nam, “A Comprehensive Study on EMI Shielding Performance of Carbon Nanomaterials-Embedded CFRP or GFRP Composites,” *Polymers (Basel)*, vol. 14, no. 23, p. 5224, Dec. 2022, doi: 10.3390/polym14235224.

[22] C. Tong, *Advanced Materials and Components for 5G and Beyond*, vol. 327. Cham: Springer Nature Switzerland, 2022. doi: 10.1007/978-3-031-17207-6.

[23] M. S. Sarto and A. Tamburrano, “Innovative Test Method for the Shielding Effectiveness Measurement of Conductive Thin Films in a Wide Frequency Range,” *IEEE Trans Electromagn Compat*, vol. 48, no. 2, pp. 331–341, May 2006, doi: 10.1109/TEMC.2006.874664.

[24] A. Tamburrano and M. S. Sarto, “Electromagnetic characterization of innovative shielding materials in the frequency range up to 8 gigahertz,” in *2004 International Symposium on Electromagnetic Compatibility (IEEE Cat. No.04CH37559)*, IEEE, pp. 551–556. doi: 10.1109/ISEMC.2004.1349857.

[25] A. Tamburrano, D. Desideri, A. Maschio, and M. Sabrina Sarto, “Coaxial Waveguide Methods for Shielding Effectiveness Measurement of Planar Materials Up to 18 GHz,” *IEEE Trans Electromagn Compat*, vol. 56, no. 6, pp. 1386–1395, Dec. 2014, doi: 10.1109/TEMC.2014.2329238.

[26] M. Kowal, S. Kubal, and R. J. Zielinski, “Measuring the shielding effectiveness of large textile materials in an anechoic chamber,” in *International Symposium on Electromagnetic Compatibility - EMC EUROPE*, IEEE, Sep. 2012, pp. 1–4. doi: 10.1109/EMCEurope.2012.6396852.

[27] C. L. Holloway, D. A. Hill, J. Ladbury, G. Koepke, and R. Garzia, “Shielding effectiveness measurements of materials using nested reverberation chambers,” *IEEE Trans Electromagn Compat*, vol. 45, no. 2, pp. 350–356, May 2003, doi: 10.1109/TEMC.2003.809117.

[28] F. B. J. Leferink, “High field strength in a large volume: the intrinsic reverberation chamber,” in *1998 IEEE EMC Symposium. International Symposium on Electromagnetic Compatibility. Symposium Record (Cat. No.98CH36253)*, IEEE, pp. 24–27. doi: 10.1109/ISEMC.1998.750054.

[29] V. M. Primiani *et al.*, “Reverberation chambers for testing wireless devices and systems,” *IEEE Electromagn Compat Mag*, vol. 9, no. 2, pp. 45–55, 2020, doi: 10.1109/MEMC.2020.9133241.

[30] E. Tourounoglou, V. Gkatsi, A. Roc’h, R. Vogt-Ardatjew, H. Schipper, and F. Leferink, “Influence of Planar Material Size and Position on Shielding Effectiveness

Measurements using the Dual Waveguide Method," in *2019 International Symposium on Electromagnetic Compatibility - EMC EUROPE*, IEEE, Sep. 2019, pp. 707–711. doi: 10.1109/EMCEurope.2019.8871968.

[31] E. Hariya and U. Masahiro, "Instruments for Measuring the Electromagnetic Shielding Effectiveness," in *1984 International Symposium on Electromagnetic Compatibility*, IEEE, Oct. 1984, pp. 1–6. doi: 10.1109/ISEMC2.1984.7568140.

[32] A. Manara, "Measurement of material shielding effectiveness using a dual TEM cell and vector network analyzer," *IEEE Trans Electromagn Compat*, vol. 38, no. 3, pp. 327–333, 1996, doi: 10.1109/15.536062.

[33] A. C. Marvin, L. Dawson, I. D. Flintoft, and J. F. Dawson, "A Method for the Measurement of Shielding Effectiveness of Planar Samples Requiring No Sample Edge Preparation or Contact," *IEEE Trans Electromagn Compat*, vol. 51, no. 2, pp. 255–262, May 2009, doi: 10.1109/TEMC.2009.2015147.

Appendix A. SCIENTIFIC CONTRIBUTIONS

This section includes a list of all the scientific publications and conferences derived from this Ph.D. work in chronological order.

A.1 Peer-reviewed scientific articles in journals

Amaro, A., Suarez, A., Tamburrano, A., Torres, J., Marra, F., Martinez, P. A., Galindo, B., Soriano, N., Victoria, J., and Alcarria, A. (2023a). EMI Shielding Effectiveness Study for Innovative Carbon Nanotube Materials in the 5G Frequency Region. *IEEE Transactions on Electromagnetic Compatibility*, 65(1), 177–185.

https://doi.org/10.1109/TEMC.2022.3209708

Amaro, A., Suarez, A., Torres, J., Martinez, P. A., Herraiz, R., Alcarria, A., Benedito, A., Ruiz, R., Galvez, P., and Penades, A. (2023). Shielding Effectiveness Measurement Method for Planar Nanomaterial Samples Based on CNT Materials up to 18 GHz. *Magnetochemistry*, 9(5), 114.

https://doi.org/10.3390/magnetochemistry9050114

Amaro, A., Torres, J., Suarez, A., Herraiz, R., Martinez, P.A., Soret, J., Garcia-Olcina, R. and Alcarria, A. (2025). Determination of Electromagnetic Shielding Effectiveness Using an Enhanced Absorber Box Method: Theoretical, Simulation, and Experimental Approaches. *Measurement Science and Technology*, IOP Publishing, 36(7).

https://doi.org/10.1088/1361-6501/ade55a

A.2 Peer-reviewed scientific articles in conferences

Martinez, P. A., Victoria, J., Torres, J., Suarez, A., Alcarria, A., Amaro, A., Galindo-Galiana, B., Losada-Fernandez, C., Ramirez-Monsell, V., & Lopez-Rius, B. (2021). Analysis of EMI Shielding Effectiveness for plastic fiber composites in the 5G sub-6 GHz band. 2021 Joint IEEE International Symposium on Electromagnetic Compatibility Signal and Power Integrity, and EMC Europe, EMC/SI/PI/EMC Europe 2021.

https://doi.org/10.1109/EMC/SI/PI/EMCEurope52599.2021.9559349

Appendix B. List of abbreviations

This section provides a list of all abbreviations used in this Ph.D. work, organized in alphabetical order.

ABS	Acrylonitrile Butadiene Styrene
ASTM	American society for testing and materials
CFRP	Carbon Fiber Reinforced Polymers
CNTs	Carbon Nanotubes
CSH	Coaxial Sample Holder
EMC	Electromagnetic Compatibility
EMI	Electromagnetic Interference
FEM	Finite Element Method
GFRP	Glass Fiber Reinforced Polymers
IEEE	Institute of Electrical and Electronic Engineers
JCR	Journal Citation Reports
MUT	Material Under Test
MWCNTs	Multi-walled Carbon Nanotubes
PP	Polypropylene
RAM	Radio-Absorbent Material
SE	Shielding Effectiveness
SJR	SCImago Journal Rank
SWCNTs	Single-walled Carbon Nanotubes
TEM	Transverse Electromagnetic Mode
VNA	Vector Network Analyzer